

Diss. ETH NO. **24009**

**Investigation of Silicon- and/or Nitrogen-containing  
Phosphorus-based Compounds as Flame Retardants  
for Cotton Textiles**

A thesis submitted to attain the degree of  
DOCTOR OF SCIENCES of ETH ZURICH  
(Dr. sc. ETH Zurich)

presented by

***Jia En Low***

*Master of Science, ETH Zurich*

*born October 15, 1984*

citizen of Malaysia

accepted on the recommendation of

*Prof. Dr. H. Grützmacher, examiner*

*Prof. Dr. A. Togni, co-examiner*

*Prof. Dr. J. Levalois-Grützmacher, co-examiner*

2017





半畝方塘一鑑開  
天光雲影共徘徊  
問渠哪得清如許  
為有源頭活水來

南宋·朱熹

*Dedicated to my parents and family.*





## **Acknowledgements**

I would like to express my deepest gratitude, to Prof. Dr. Hansjörg Grützmacher for the opportunity to carry out an exciting PhD project and your confidence in my work. A big thank you also to Prof. Dr. Joëlle Levalois-Grützmacher for your supervision, patience and invaluable support in guiding me throughout this experience.

Next I would like to express big thanks to Prof. Dr. Antonio Togni for your kind acceptance to be my co-examiner. Your advice improving this thesis are invaluable.

Special thanks goes to Dr. Hartmut Schönberg for his kind and patient assistance in administrative issues and issues concerning technical and research equipment. I would like to extend my gratitude to Christine Rüegg for providing a wonderful administrative, moral and emotional support throughout this journey.

To Xiuxiu, Johanna, Vijay and Jieping, thank you for the superb moments spent together as labmates, and the valuable emotional support at all times.

Additionally I would like to thank all current and former colleagues in the Grützmacher group, namely Dominikus, Amos, Matt, Vito, Yanbo, Andreas, Mark, Erik, Riccardo, Thomas, Jan, Monica, Fabian, Fernando, Bruno, Esther, Pascal, Xiaodan, Alex and Gustavo. Thank you for all the fun times we spent together, fruitful discussions and delicious foods (and beer).

I have to thank my colleagues at EMPA St. Gallen for the use of their PCFC instrument. Thank you, Dr. Sabyasachi Gaan, for the kind permission, your input and support in this research work. Big thank yous to Timea, Milijana, Shuyu, Elisabeth and Khalifah for all the necessary assistance rendered.

Thank you also to our collaboration partners, especially Julien Bardon at the Luxembourg Institute of Science and Technology (LIST) for the great opportunity and moments to collaborate on a new plasma instrument.

To my family and friends for their continual support and confidence. Mum, dad, JW, JS and Iris, thank you for your unconditional love and support. No words can express how lucky I am to have you guys through the journey, KS, ZY, CL, YC, YH, KO, CC and Cheng. Trong Tan and Dawn, for being solid support pillars during my most vulnerable moments despite being tens of thousands of kilometres away. Imants, Mari Ángeles, Manuela and Esther, you are always my inspiration. Aman, Cherie and Charm, always being there regardless of the distance between us.

Without all of you here, I will not be where I am today. 能与你们相识，是我的荣幸。





## **Abstract**

One of the most abundant natural polymers on Earth, cellulose-based cotton are among the most widely applied materials, especially as clothing and furniture. Unfortunately, its relative ease of burning poses a great risk to fire. With rapid improvement in living standards, there is a growing demand to comply with the requirements for personal and environmental safety. The challenge therefore remains in search of the safest, most efficient and durable flame retardant for cotton textiles.

Phosphorus has been one of the most extensively studied element, as phosphorylated cellulose undergo a thermal degradation pathway that suppresses depolymerisation and releases less heat. Additional presence of nitrogen can facilitate this process, improving the flame retardant behaviour of cotton textiles (Phosphorus-nitrogen synergism).

For this reason, the main focus of this work is on organophosphorus compounds with nitrogen. To exploit its low toxicity, we also explored the possibility of incorporating silicon into the chemical formula of new flame retardants.

In the literature, a wide variety of investigations can be found using nitrogen-containing organophosphorus compounds as flame retardants to exploit the phosphorus-nitrogen synergism. Commercially, Pyrovatex® or Proban® are used in firefighting suits. However, to render these products durable, high-temperature curing processes using crosslinking or coupling agents are required. This results in the processed textile becoming rigid and inflexible, limiting its application range. Thus, maintaining the physical properties of the cotton textiles has subsequently been part of the requirements on the development of new flame retardants.

The primary objective of this work is to explore via structure-to-property relationships new formulations of flame retardants which are efficient, durable, environmentally benign, and maintain physical properties of cotton textiles. This objective is achieved via chemical synthesis and characterisation of various structurally related compounds, followed by the determination of flammability properties and surface characterisation of the cotton textiles treated with flame retardant compounds.

To study the possibility of incorporation of silicon, two approaches were employed. As the first approach, we co-polymerised organosilicon with organophosphorus monomers using plasma-induced graft polymerisation (PIGP) technique. Another approach is to explore flame retardants containing phosphorus and silicon in their structure. This is inspired from a previous work which reported on an efficient flame retardant, tetrakis(trimethylsilyl) hypophosphate. Using this as the reference, we investigated structurally related compounds, including

phosphate esters and silyl esters of hypophosphates, pyrophosphates, iminodiphosphates, and silylated phosphoramidates. In addition, we investigated as well phosphorohydrazidates, which are related to phosphazenes. The final objective of this study is then to render the FR treated cotton textiles resistant to water rinsing by grafting a protective layer of polymer via PIGP process.

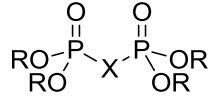
	<b>X</b>	<b>Name</b>	<b>R</b>	<b>Name</b>
	<b>nothing</b>		Hypophosphate	<b>Et</b>
<b>O</b>		Pyrophosphate	<b>SiMe<sub>3</sub></b>	Silyl Ester
<b>NH</b>		Imidodiphosphate		
<b>NH-NH</b>		Phosphorohydrazidate		

Figure I: Names and structures of the investigated compounds as flame retardants on cotton textiles

The first approach in the co-polymerisation of silicon- with phosphorus-based monomers on cotton textiles met with limited improvement in flame retardant efficiency.

In the second approach, investigations indicate significantly superior flame retardant efficiency in textiles treated with phosphate silyl esters relative to those with phosphate esters. This is correlated to their smaller sizes because of desilylation, and easier phosphorylation at room temperature. In addition, it is also possible to combine phosphorus-nitrogen synergism into the silylated system to give the best flame retardant, tetrakis(trimethylsilyl) iminodiphosphate. Further analyses reveal a correlation between the enhancement in flame retardancy of textiles treated with phosphate silyl esters and the partial room temperature phosphorylation of cellulose. By protecting the FR treated textiles with a hydrophobic polymer on the surface, water repellence and rinse resistance is achieved on these textiles.

## **Zusammenfassung**

Baumwolltextilen, die aus Zellulosefasern bestehen, gehören den kommerziell häufigst verwendeten organischen Polymeren der Welt. Die Brennbarkeit der Baumwolltextilen ist aber ein noch zu lösendes Problem. Aufgrund der schnell wachsenden Bevölkerungszahlen und Lebensstandards gewinnt die Nachfrage an persönlicher und ökologischer Sicherheit an Bedeutung. Aus diesem Grund bleibt heutzutage die Herausforderung bestehen, die sichersten, effizientesten und waschfestesten Flammschutzmittel für Baumwolltextilen zu entwickeln.

Phosphor ist das am weitesten untersuchte Element in der Anwendung als Flammschutzmittel für Baumwolltextilen. Während der thermischen Zersetzung der phosphorylierten Zellulose werden Depolymerisation und Wärmefreisetzung reduziert. Die Anwesenheit von Stickstoff in der Verbindung führt zur Verstärkung der Flammschutzeigenschaft.

Daher ist diese Arbeit auf organische Phosphatverbindungen fokussiert, welche auch Stickstoff enthalten. Wegen der geringeren Giftigkeit wurde auch die Möglichkeit erforscht, Silizium in die neuen Flammschutzmittel zu integrieren.

Dank der Synergie zwischen Phosphor und Stickstoff können viele Berichte in der Literatur gefunden werden, in denen Flammschutzmittel aus diesen beiden Elementen untersucht werden. Zur Verbesserung der Dauerhaftigkeit von kommerziellen Flammschutzmitteln, wie zum Beispiel Pyrovatex® und Proban®, werden oft Haftungsverfahren verwendet. Infolgedessen sind diese verarbeiteten Textilien oft starr und weniger bequem. Dies zeigt, dass neue Flammschutzmittel erfunden werden müssen, die die physikalischen Eigenschaften der Textilien möglichst wenig verändern.

Das erste Ziel dieser Dissertation ist es, durch die Struktur-Eigenschaft-Beziehung neuer Flammschutzmitteln zu entwickeln, die sowohl effizient als auch dauerhaft umweltfreundlich sind. Um dieses Ziel zu erreichen, werden neue verwandte chemische Verbindungen synthetisiert, charakterisiert und auf ihre Flammschutzeigenschaften geprüft.

Zur Erforschung der möglichen Flammschutzeigenschaften von Silizium werden zwei Ansätze verfolgt. In dem ersten Ansatz werden Organosilizium und -phosphor Monomere auf der Oberfläche von Baumwolltextilen durch Plasma co-polymerisiert. Inspiriert von einer vorherigen Arbeit werden im anderen Ansatz chemische Verbindungen untersucht, die Phosphor und Silizium enthalten. Verschiedene strukturell verwandte Verbindungen werden erforscht, nämlich Phosphatester und Silylester der Hypophosphate, Diphosphate, Iminodiphosphate und silylierten Phosphoramidate.

Aufgrund der strukturellen Verwandtschaft mit Phosphazenen werden auch Phosphorohydrazidate untersucht. Das letzte Ziel dieser Dissertation ist es, die Flammenschutzmittel enthaltenden Baumwolltextilen mit hydrophoben Monomeren durch Plasmabehandlungen wasserdicht zu machen.

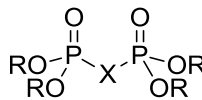
	<b>X</b>	<b>Name</b>	<b>R</b>	<b>Name</b>
		<b>nichts</b>	Hypophosphat	<b>Et</b>
	<b>O</b>	Diphosphat	<b>SiMe<sub>3</sub></b>	Silylester
	<b>NH</b>	Imidodiphosphat		
	<b>NH-NH</b>	Phosphorohydrazidat		

Diagramm: Namen und Strukturen der als Flammenschutzmittel für Baumwolltextilen untersuchten Verbindungen.

Unsere Ergebnisse zeigen beschränkte Verbesserungen der Flammschutzeigenschaften bei Textilien, auf deren Oberflächen Silizium- und Phosphorbasierte Monomere polymerisiert wurden.

Im zweiten Ansatz hingegen werden ausgezeichnete Flammschutzeigenschaften bei Textilien festgestellt, welche mit Silylestern behandelt wurden. Zudem konnte auch gezeigt werden, dass Silylester und der Phosphor-Stickstoff-Synergismus in Iminodiphosphat-silylester kombiniert werden können, um das bisher beste Flammschutzmittel für Baumwolltextilen zu ergeben.

Weitere Untersuchungen zeigen einen Zusammenhang zwischen den hervorragenden Flammschutzeigenschaften der mit Silylestern behandelten Textilien, der teilweisen Desilylierung, der kleinere Molekülgrösse und der Phosphorylierung der Zellulose bei Raumtemperatur. Zuletzt können durch die Polymerisierung von hydrophoben Monomeren die flammgeschützten Textilien wasserdicht und auswaschresistent gemacht werden.

Acknowledgements.....	i
Abstract.....	iii
Zusammenfassung .....	v
Chapter 1 Introduction .....	9
1.1 Fire Statistics and the Need for Flame Retardants.....	10
1.2 Thermal Decomposition of Cellulose .....	11
1.3 The Fire Tetrahedron .....	13
1.4 Gas phase and Condensed Phase Flame Retardants .....	13
1.5 Measurement of Flame Retardant Properties .....	16
1.5.1 Thermogravimetric and Evolved Gas Analysis (TGA-IR-MS).....	16
1.5.2 Limiting Oxygen Index (LOI).....	20
1.5.3 Pyrolysis Combustion Flow Calorimetry (PCFC).....	21
1.6 Imparting Washing Durability.....	22
1.7 Commercially available Phosphorus-based Flame Retardants.....	23
1.8 Research Investigations of New Phosphorus-based Structures as Flame Retardants .....	24
1.8.1 Flame Retardants based on Phosphorus and Nitrogen .....	24
1.8.2 Phosphoramidate Flame Retardant with Wash Durable Properties .....	25
1.8.3 Silicon-based Flame Retardants Applied on Cotton Textiles .....	26
1.9 Objectives and Outline of this Thesis.....	27
Chapter 2 Preliminary Studies: Graft co-polymerisation of DEAE PN and Silicon-containing monomers on Cotton Textiles.....	31
2.1 Introductory Remarks.....	32
2.2 Kinetics of Homopolymerisation <sup>42,43</sup> .....	32
2.3 Plasma Induced Graft Polymerization (PIGP) Process.....	33
2.4 Co-polymerisation of DEAE PN with APTMS .....	34
2.4.1 Flammability Measurements.....	34
2.4.2 Thermal Decomposition and Evolved Gas Analyses .....	38
2.5 Concluding Remarks.....	42
Chapter 3 Synthesis of New Flame Retardant Compounds .....	43
3.1 Introductory Remarks.....	44
3.2 Phosphate Esters.....	44
3.2.1 Tetraethyl Hypophosphate (PP-OEt) .....	44
3.2.2 Tetraethyl Pyrophosphate (POP-OEt).....	46
3.3 Synthesis of Phosphate Silyl Esters .....	47
3.3.1 Tetrakis(trimethylsilyl) Hypophosphate (PP-OTMS) .....	47
3.4 Diethyl Phosphorohydrazidate (PNN-OEt) and N, N'- Bis(diethyl)phosphoryl Hydrazidate (PNNP-OEt).....	49
3.5 Diethyl N-Trimethylsilyl Phosphoramidate (P-NTMS) .....	51
3.7 Concluding Remarks.....	57
Chapter 4 Phosphorus and Silicon - Phosphate Silyl Esters .....	59
4.1 Earlier Investigations on Tetrakis(trimethylsilyl) Hypophosphate .....	60

4.2 The Objective of our investigation in this Chapter .....	62
4.3 Impregnation of Flame Retardants onto Cotton Textiles .....	63
4.4 Flammability Studies of the FR-treated Cotton Textiles.....	64
4.4.1 LOI measurements.....	64
4.4.2 Thermal Decomposition Studies of various compounds on textiles.....	68
4.4.3 Heat Release Studies on the Flame Retardants on Cotton Textiles .....	73
4.5 Surface Analyses of Cotton Textiles treated with Phosphate Silyl Esters .....	78
4.5.1 Surface Morphology and Profiling of Elemental Distribution via EDX Spectroscopy .....	78
4.5.2 Characterization of FR-treated textiles by Solid-state NMR Spectroscopy.....	79
4.5.3 X-Ray Photoelectron Spectroscopy (XPS) Analysis .....	81
4.6 Concluding Remarks.....	86
Chapter 5 Phosphorus, Nitrogen and Silicon: Combination Possible for enhanced FR properties? ...	89
5.1 Introductory Remarks.....	90
5.2 Impregnation of FRs onto cotton textile .....	90
5.3 Flammability of the FR treated cotton textiles (LOI) .....	91
5.4 Thermal Decomposition and Evolved Gas Analyses of the FR-treated cotton textiles .....	93
5.5 Heat Release Analyses of FR-treated cotton textiles .....	95
5.6 Concluding Remarks.....	98
Chapter 6 Phosphorohydrazidates as Flame Retardants on Cotton textiles .....	99
6.1 Introductory Remarks.....	100
6.2 Impregnation of the FR species on cotton textiles.....	100
6.3 Flammability Measurements for FR impregnated cotton textiles with LOI.....	100
6.4 Thermal Decomposition Analysis of Cotton Fabrics Impregnated by PNN-OEt and PNNP-OEt .....	102
6.5 Heat Release Studies of Phosphorohydrazidates on Cotton textiles .....	103
6.6 Concluding Remarks.....	104
Chapter 7 Protection of Phosphate Silyl Ester Treated Cotton Textiles.....	105
7.1 Plasma as a Source of Energy for Polymerization .....	106
7.2 Monomer Impregnation and the Plasma-Induced Graft Polymerization (PIGP) Process .....	106
7.2.1 Impregnation of AC8 monomer on the FR pre-treated textiles.....	107
7.2.2 PIGP Process .....	107
7.2.3 Water Repellence Measurement (Schmerber Pressure) .....	108
7.2.4 Water Rinsing Test.....	110
7.3 Treatment of Cotton Textiles with Atmospheric Pressure Plasma .....	111
7.3.1 Surface Analyses and Flammability Test of the HMDSO-Deposited FR Cotton Textiles .	112
7.3.2 Thermal Degradation and Heat Release Profile of Plasma treated FR textiles .....	114
7.4 Concluding Remarks.....	116
Chapter 8 Conclusions and Outlook.....	117
8.1 Conclusions from this thesis by chapter.....	118
8.2 The Overview.....	119

8.3 Outlook.....	120
Chapter 9 Experimental, Miscellaneous and Appendices .....	123
9.1 Chemicals and Materials.....	124
9.2 Synthesis of Flame Retardant Compounds.....	124
9.2.1 Tetraethyl Hypophosphate (PP-OEt) .....	124
9.2.2 Tetraethyl Pyrophosphate (POP-OEt).....	125
9.2.3 Tetrakis(trimethylsilyl) Pyrophosphate (POP-OTMS) .....	126
9.2.4 Diethyl Phosphorohydrazidate (PNN-OEt) and N, N'- Bis(diethyl)phosphoryl Hydrazidate (PNNP-OEt) <sup>54</sup> .....	126
9.2.5 N-Trimethylsilyl Phosphoramidate (PN-TMS).....	128
9.2.6 Tetrakis(trimethylsilyl) Imidodiphosphate (PNP-OTMS).....	129
9.3 Preparation of Flame Retardant-Impregnated Cotton Textile Sample.....	131
9.4 Plasma Treatment of the Textiles .....	132
9.5 Characterization of Flame Retardancy .....	132
9.6 Characterization Methods for Compounds and Surface Modified Textiles .....	134
Appendix .....	135
Chapter 10 Bibliography .....	137





# Table of Figures

Figure 1.1: Statistics showing deaths per million residents by countries in Europe from 2008 to 2010 based on a bulletin published by World Fire Statistics in 2014 <sup>3</sup> .....	10
Figure 1.2: The thermal decomposition process of cellulose in cotton textile.....	12
Figure 1.3: The Fire Tetrahedron .....	13
Figure 1.4: Thermal decomposition profile (TGA) and its first derivative (DTG) of cotton textile.....	17
Figure 1.5: 3D FTIR spectrum of the decomposition of a cotton textile sample. ....	18
Figure 1.6: FTIR spectrum of evolved gases from the decomposition of cotton textile obtained at 370°C and at 668°C.....	18
Figure 1.7: The intensity of MID signals of $m/z = 18$ ( $H_2O$ ) and $44$ ( $CO_2$ ) with temperature during the pyrolysis of cotton textile (TG in black).....	19
Figure 1.8: A generalized illustration of an LOI measuring instrument.....	20
Figure 1.9: The heat release profile of cotton textile measured at a heating rate of $1\text{ K s}^{-1}$ .....	21
Figure 1.10: Histogram of the frequency of publications containing the keywords ‘phosphorus nitrogen synergism’ based on search results generated from SciFinder. ....	25
Figure 1.11: DEAEPN and the use of a low pressure radio frequency plasma reactor for the PIGP process .....	26
Figure 1.12: A histogram of the search results based on the keywords ‘silicon flame retardant cotton textile fabrics’.....	27
Figure 1.13: The structures of the silicon-containing monomer 3-acryloxypropyltrimethoxysilane (APTMS) and diethyl (2-acryloxyethyl) phosphoramidate (DEAEPN).....	28
Figure 1.14: Phosphorohydrazidate molecules investigated for their FR properties .....	30
Figure 2.1: The structures of DEAEPN (left) and APTMS (right).....	32
Figure 2.2: The kinetics of polymerisation of APTMS, with that of DEAEPN <sup>27,31</sup> shown as a comparison.....	33
Figure 2.3: The structure of photoinitiator BAPO (left) and cross-linking agent EGDA (right).....	34
Figure 2.4: A possible explanation for the better affinity of APTMS on cotton fabrics. ....	37
Figure 2.5: TG curves of untreated cotton textile and textiles with 10 wt% APTMS or DEAEPN.....	38
Figure 2.6: TG curves of untreated textile and textiles treated with co-polymers of DEAEPN and APTMS at various amounts. ....	39
Figure 2.7: FTIR spectra of evolved species obtained at the end of mass loss step during the decomposition of untreated textile, DEAEPN treated textile and poly-DEAEPN.....	40
Figure 2.8: FTIR spectra of evolved species obtained from the end of mass loss step for untreated textiles. APTMS-treated textiles and polymerised APTMS.....	41
Figure 3.1: Structures of various compounds whose syntheses are presented in this chapter.....	44
Figure 3.2: The progress of reaction with proton-coupled <sup>31</sup> P NMR spectroscopy. ....	46
Figure 3.3: The synthesis of <b>POP-OTMS</b> in accordance to Wessjohan et al <sup>53</sup> .....	48
Figure 3.4: The solid state structure of <b>PNNP-OEt</b> .....	50
Figure 3.5: The solid state structure of <b>P-NTMS</b> .....	52
Figure 3.6: The <sup>31</sup> P NMR spectrum of <b>B2</b> in its neat liquid obtained at room temperature. ....	55
Figure 4.1: The decrease in the wt% loading of a cotton sample treated with <b>PP-OTMS</b> after exposure to air.....	60
Figure 4.2: Investigation of two possibilities of origin of the LOI behavior discovered in <b>PP-OTMS</b> on cotton textiles. ....	62
Figure 4.3: Impregnation of FR compounds onto the surface of cotton textiles .....	63
Figure 4.4: The variation of LOI with increasing phosphorus content for cotton textiles treated with <b>PP-OEt</b> and with <b>POP-OEt</b> .....	65
Figure 4.5: The variation of LOI with increasing phosphorus content for cotton textiles treated with <b>PP-OTMS</b> and with <b>POP-OTMS</b> . ....	66
Figure 4.6: The variation of LOI with increasing phosphorus content for cotton textiles treated with <b>P-OTMS</b> and with <b>H<sub>3</sub>PO<sub>4</sub></b> .....	67
Figure 4.7: TGA and DTG curves of <b>PP-OEt</b> , <b>POP-OEt</b> , untreated textiles and textiles impregnated with phosphate esters, <b>PP-OEt</b> and <b>POP-OEt</b> .....	69

Figure 4.8: TGA and DTG curves of <b>PP-OTMS</b> , <b>POP-OTMS</b> , untreated textiles and textiles impregnated with phosphate silyl esters, <b>PP-OTMS</b> and <b>POP-OTMS</b> .....	70
Figure 4.9: TGA and DTG curves of untreated textiles and textiles impregnated with <b>P-OTMS</b> and <b>H<sub>3</sub>PO<sub>4</sub></b> .....	72
Figure 4.10: Heat release profiles of untreated textiles and textiles treated with <b>PP-OEt</b> and <b>POP-OEt</b> .....	73
Figure 4.11: Heat release profiles of untreated textile and textiles treated with <b>PP-OTMS</b> and <b>POP-OTMS</b> .....	74
Figure 4.12: Heat release profiles of untreated textile and textile samples treated with <b>H<sub>3</sub>PO<sub>4</sub></b> and <b>P-OTMS</b> .....	75
Figure 4.13: <b>SEM</b> Images and the corresponding EDX spectra of (i) untreated cotton textile; (ii) cotton textile treated with <b>PP-OTMS</b> .....	78
Figure 4.14: Solid-state CP-MAS (a) <sup>31</sup> P (b) <sup>13</sup> C NMR spectra of textiles treated with <b>P-OTMS</b> at 5% P. The asterisks (*) denote spinning sidebands.....	80
Figure 4.15: XPS Spectra of untreated and cotton fabrics treated with <b>P-OTMS</b> .....	82
Figure 4.16: High-resolution scans of (i) C 1s; (ii) P 2p for <b>P-OTMS</b> treated cotton textiles.....	83
Figure 4.17: Room temperature phosphorylation of the cellulose with the proposed mechanism.....	85
Figure 4.18: The influence of molecular sizes in phosphate ester and 'naked' phosphates (denoted as FR) on the packing density and access to more OH sites for phosphorylation.....	86
Figure 4.19: For phosphorylation to occur, (a) the ester groups in phosphate esters are less easily cleaved, hence requires an additional step with heat before phosphorylation; (b) since desilylation of phosphate silyl ester FRs takes place readily at room temperature facilitating phosphorylation of cellulose to take place.....	87
Figure 5.1: Structure of (from left to right) <b>P-NH<sub>2</sub></b> , <b>P-NTMS</b> , <b>PNP-OEt</b> , <b>PNP-OTMS</b> under investigation in this chapter.....	90
Figure 5.2: Variation of LOI to increasing phosphorus contents for textiles treated with <b>P-NH<sub>2</sub></b> and <b>PN-TMS</b> .....	91
Figure 5.3: The variation of LOI with increasing phosphorus content for cotton textiles treated with <b>PNP-OEt</b> , <b>PNP-OTMS</b> and <b>POP-OTMS</b> .....	92
Figure 5.4: TGA and DTG curves of <b>P-NH<sub>2</sub></b> , <b>PN-TMS</b> , untreated cotton textiles and textiles treated with <b>P-NH<sub>2</sub></b> and <b>P-NTMS</b> .....	93
Figure 5.5: TGA and DTG curves of <b>PNP-OTMS</b> , <b>PNP-OEt</b> and <b>POP-OTMS</b> on cotton textiles.....	94
Figure 5.6: Heat release curves of textiles treated with <b>P-NH<sub>2</sub></b> and <b>P-NTMS</b> .....	95
Figure 5.7: Heat release curves of cotton textiles treated with <b>PNP-OTMS</b> and that with <b>POP-OTMS</b> .....	96
Figure 6.1: Diethyl Phosphorohydrazidate ( <b>PNN-OEt</b> ) and N,N'-bis(diethyl) phosphoryl hydrazidate ( <b>PNNP-OEt</b> ).....	100
Figure 6.2: The variation of LOI with FRs of various phosphorus content on cotton textile.....	101
Figure 6.3: TGA and DTG curves of cotton textile and textiles impregnated with <b>PNN-OEt</b> and <b>PNNP-OEt</b> at 3% P.....	102
Figure 6.4: The HR curves of untreated textile and textiles treated with <b>PNN-OEt</b> and <b>PNNP-OEt</b> .....	103
Figure 7.1: The structure of 1,1,2,2, tetrahydroperfluorodecyl acrylate (AC8) monomer.....	106
Figure 7.2: Repellent properties of poly-AC8 grafted cotton textiles towards water and oil.....	108
Figure 7.3: Schmerber pressures of virgin cotton fabric after plasma treatment under various conditions.....	109
Figure 7.4: The experimental setup of the atmospheric argon plasma coupled with deposition capabilities. (With permission from Dr. Julien Bardon, Luxembourg Institute of Science and Technology, LIST).....	112
Figure 7.5: The SEM micrograph (left bottom) and EDX images with the elemental spectra (right) for control (top right) and coated fabric samples (bottom right).....	113
Figure 7.6: TGA spectra of untreated textile and textiles treated under various conditions.....	114
Figure 7.7: Heat release curves of untreated textile and textile sample treated under various conditions.....	115
Figure 8.1: The chemical structure of a proposed silyl ester derivative of DEAEPN.....	121
Figure 8.2: Cyclic phosphate esters with an oxygen (left) or a nitrogen (right) bridge.....	121

## List of Abbreviations

APTMS	3-Acryloxypropyl Trimethoxysiloxane
BAPO	Bis acyl Phosphine Oxide
CLA	Cross Linking Agent
DCM	Dichloromethane
DEAEPN	Diethyl (2-acryloxyethyl) phosphoramidate
EGDA	Ethylene glycol diacrylate
FR	Flame Retardant
(FT)IR	(Fourier Transformed) Infra-Red
GDP	Gross Domestic Product
LOI	Limiting Oxygen Index
MS	Mass Spectrometry
NMR	Nuclear Magnetic Resonance
PCFC	Pyrolysis Combustion Flow Calorimetry
PI	Photoinitiator
PIGP	Plasma-induced Graft Polymerization
P-OTMS	Tris(trimethylsilyl) Phosphate
PNP-OEt	Tetraethyl Imidodiphosphate
PNP-OTMS	Tetrakis(trimethylsilyl) Imidodiphosphate
PNNP-OEt	N,N'-bis(diethyl) phosphoryl hydrazidate
PNN-OEt	Diethyl phosphorohydrazidate
POP-OEt	Tetraethyl Pyrophosphate
POP-OTMS	Tetrakis(trimethylsilyl) Pyrophosphate
PP-OEt	Tetraethyl Hypophosphate
PP-OTMS	Tetrakis(trimethylsilyl) Hypophosphate
THF	Tetrahydrofuran



# **Chapter 1**

## **Introduction**

## 1.1 Fire Statistics and the Need for Flame Retardants

In a study published by World Fire Statistics<sup>1</sup> in 2014, 38.8% of all fires across the world originated in homes and buildings. Annually, as many as 300 thousand deaths occur globally because of fire related burns<sup>2</sup>. 90% of these fire deaths are attributed to home fires and fires originating from building enclosures<sup>1</sup>. The direct and indirect costs of fire incur up to an overall 1% of the GDP<sup>2</sup> among the developed countries.

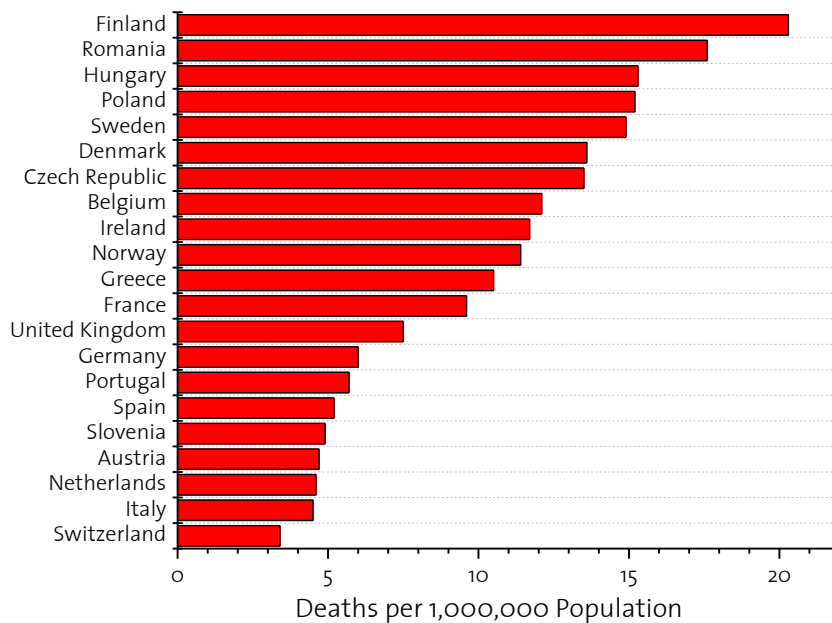


*Figure 1.1: Statistics showing deaths per million residents by countries in Europe from 2008 to 2010 based on a bulletin published by World Fire Statistics in 2014<sup>3</sup>.*

In Europe there are up to 2.5 million annual cases of fire, with up to 25 thousand deaths and 250 thousand injuries<sup>1</sup>. Figure 1.1 shows the number of fire deaths in various countries per 1 million inhabitants, with Finland and Romania reporting the highest number of casualties at 20 and 18 deaths per million residents from 2008 to 2010. Half of the countries listed in this statistics reported more than 10 deaths per million population. In the same period, Switzerland reported 3.5 deaths per 1 million inhabitants, the lowest among the listed countries.

Frequently, these fires are ignited from upholstered furniture, which is common in modern households today. They spread rapidly within enclosures containing textile furniture, especially from vertically hanged curtains at the corners of the room. Despite its widespread and extensive use in various applications as clothing, upholstered furniture and embroidery,

cotton textiles catch fire easily and their high flammability remains a major disadvantage. Therefore, controlling the flammability of this natural fabric is a crucial task. This necessitates flame retardants to inhibit fire propagation through artificial reduction of the flammability of cotton textiles. Before we look into how flame retardants function on these cellulosic fabrics, we need to first understand the decomposition chemistry and kinetics of cellulose, which is the main component of cotton fibres.

## ***1.2 Thermal Decomposition of Cellulose***

In the following Figure 1.2, the various stages and processes in the thermal degradation of cellulose are illustrated. In general, these stages are related to different states of the cellulose polymer at specific temperature ranges. The major processes in the degradation are (i) dehydration, which releases water and (ii) depolymerisation, which originates from the cleavage of glycosidic bonds and releases carbon monoxide or carbon dioxide.

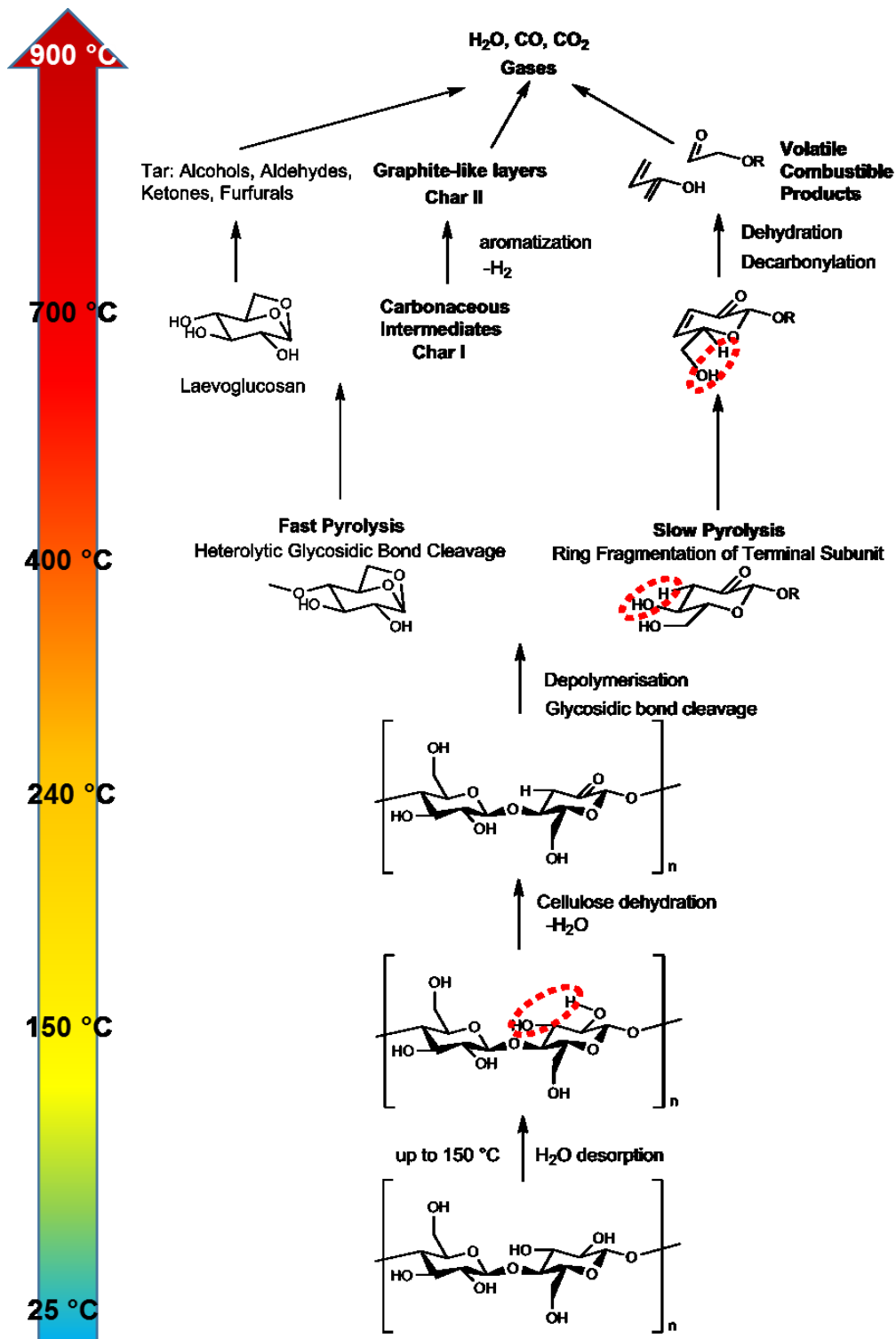


Figure 1.2: The thermal decomposition process of cellulose in cotton textile.

The initial degradation stage involves desorption of surface-physisorbed water, which takes place from ambient temperature to about 150°C. Between 150°C and 240°C, dehydration starts to occur on the subunits of the cellulose chains. From 240°C to 400°C, the



decomposition process is mainly depolymerisation, where glycosidic linkages are cleaved. This is the stage of greatest weight loss into the volatile phase, where the resultant products are dependent on the rate of pyrolysis. While slow pyrolysis promotes ring fragmentation of terminal glycopyranose subunits, heterolytic cleavage of glycosidic bonds predominates in the fast pyrolytic step<sup>4</sup>. This leads to the formation of laevoglucosan<sup>4-9</sup>, an intermediate which precedes further decomposition at higher temperature into flammable tar and simpler organic products. Carbonaceous char are also generated. Increasing the temperature from 700°C then initiates the aromatisation of the char into graphite-like products. Beyond 800°C, further decomposition generates final products of CO, CO<sub>2</sub> and H<sub>2</sub>O.

### **1.3 The Fire Tetrahedron**

In the search for flame retardants for cotton textiles, it is necessary to understand the crucial conditions to sustain combustion processes. These conditions can be illustrated in terms of a fire tetrahedron (Figure 1.3), where three sources, heat, oxygen and fuel, when balanced will induce a chain of chemical reactions responsible for fire propagation. The removal of any of these abovementioned sources will result in the fire being extinguished. Flame retardants function in inhibiting or removing one or more of these conditions to extinguish the fire.

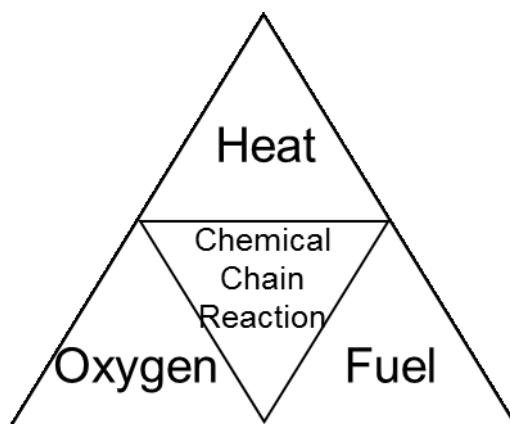
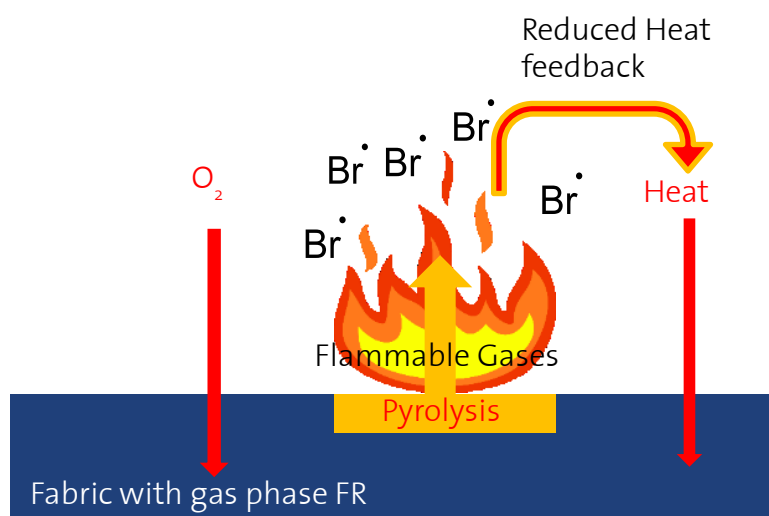


*Figure 1.3: The Fire Tetrahedron*

### **1.4 Gas phase and Condensed Phase Flame Retardants**

To date, two general modes of actions have been identified for flame retardants on cotton textiles. They work either in the gas phase or in the condensed phase.

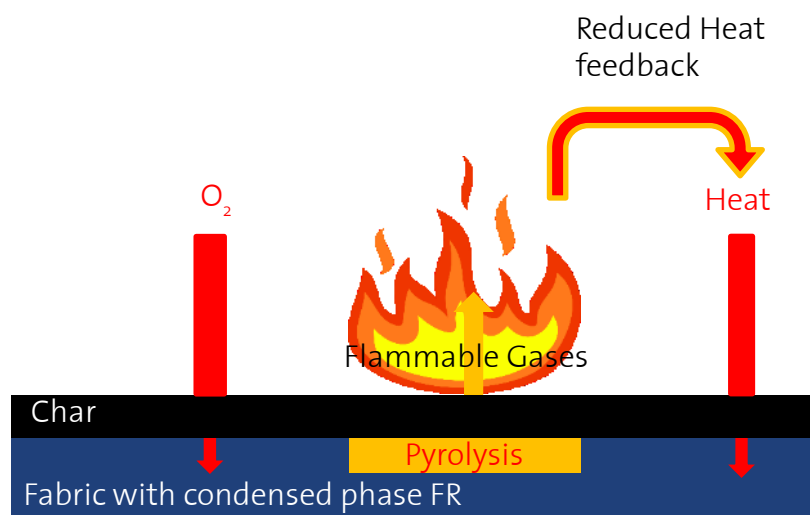
Gas phase flame retardants proceed by releasing radicals into the combustion mixture during thermal decomposition (Scheme 1.1). Acting as scavengers, these radicals then in turn inhibit free radical reactions during combustion by recombination reactions.



*Scheme 1.1: Mode of action of gas phase flame retardants on cotton textiles.*

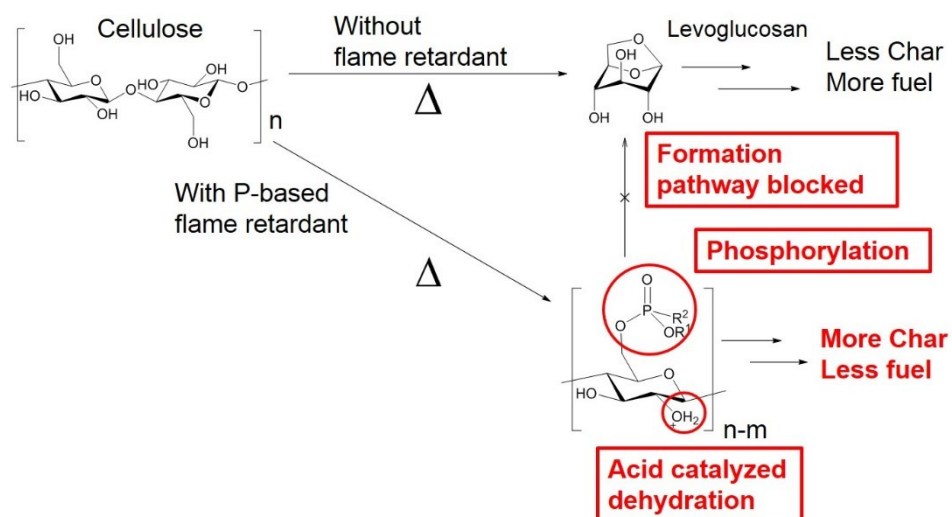
In the past, halogenated flame retardants, for example decabromodiphenyl ether<sup>10</sup> are among the most popular for cotton textiles. They typically contain high amounts of halogens because of their efficiency in acting as radical scavengers during the combustion process. As a result, the exothermic processes are limited, the system cools down and the supply of fuels is suppressed. However, halogenated flame retardants sometime pose greater health risk during fires. Also, the risk they induce to the environment is another great disadvantage that far outweighs their benefits.

On the other hand, condensed phase flame retardants act directly on the substrates by interfering with the thermal decomposition process (Scheme 1.2). Their presence usually promotes the formation of a layer of char and also acid-catalysed dehydration reactions. This layer of char acts as insulator, severely limiting further depolymerisation reactions which would otherwise generate fuels as a feedback into the burning flame.



Scheme 1.2: Mode of action of condensed phase flame retardants on cotton textiles.

Contrary to halogenated flame retardants, phosphorus-based flame retardants are known as condensed phase flame retardants, as they react with the cellulose chain at elevated temperatures via phosphorylation of the C6 primary alcohol functional group<sup>11</sup>. This inhibits the formation pathway towards levoglucosan, a key intermediate resulting from the depolymerisation of cellulose chains, and promotes the formation of char, limiting further depolymerisation to generate fuel as a feedback to the fire (Scheme 1.3).



Scheme 1.3: Phosphorylation as a crucial step in the action of condensed phase flame retardants

Because of their close relation to the chemistry of thermal decomposition of cellulose, our work in this thesis mainly involves phosphorus-based compounds which are mostly condensed phase flame retardants. Understanding the chemistry of this thermal degradation is an important step into search for the chemical formulation of the most efficient flame retardant for cotton textiles.

## **1.5 Measurement of Flame Retardant Properties**

While there has been no consensus of a standardised method of measuring flammability of the substances, there are a number of instruments currently widely used to measure the effectiveness of flame retardants. In this thesis, we rely our investigation on these instruments which allow flammability measurement by Limiting Oxygen Index (LOI), thermal decomposition and evolved gas analysis by TGA-FTIR-MS, and heat release studies by Pyrolysis Combustion Flow Calorimetry (PCFC).

### **1.5.1 Thermogravimetric and Evolved Gas Analysis (TGA-IR-MS)**

This is a hyphenated technique combining three different types of analytical instruments: thermogravimetric analysis (TGA), Fourier-transformed infrared spectroscopy (FTIR) and mass spectrometry (MS).

This technique uses TGA as the principal instrument, with FTIR and MS connected allowing analysis of evolved gases. Samples of about 2 mg are typically placed onto a crucible and heated at a specific heating rate (e.g. 10 K min<sup>-1</sup>) under an argon flow of 50 ml min<sup>-1</sup>. During pyrolysis, the residual mass of sample on the crucible is monitored, while evolved gases and volatiles are transported through transfer lines onto FTIR and mass spectrometers, where the respective vibrational modes and mass-to-charge ratios of the evolved species could be identified.

TGA measures the net change in the sample mass, and it reflects the sum of all reactions taking place during pyrolysis. Thermal decomposition curve are expressed as percentage of original weight against the time or temperature. Important TGA parameters include the onset decomposition temperature ( $T_{onset}$ ) and the mass loss in percent.

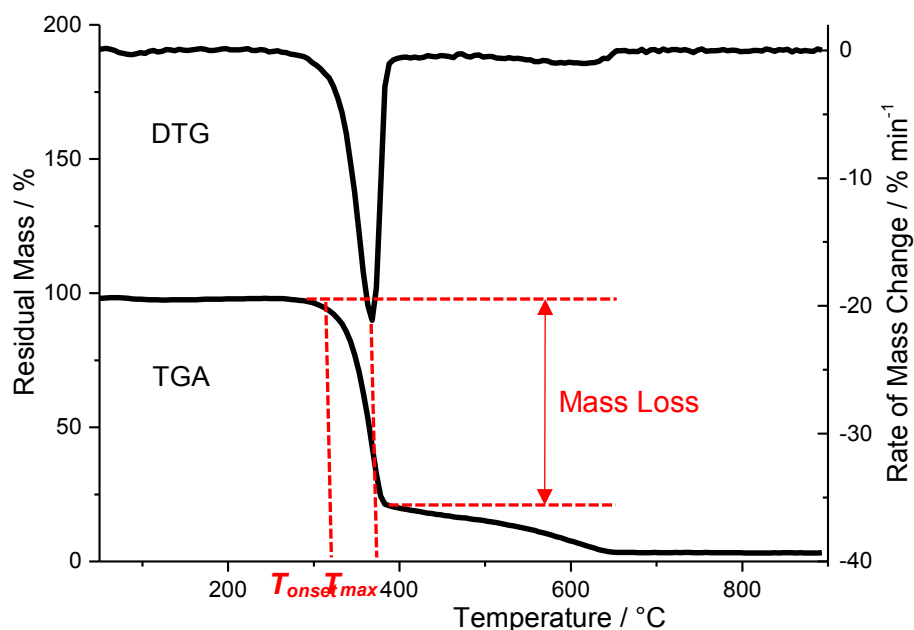


Figure 1.4: Thermal decomposition profile (TGA) and its first derivative (DTG) of cotton textile.

The TG curve of cotton textile (Figure 1.4) contains two major mass loss steps. The first step sees a larger mass loss (75%) between 345°C and 397°C, while the second step consists of a smaller mass loss step (15%) over a wider temperature range (397°C – 655°C).

The important parameters and their corresponding values for cotton textile samples are summarized in the following Table 1.1:

	Step 1	Step 2
$T_{onset} / ^\circ\text{C}$	344.7	556.4
<b>Mass Loss / %</b>	78.8	13.6
$T_{max} / ^\circ\text{C}$	368.8	621
<b>Residue at 900 °C, <math>\mu</math> / %</b>		3.2

Table 1.1: Important TGA parameters and their corresponding values for cotton textiles

Evolved from the pyrolysis process, volatile species are transported through a transfer line to the detector for FTIR spectrometer, which detects the absorption from various vibrational modes of the volatile species. The following Figure 1.5 illustrates the FTIR spectrum obtained from the evolved gas analysis of pyrolysis products from cotton textile decomposition. This is a 3-dimensional spectrum with wavenumber, absorbance and temperature at the respective x, y and z-axes.

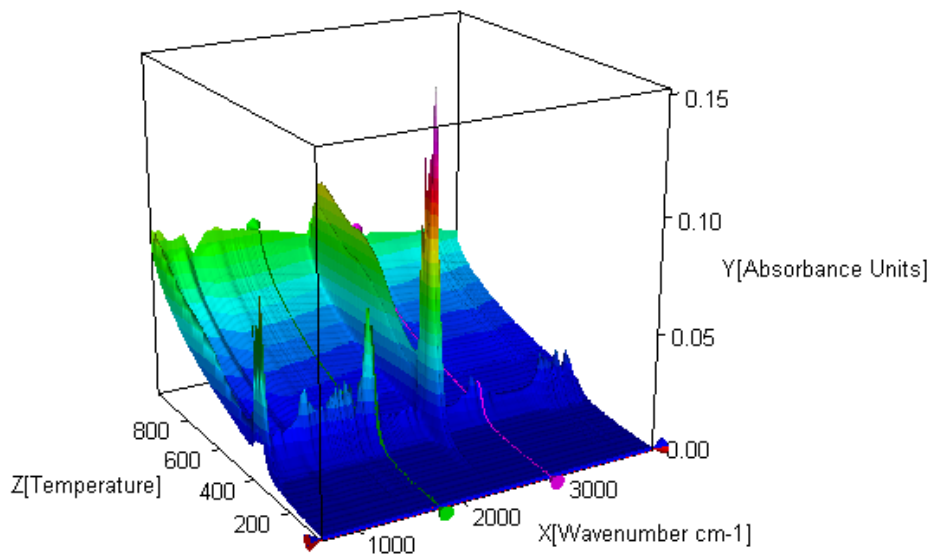


Figure 1.5: 3D FTIR spectrum of the decomposition of a cotton textile sample.

In addition, individual spectra at different temperatures could be extracted and presented for further analysis of various stages of the decomposition. In this case, the FTIR spectra of the volatile products obtained at 370°C and 668°C are presented in the following Figure 1.6.

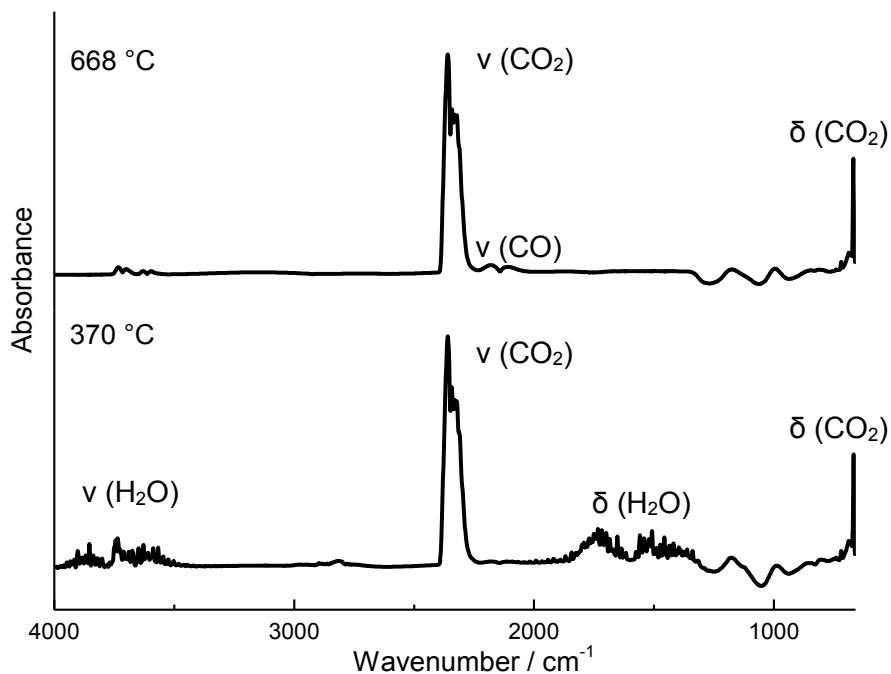


Figure 1.6: FTIR spectrum of evolved gases from the decomposition of cotton textile obtained at 370°C and at 668°C.

Assignments of the detected absorptions are summarized in the following Table 1.2.

Wavenumber / $\text{cm}^{-1}$	Type of Absorption	Assignment
4000 – 3000	Broad, medium	$\nu$ (H–O–H), water
2990	Medium	$\nu$ ( $\text{sp}^3$ C–H), organic products
2300	Sharp, intense	$\nu$ (O–C–O), carbon dioxide
2100 – 2000	Broad, weak	$\nu$ (C–O), carbon monoxide
1800 – 1300	Broad, medium	$\delta$ (H–O–H), water
668	Sharp, medium	$\delta$ (O–C–O), carbon dioxide

Table 1.2: Absorptions detected in the gases evolved from the pyrolysis of cotton textile.

Another hyphenated technique, mass spectrometry (MS) provides the mass-to-charge ratios of evolved species from the decomposition process. In the following spectra in Figure 1.7, we can see how the multi-ion detection (MID) currents for  $m/z$  18 (water) and 44 (carbon dioxide) vary with increasing temperature.

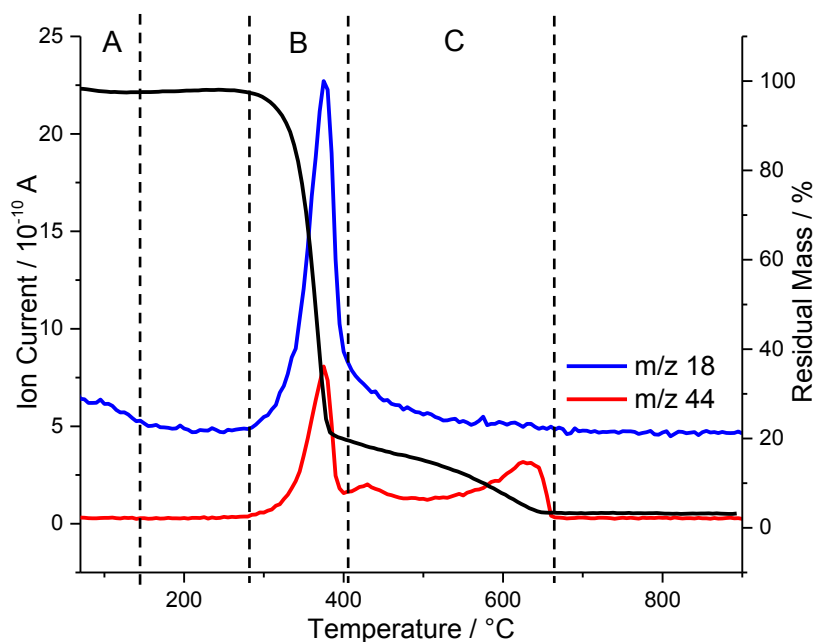


Figure 1.7: The intensity of MID signals of  $m/z = 18$  ( $\text{H}_2\text{O}$ ) and 44 ( $\text{CO}_2$ ) with temperature during the pyrolysis of cotton textile (TG in black).

In summary, a small bump in the MID signal of water ( $m/z$  18) occurs between  $80^\circ\text{C}$  and  $105^\circ\text{C}$  (A). This is attributed to desorption of water from the surface of textiles. Between  $245^\circ\text{C}$  and  $405^\circ\text{C}$  is a fast mass loss step (B), during which maxima in the ion current signals for both water ( $m/z$  18) and carbon dioxide ( $m/z$  44) are detected. This indicates that depolymerisation and combustion are dominant during this mass loss. In the following mass loss step (C)

between 405°C and 655°C, two smaller maxima are observed in the ion current of carbon dioxide at 415°C and 650°C. In contrast, the ion current for water remains relatively low. This shows that decarbonylation occurs mainly during this phase. From the MID curves one could trace, through its mass-to-charge ratio ( $m/z$ ), how the evolution of each product changes through the course of the thermal decomposition process. This gives further information about the process taking place during the mass loss step of a substance.

### **1.5.2 Limiting Oxygen Index (LOI)**

LOI is one of the earliest established methods of measuring flammability<sup>12</sup>. Typically, a sample of 5 cm x 10 cm dimension is fixed in a gas chamber, through which a mixture of nitrogen and oxygen gases in adjustable volumes are introduced. The sample is then subjected to a candle-like burning from the top (Figure 1.8). According to the ASTM D-2563<sup>13</sup>, LOI is defined as minimum amount of oxygen required to sustain the longitudinal burning of the sample from the top to the bottom (candle-like combustion). The LOI value of a cotton textile sample is **17.5 ± 0.2**. LOI gives a good first indication of flammability because it is a fast and easy method of measurement.

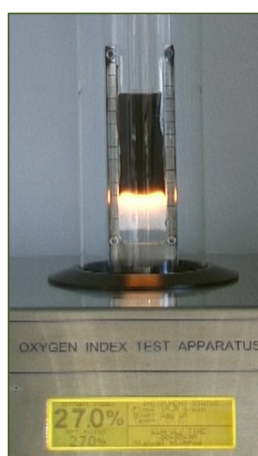


*Figure 1.8: A generalized illustration of an LOI measuring instrument.*



### 1.5.3 Pyrolysis Combustion Flow Calorimetry (PCFC)

The pyrolysis combustion flow calorimetry (PCFC) is a relatively new instrument for the measurement of flame retardant properties, being developed only in 1990s<sup>14</sup>. Owing to the small sample size in microgram scale, this technique is sometimes also called Microscale Combustion Calorimetry (MCC). For consistency, we refer this technique throughout this thesis as PCFC.

A typical setup of a PCFC instrument consists of a piston which holds the sample placed on a crucible<sup>15</sup>. The loaded piston is then placed into the pyrolyser, which is controlled by a temperature programme. Typically, a sample of about 2 mg is weighed, placed on an alumina crucible, and heated at a rate of  $1 \text{ K s}^{-1}$ . During pyrolysis, the products undergo combustion in the combustion chamber. The amount of oxygen consumed in this process is measured. The rate of heat release at a given temperature is calculated from the amount of oxygen consumed during combustion using the principle of oxygen consumption calorimetry<sup>16</sup>, where 13.1 MJ is released per kilogram of oxygen consumed during combustion.

The heat release profile is expressed in the heat release rate (HRR) against temperature, as shown in Figure 1.9.

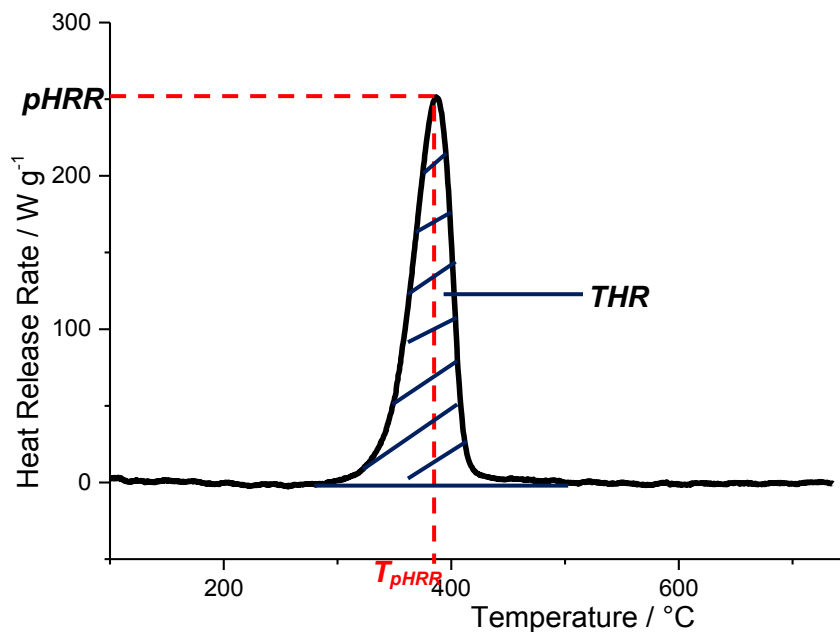


Figure 1.9: The heat release profile of cotton textile measured at a heating rate of  $1 \text{ K s}^{-1}$ .

The area under the HRR curve gives the total amount of heat released (THR) in the combustion of pyrolysis products from a sample of given mass. A reduction of THR values is

characteristic of the presence of flame retardants. The ratio of **THR** to the heating rate gives the Heat Release Capacity (**HRC**), which is an intrinsic property of a given substrate (with or without flame retardant). Self-extinguishing materials typically exhibit **HRC** values below 100 kJ K<sup>-1</sup> g<sup>-1</sup>. Besides that, the temperature at maximum heat release, or **T<sub>pHRR</sub>**, is often reduced in the presence of flame retardants, accompanying the reduction in **THR**.

Parameter / Unit	Value
THR / kJ g <sup>-1</sup>	10.9 ± 0.1
HRC / kJ K <sup>-1</sup> g <sup>-1</sup>	254 ± 3
T <sub>pHRR</sub> / °C	394 ± 3

Table 1.3: Important parameters of PCFC and the corresponding values for cotton textiles.

## 1.6 Imparting Washing Durability

One of the most important requirement of flame retardants after their application on cotton textiles is their resistance to washing, since such cotton textiles will often be subjected to repeated laundering processes. The leaching of phosphorus-based flame retardants are of particular concern<sup>17</sup> because most importantly, this directly leads to the loss of flame retardant properties of the textiles. Besides that, leaching is also a source of pollutant to the environment. Schreder *et al* in an article published by 2014<sup>17</sup> quantified and highlighted the seriousness of the consequences of leaching of flame retardants from the textiles, which not only pollutes the environment, but are also potential health hazards should they undergo bioaccumulation.

Therefore, the flame retardant molecules should ideally be chemically reacted, or grafted to the surface of the cotton textiles to prevent them from being washed away during the laundering processes. These processes can be achieved using methods such as esterification, etherification or graft-polymerisation reactions. Esterification and etherification involves chemical introduction of additional functional groups to make cellulose esters, nitrates<sup>18</sup>, acetates or methyl cellulose. However, this method requires treatment of textiles with sulphuric or acetic acids<sup>19</sup>, which often leads to a change in physical properties of the modified cellulose. Other modifications include the formation of cross-linked or resinification products by reacting bi- or polyfunctional groups to the cellulose chains<sup>20</sup>. These methods are reported to bring structural stability and crease resistance to the cellulose matrix<sup>21</sup>.

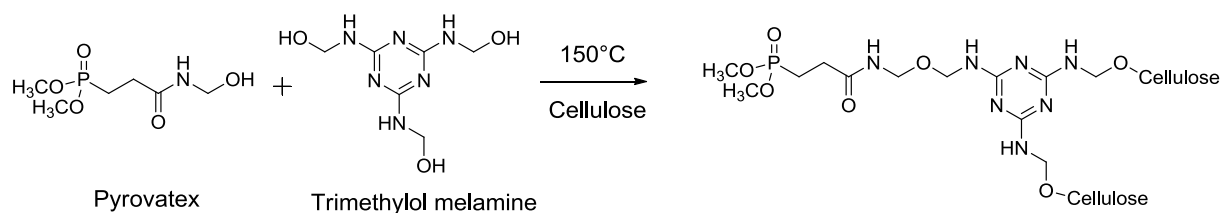
On the other hand, graft-polymerisation reactions<sup>19,22</sup> involves the simultaneous polymerisation of a monomer and the formation of a bond between the chain and the surface of cotton. This can be achieved by either "grafting-from", "grafting-through" or "grafting-to"

methods<sup>19,23</sup>. The “grafting-from” method involves the formation of polymer chains from initiation sites on the cotton textiles. The “grafting-through” approach involves the copolymerisation of a cellulose macromonomer and a low molecular weight co-monomer. In the “grafting-to” method, the active end-functional groups of pre-formed polymer chains are coupled with the functional groups on the cellulose backbone. Because of its advantage of direct access to the reactive groups of cellulose backbone, the “grafting-from” approach is the more widely applied method. Overall, these processes involve either radical or chain transfer polymerisation reactions to achieve the grafting. Although the conditions for these approaches are challenging to control, it is possible to employ this technique under mild conditions to preserve the physical properties of the textiles.

## 1.7 Commercially available Phosphorus-based Flame Retardants

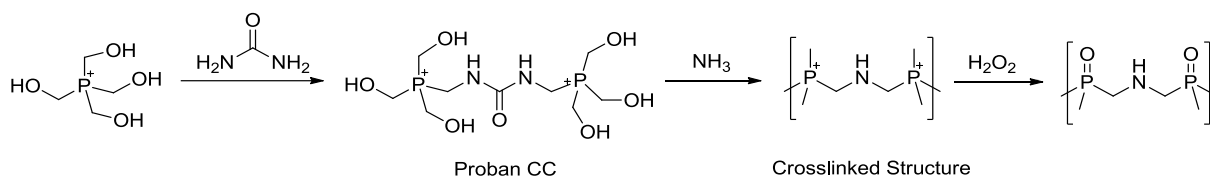
Currently, there are commercially available flame retardants<sup>24</sup> for application on cotton textiles. Among the most widely used examples include Pyrovatex® and Proban®.

Pyrovatex® (Huntsman, formerly Ciba), is a phosphonate molecule that contains a phosphate centre and a nitrogen atom in the form of an amide bond (Scheme 1.4). Currently, Pyrovatex® is widely used as the fire resistant clothing for the fire fighters. However, a crosslinking agent at 20% to 25% to the weight of textile, together a high temperature curing step at 150°C for 5 minutes, is necessary to confer washing durability on cotton textiles. As a result of this process, the tear strength in particular is severely compromised after such treatment<sup>15</sup>.



*Scheme 1.4: Treatment of Cellulose with Pyrovatex®, using trimethylol melamine as the crosslinking agent.*

The second product, Proban® exists initially as a monomer, which then with urea forms an insoluble polymer supported on cotton textile<sup>25</sup>. In this case, the required treatment steps involve using corrosive ammonia and hydrogen peroxide, an oxidizing agent.



*Scheme 1.5: Treatment of cellulose with Proban®*

As the treatment often involve using very high loading (25 wt% phosphorus-based precursor and 15 wt% urea), Proban®-processed textiles are often stiff and softeners, typically at 5 g/L, also have to be used as a post-treatment step<sup>25</sup>. Besides, the treated textiles also typically contain undesired formaldehyde, a known carcinogen, hence posing particular danger to the health of the industrial workers.

For these reasons, both Pyrovatex® and Proban® are not recommended for use on furniture textiles<sup>25</sup>, and the search for a more robust and durable flame retardants remains.

## **1.8 Research Investigations of New Phosphorus-based Structures as Flame Retardants**

### **1.8.1 Flame Retardants based on Phosphorus and Nitrogen**

For application on cotton textiles, the enhancement of nitrogen on the performance of phosphorus-based flame retardants (phosphorus-nitrogen synergism) is a well-known effect which has been extensively studied in the literature over the decades<sup>26–29</sup>. A search on the keywords ‘phosphorus nitrogen flame retardant cotton textiles’ returned 500 publications since 1965 (Figure 1.10), with the highest number of articles published in 2015.

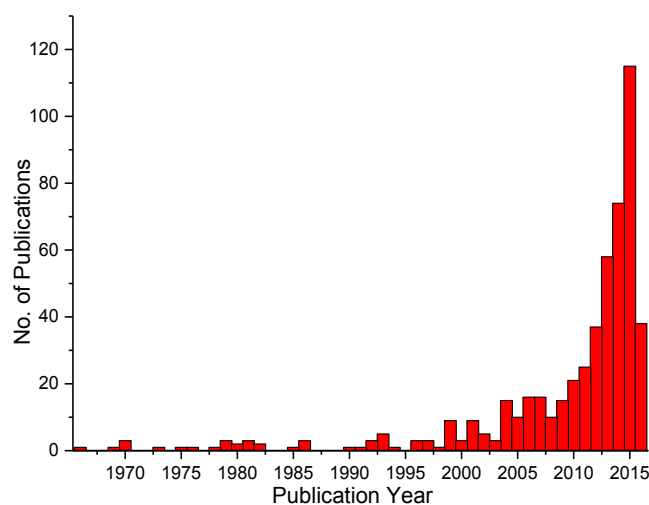


Figure 1.10: Histogram of the frequency of publications containing the keywords 'phosphorus nitrogen synergism' based on search results generated from SciFinder.

Nitrogen can either be incorporated into the molecular structure or as another molecule in a mixture with phosphorus-based compounds. Examples for the former includes alkyl phosphoric triamides<sup>26</sup>, phosphoramidates<sup>29–31</sup> and the commercial Pyrovatex® and Proban®<sup>25</sup>. Examples of mixtures that have been reported in the literature include phosphoric acid derivatives in combination with urea or melamine, or their derivatives<sup>26</sup>. All of these systems have demonstrated that the phosphorus-based flame retardants are significantly enhanced in the presence of nitrogen.

### 1.8.2 Phosphoramidate Flame Retardant with Wash Durable Properties

Studies from former members of our group, such as Ruffin<sup>32</sup>, Tsafack<sup>27,31</sup>, Prinz<sup>6</sup> and Salimova<sup>5</sup> involved phosphoramidate compounds. Salimova<sup>5</sup> reported that phosphoramidates display excellent flame retardant properties because of their ability to interact with the cotton textile surface owing to their basic nature. In particular, phosphoramidates with primary and secondary amine groups are expected to exhibit good flame retardant properties because their polarity facilitates interaction with the surface of cotton textiles. Combining flame retardancy and washing durability, Tsafack<sup>31</sup> first reported a wash durable phosphoramidate flame retardant with the synthesis and application of diethyl (2-acryloxyethyl) phosphoramidate (DEAEPN) (Figure 1.11) on cotton textile.

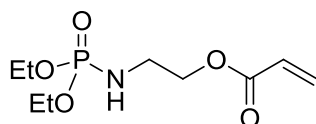
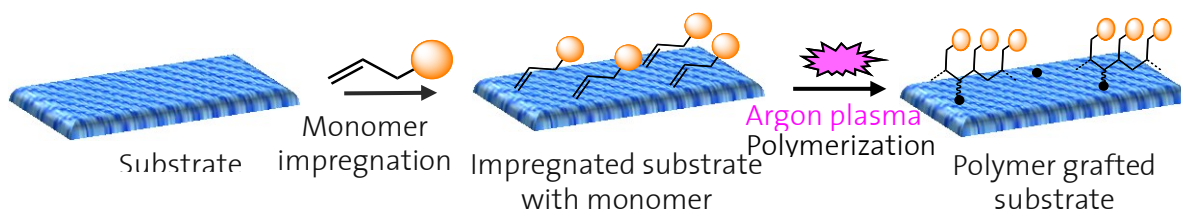


Figure 1.11: DEAEPN and the use of a low pressure radio frequency plasma reactor for the PIGP process

The acrylate functional group of the molecule allows polymerisation and surface grafting to take place through the plasma-induced graft polymerisation (PIGP) process (Scheme 1.6)<sup>31</sup>. This technique exploits low pressure argon plasma generated under room temperature as an energy source to not only activate the surface of cotton textiles by generating high energy radicals<sup>31</sup>, but also simultaneously induce polymerisation of the monomers. The resulting polymers would be grafted onto the surface, conferring chemical resistance towards laundering.



Scheme 1.6: A schematic diagram of the PIGP process

In the presence of cross-linking<sup>5,31,33</sup> and coupling agents<sup>6</sup>, the yield of grafting can also be enhanced. This has been studied in depth by Prinz and the results thereof are reported in her thesis<sup>6</sup>.

### 1.8.3 Silicon-based Flame Retardants Applied on Cotton Textiles

Recently, there is a growing interest on silicon-containing compounds for application as flame retardants. Relative to phosphorus and nitrogen-based flame retardants, silicon-containing flame retardants are less extensively studied, but are recently receiving increasing attention in the literature. A search on the keywords 'silicon flame retardant cotton textile fabric' returned

a total of 26 publications (Figure 1.12), from which there are only a total of 10 reports being published from 2012 to 2016.

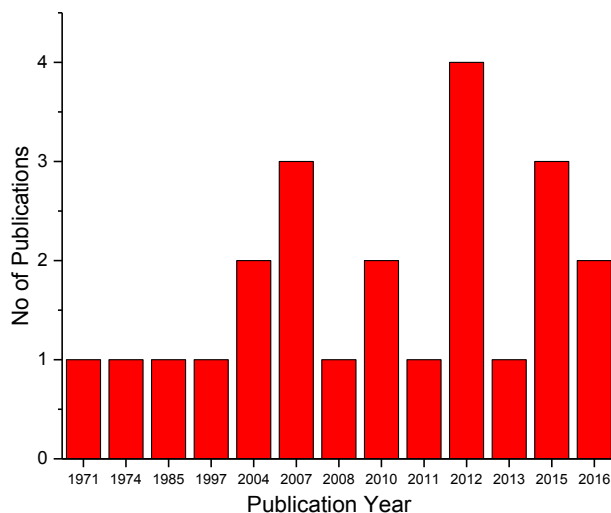


Figure 1.12: A histogram of the search results based on the keywords 'silicon flame retardant cotton textile fabrics'

Even then, the focus on purely silicon-based compounds as flame retardants is relatively limited. Instead, most of these publications report on attempts to combine silicon and phosphorus-based flame retardants. This is achieved by either co-polymerisation of phosphorus and silicon-based monomers<sup>24,34–36</sup>, or by doping phosphorus and nitrogen based compounds onto silica generating precursors<sup>36</sup>. In these reports, the authors claim that they have succeeded in the combination because of the higher char yields obtained, however the exact way in which the silicon-containing compounds interfere with the thermal decomposition of the substrate remains unclear.

## 1.9 Objectives and Outline of this Thesis

Alongi *et al*<sup>4</sup> listed the following desired properties suggested by Horrocks<sup>10</sup> of an ideal flame retardant, other than excellent flame retardant properties, for application on cotton textiles:

1. They should be easily applied onto cotton textile.
2. No formaldehyde should be released in the process of application.
3. They should be relatively cheap to produce.
4. They should possess low biological and environmental toxicity.

The main objective of this thesis is to explore the possibility of including silicon to enhance the

flame retardant properties of cotton textile alongside phosphorus and nitrogen. To achieve this objective, two possible strategies can be employed.

The first strategy involves the simultaneous graft polymerisation of a physical mixture of phosphoramidate and silicon-containing monomers on cotton textiles (Figure 1.13).

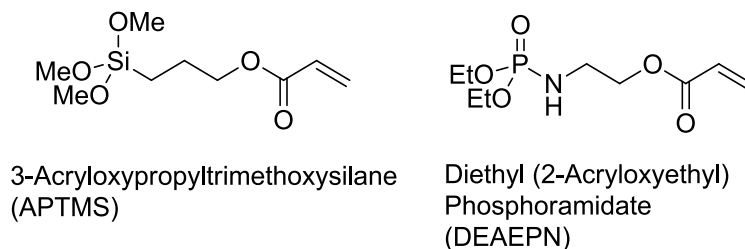
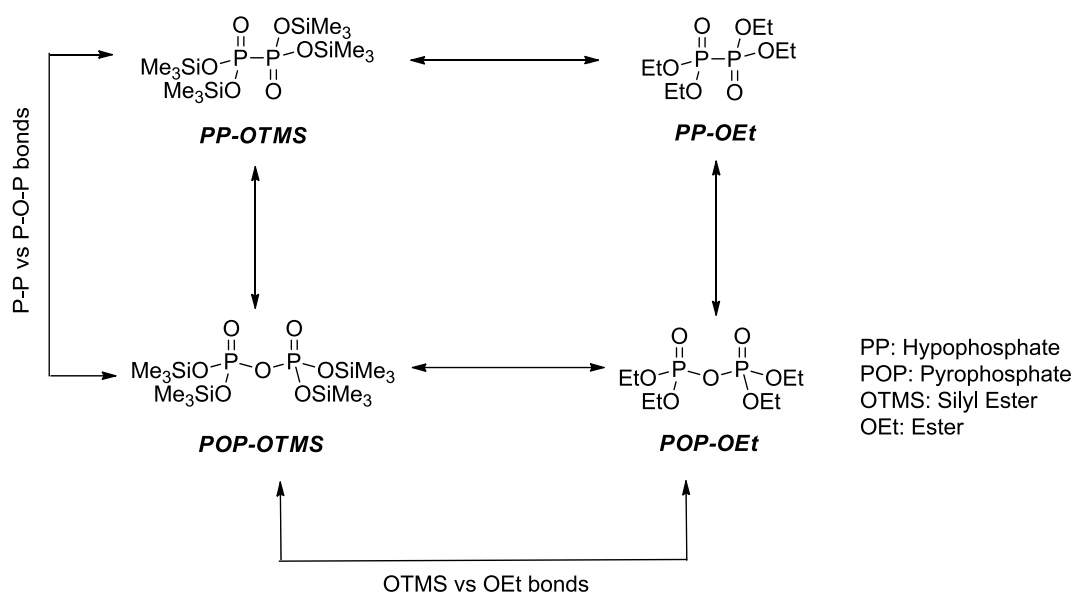


Figure 1.13: The structures of the silicon-containing monomer 3-acryloxypropyltrimethoxysilane (APTMS) and diethyl (2-acryloxyethyl) phosphoramidate (DEAEPN).

Similar to the studies published in the literature involving silica-generating reactions doped with phosphorus-based flame retardants and nitrogen compounds, this is considered as a preliminary study and the results are presented in Chapter Two. The chemical synthesis of all new compounds relevant to our studies in this thesis are reported and discussed in Chapter Three.

An alternative strategy involves the incorporation of silicon into the chemical formulae of the flame retardant compounds. In this aspect, the easiest way is to convert the phosphate ester side chains via silylation to phosphate silyl ester. Previously, Ruflin<sup>32,37</sup> reported the synthesis of hypophosphate silyl ester using an alternative route. Applied on cotton textiles, this compound displayed excellent flame retardant properties, exceeding even that of best phosphoramidate-based flame retardants we developed on the same phosphorus loading. Here, we are interested to determine if the enhancement of the flame retardant properties has a correlation to (i) a modified phosphorus centre through the formation of a phosphorus-phosphorus bond, or (ii) silylation of phosphate ester into phosphate silyl ester. To verify these hypotheses, we conduct a structure-to-property investigation by the synthesis and characterisation of structurally related compounds, including those depicted in Scheme 1.7. The detailed results are described and discussed in Chapter Four.

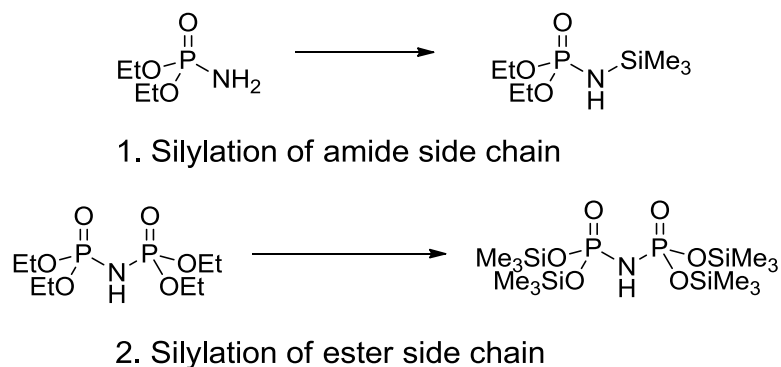




Scheme 1.7: An illustration of structurally related compounds to tetrakis(trimethylsilyl) hypophosphate.

Chapter Five describes our results in the exploration of the possibility to combine both effects of including silyl ester and the phosphorus-nitrogen cooperativity on the flame retardant properties. This could be achieved via two ways, either by the silylation of the amide side chain or the phosphate ester into phosphate silyl ester.

Similar to that in Chapter Four, we then also investigated the structure to property relationship of each of these compounds.



Scheme 1.8: Illustration of the two possibilities of achieving an enhancement of phosphorus-based flame retardants with nitrogen and silicon.

In particular, tetrakis(trimethylsilyl) imidodiphosphate (depicted in Scheme 1.8 above) and its subsequent comparison to the oxygen-bridging analogue, tetrakis(trimethylsilyl) diphosphate, will shed a light on the possibility of a combination of both effects. In addition to this, its properties will also be compared with recently published studies by Wang *et al*<sup>88</sup> and Przybylak *et al*<sup>89</sup>. In their investigations, the former have attempted to modify the cotton textiles with organosilicon-functionalized cyclotriphosphazene, while the latter similarly treated the textiles with phosphorus-based flame retardant compounds.

Polyphosphazenes are well known to exhibit excellent flame retardant properties<sup>40</sup>. Mayer-Gall *et al*<sup>41</sup> in 2015 described their successful synthesis of a permanent flame retardant finishing of textiles with allyl-functionalized polyphosphazenes on cotton textiles, achieving LOI values of 26.7 at 3.6 wt% of P-content on the weight of the textile. Structurally related to phosphazenes, phosphorohydrazidates have to date not been tested for their flame retardant properties. It is therefore in our interest to find out if phosphorohydrazidates will also perform as flame retardants. In Chapter Six, we report our study into the flame retardant properties of two phosphorohydrazidate derivatives (Figure 1.14) on cotton textiles.

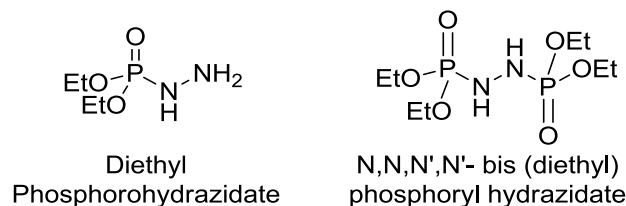


Figure 1.14: Phosphorohydrazidate molecules investigated for their FR properties

While the main focus of this thesis is on the study of structure-to-property relationship of flame retardants on cotton textiles, most of the compounds other than the two monomers, DEAEPN and APTMS, will not be durable to washing processes. Therefore washing durability has to be addressed. To this end, we aim to protect these FR treated textiles from water by grafting and polymerisation of a fluorine-rich hydrophobic monomer on the surface of cotton textile through the PIGP process. As a model compound, we use the commercially available tris(trimethylsilyl) phosphate as flame retardant to study the consequences of having a perfluorinated polymer on the surface of the FR pre-treated cotton textile. The results of this study are detailed in Chapter Seven.

In summary, the content of this thesis is organised into the following chapters:

<b>Chapter</b>	<b>Topic</b>
<b>Two</b>	Preliminary Studies: Co-polymerisation of P and Si containing monomer
<b>Three</b>	Synthesis of New Flame Retardant Compounds
<b>Four</b>	The FR Properties of Phosphate Silyl Esters and Phosphate Esters
<b>Five</b>	Phosphorus, Nitrogen and Silicon: Combination Possible on the FR Property?
<b>Six</b>	Phosphorohydrazidates as Flame Retardants
<b>Seven</b>	Plasma Treatment of Textiles Pre-Treated with Flame Retardants
<b>Eight</b>	Conclusions and Outlook
<b>Nine</b>	Experimental, Miscellaneous and Appendices
<b>Ten</b>	Bibliography

Table 1.4: A summary of the chapters in this thesis and their corresponding topics.

## **Chapter 2**

### **Preliminary Studies: Graft co-polymerization of DEAEPN and Silicon-containing monomers on Cotton Textiles**

## 2.1 Introductory Remarks

This chapter describes our investigation at combining phosphorus, nitrogen and silicon via the co-polymerisation of diethyl (2-acryloxyethyl) phosphoramidate (DEAEPN) and silicon-containing monomers.

In this study, we used 3-acryloxypropyl trimethoxysilane (APTMS) as the silicon-containing monomer, which is commercially available.



Figure 2.1: The structures of DEAEPN (left) and APTMS (right)

## 2.2 Kinetics of Homopolymerisation<sup>42,43</sup>

Before conducting co-polymerisation experiments, it is necessary to determine the susceptibility of each of the monomers, namely APTMS and DEAEPN, towards free-radical polymerisation induced by the plasma process. By means of Ar plasma and bis-acylphosphine oxide (BAPO) as the photoinitiator at 5% to the weight of APTMS, the kinetics of polymerisation of APTMS was determined and compared with that of DEAEPN<sup>33</sup>. Ar plasma induced polymerisation is performed at different times varying from 5 to 20 minutes at an interval of 5 minutes. The conversion is analysed by <sup>1</sup>H NMR spectroscopy. The remaining monomer is extracted with a defined amount of CDCl<sub>3</sub> as the polymer is insoluble in the same solvent. The amount of monomer is analysed via NMR in the presence of a capillary filled with decamethylpentasiloxane as the internal standard. From the ratio of the integral of the internal standard and that of the methylene groups in the remaining monomer, the relative concentrations of monomers after different treatment times can be determined.

Figure 2.2 depicts the relative amount of respective monomers remaining after a stipulated treatment time under argon plasma.

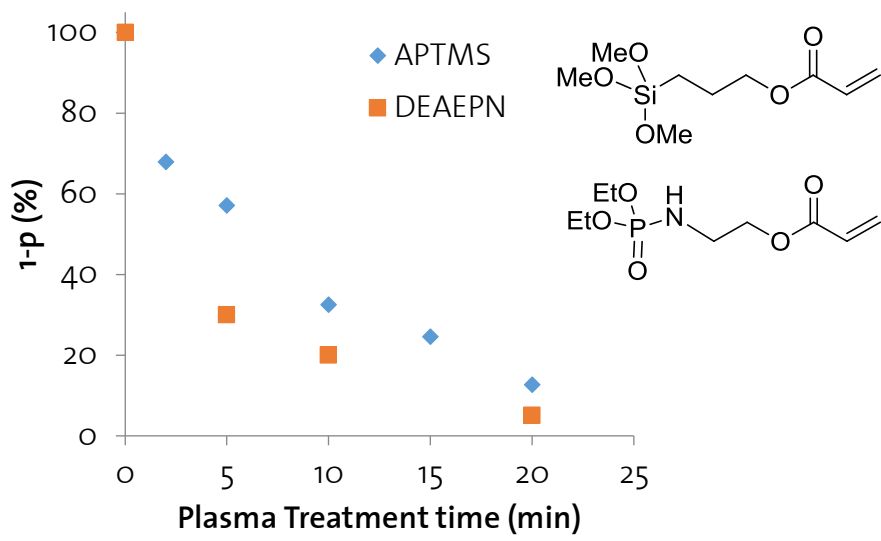


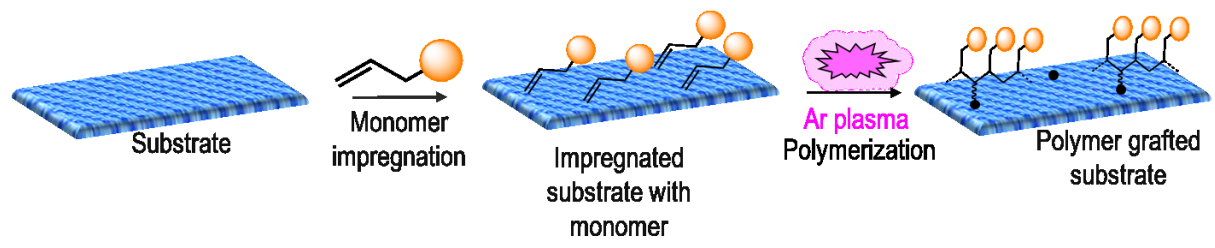
Figure 2.2: The kinetics of polymerisation of APTMS, with that of DEAEPN<sup>27,31</sup> shown as a comparison.

Compared to DEAEPN, we could observe a slower conversion rate for APTMS under the same conditions of plasma treatment. After 5 minutes of plasma treatment, only 30% DEAEPN is left as monomer, while almost 60% of APTMS remains unreacted. At 20 minutes of plasma treatment, almost all DEAEPN monomer is converted into polyDEAEPN. However, 10% of APTMS still remain as monomers.

Although APTMS displays a slower kinetics of homopolymerisation, its conversion rate is still comparable to that of DEAEPN. For this reason, we proceed to co-polymerise APTMS with DEAEPN in the presence of photoinitiators and cross-linking agents to form a network of polymer chains with improved grafting on cotton textile.

### 2.3 Plasma Induced Graft Polymerization (PIGP) Process

After the investigation of the kinetics of polymerization, we proceed with the grafting and polymerization of the respective monomers on the surface of cotton textiles using the PIGP process. This method has been illustrated in Scheme 2.1.



Scheme 2.1: Grafting monomers on the surface of textiles using PIGP Process, using a low pressure and low temperature argon plasma

The PIGP process for cotton textiles<sup>6,22,31</sup> involves the following steps:

1. Impregnation of the monomer on the cotton textile surface

In this step, the monomer (amount varied between 5% and 20% to the weight of textile) is typically dissolved in a volatile organic solution containing a photoinitiator (PI) (5% to the weight of the monomer) and a cross-linking agent (CLA) (10% to the weight of the monomer). Since the flammability of the FR-treated textile is directly related to the phosphorus content, and the indicator of good flame retardancy is usually set at LOI of 26 at 3% P on the cotton textiles<sup>44</sup>, the FR monomer is usually added up to 20% to the weight of textile. To understand the effect of relative concentrations of APTMS and DEAEPN to the flammability in this study, we also varied the relative amount of APTMS and DEAEPN based on the ratio of phosphorus to silicon. The photoinitiator, as the name suggests, forms radicals through the homolysis of the phosphorus-carbon bond under irradiation and initiates polymerization reactions. The cross-linking agent promotes the formation a network of polymer chains to improve the grafting on cotton textile.

We use for the experiments reported in this thesis bis(acyl) phosphine oxide (BAPO) as the photoinitiator and ethylene glycol diacrylate (EGDA) as the cross-linking agent.



Figure 2.3: The structure of photoinitiator BAPO (left) and cross-linking agent EGDA (right)

2. Treatment of the monomers under low temperature and pressure argon plasma

The impregnated textile samples are then brought to the low pressure chamber, where they are then exposed to the Ar plasma. A typical treatment takes place for a maximum of 20 minutes in order to ensure the maximum conversion of the monomers into polymers.

## 2.4 Co-polymerisation of DEAEPN with APTMS

### 2.4.1 Flammability Measurements

In the presence of BAPO and EGDA, we performed the co-polymerisation of DEAEPN with APTMS on cotton textile using the PIGP process. In all experiments, the amount of each monomer are added in a range from 2.5% to 10% to the weight of the textile. The amount of BAPO and EGDA are set constant at 5% and 10% to the total weight of the mixture of monomers. After the plasma treatment, the samples are subjected to flammability test via LOI

measurement. Table 2.1 shows the measured flammability with the monomer loadings on cotton textiles after plasma treatment.

Entry	DEAEPN loading wt% (% P)	APTMS loading wt% (% Si)	After Impregnation wt%	After plasma wt%	LOI	Char yield %
untreated fabric	-	-	-	-	17.5	3.5
1	10 (1.2)	-	9.1	8.5	23.7	17.6
2	-	10 (1.2)	8.7	6.3	17.8	6.5
3	10 (1.2)	2.5 (0.3)	10.7	10.6	23.8	18.3
4	10 (1.2)	5 (0.6)	13.3	10.7	21.5	15.5
5	10 (1.2)	7.5 (0.9)	18.9	17.7	23.7	18.9
6	10 (1.2)	10 (1.2)	19.6	18.4	23.7	18.4
7	7.5 (0.9)	10 (1.2)	17.2	14.4	22.1	17.5
8	5 (0.6)	10 (1.2)	13.1	10.5	20.3	15.7
9	2.5 (0.3)	10 (1.2)	9.5	5.6	18.5	9.9

Table 2.1: LOI and char yield with FR at various loadings on cotton textile. Wt% denotes the weight of FR in percentage relative to that of cotton textile.

First of all, one observes a slight decrease in the FR loadings in all samples after the plasma treatment. This is due to a slight etching effect of the plasma in which some of the monomers or water on the surface are removed via low pressure during the treatment. Untreated cotton textile (Entry 0) burns at LOI 17.5 and gives 3.5% char. For textiles treated with 10 wt% APTMS (Entry 2), there is a slight increase in LOI and char yield, but not as pronounced as in textiles treated with 10 wt% DEAEPN (Entry 1), where the LOI increases to 23.7 and a much larger char yield of 17.6%. Although APTMS gives a slightly higher char yield than untreated textile, there is a stronger influence from DEAEPN on the flammability of cotton textiles. Observations reveal that the LOI values appear to be dependent only on the P content regardless of the Si content on the cotton textile. Here it is apparent that the presence of Si does not affect the flammability of the cotton textile, whether or not it contains a P-based FR.

For cotton textiles treated with a mixture containing equal amount of DEAEPN and APTMS at 10 wt% each (Entry 7), the LOI equals the value obtained for the fabric treated with DEAEPN

only (Entry 2). However, a small increase in char yield is observed. As the ATPMS loading in the co-polymer on textile varies from 2.5 wt% to 7.5 wt%, the LOI also remains around 23.7, while the char yields remain between 18 and 19%. This shows that APTMS does not further enhance the flame retardancy of DEAEPN. However, when DEAEPN loading in the co-polymer on cotton textile decreases from 7.5 to 2.5 wt%, the LOI shows more significant decrease from 22.1 to 18.5. The same trend can be observed also in their char yields, from 17.5% to 9.9%. This indicates the flammability of the fabric has a direct correlation to the amount of phosphorus-containing monomer, DEAEPN. From the LOI values one observes that it has a direct correlation to P content but independent to Si content.

We next investigated the effect of washing on the FR treated cotton textiles after the plasma treatment. In accordance to the standard protocol, the FR treated samples were subjected to 60 minutes of washing at room temperature in an aqueous solution of a standard detergent at 5 g/L concentration. These samples were then rinsed with distilled water to remove excess detergent from the textiles, and then dried at 60°C before being placed in a constant atmosphere for at least 24 hours and weighed again.

Table 2.2 illustrates how the loading changes when the samples are washed after plasma treatment.

<b>Entry</b>	<b>DEAEPN loading wt%</b>	<b>APTMS loading wt%</b>	<b>After Impregnation wt%</b>	<b>After plasma wt%</b>	<b>After washing wt%</b>	<b>Grafting yield %</b>	<b>LOI</b>	<b>Char yield %</b>
<b>11</b>	10	-	8.9	8.7	5.2	60	20.5	12.9
<b>12</b>	-	10	7.6	5.3	4.8	92	18.1	7.3
<b>13</b>	10	2.5	11.0	10.7	8.9	83	20.8	16.5
<b>14</b>	10	5	12.6	12.2	10.5	84	20.7	16.0
<b>15</b>	10	7.5	16.0	13.6	11.0	88	20.8	16.3
<b>16</b>	10	10	18.5	15.5	12.5	81	21.0	15.7
<b>17</b>	7.5	10	15.0	14.2	13.1	99	21.0	14.0
<b>18</b>	2.5	10	10.8	9.4	9.1	92	19.5	9.9

*Table 2.2: Loadings of FR on cotton after plasma treatment, before and after washing step.*

After washing step, the loadings decrease for all FR-treated samples. For DEAEPN-treated textile (Entry 11) only 60% remain grafted on the fabric. Relative to the unwashed sample, the



LOI decreases to 20.5 with 12.9% char. This correlates to the decreased amount of FR, hence reduced P-content on the textile from 1.1% to 0.64%.

For APTMS-treated textile (Entry 12), the grafting yield is much higher at 92%. The char yield also increases to 7.3%. The observed changes above suggest that compared to DEAEPN, APTMS exhibits a stronger affinity towards the cotton fabrics.

For the co-polymerised samples, the decrease in loading and the corresponding LOI and char yield is also observed. For example, with APTMS and DEAEPN at 10 wt% on textile (Entry 16), the grafting yield increases to 81% relative to textile treated only with 10 wt% DEAEPN. The LOI increases to 21.0 and the char yield to 15.7%, all these values are higher than those for 10 wt% DEAEPN on textile. When DEAEPN loading is varied from 2.5% to 7.5% in the co-polymerized samples (Entries 16 to 18), the grafting yield, LOI and char yield are higher for all variations of DEAEPN content, compared to the opposite situation when APTMS loading is varied and DEAEPN is kept constant in the co-polymerised samples (Entries 13 to 16).

From the above observations, it appears that the presence of APTMS increases the grafting yield of the co-polymer on the surface of textiles. Although its presence on cotton textile does not reduce the flammability of the textile, or enhance the flame retardant properties of DEAEPN-treated textile, the presence of APTMS in the co-polymer improves its affinity on the cotton textiles. One possible explanation for this stems from its ability to react with the primary-OH group of the cellulose chain via hydrolysis during the washing or drying step, forming a covalent bond with the textile surface. Comparatively, the phosphate ester side groups are relatively stable towards hydrolysis at the treatment temperature (RT). This might explain the observed difference in affinities towards cotton textiles.

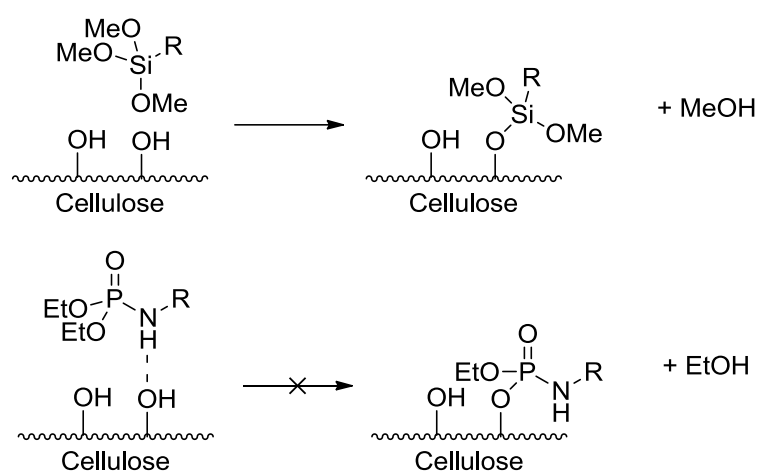


Figure 2.4: A possible explanation for the better affinity of APTMS on cotton fabrics.

## 2.4.2 Thermal Decomposition and Evolved Gas Analyses

To better understand the flammability results obtained previously from the FR systems we next measured the thermal decomposition profiles of textiles samples treated with the mixture of FR monomers at different concentrations after plasma treatment and washing procedure (Figure 2.5).

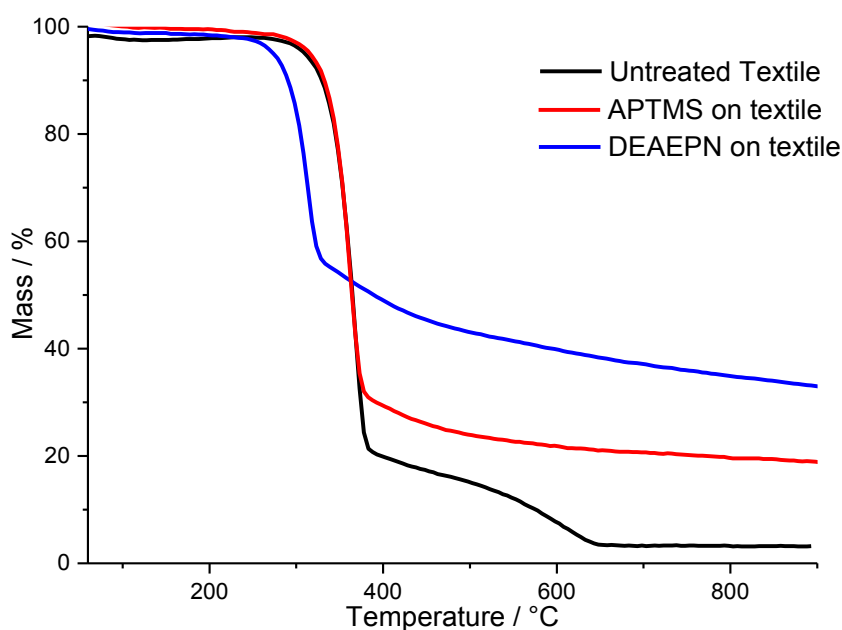


Figure 2.5: TG curves of untreated cotton textile and textiles with 10 wt% APTMS or DEAEPN.

In the presence of APTMS or DEAEPN, the thermal decomposition curves exhibit a single major mass loss step. The thermal decomposition of APTMS treated textile begins at a similar temperature to that of untreated textile, but exhibit a smaller mass loss step (70%). In addition, the slower decomposition step in untreated textile between 395°C and 655°C is no longer present for the textile with APTMS. This seems to suggest that APTMS interferes with the conversion from char I to char II at higher temperatures. This is typical as well for the formation of glassy SiO<sub>x</sub>-like protective later on the surface of the textile, which explains the stiffness of the APTMS-treated textile after plasma treatment. On the other hand, the thermal decomposition of DEAEPN treated textile shows a reduced onset temperature of decomposition, a mass loss step even smaller than APTMS, and high amounts of residue at 40% at 900°C. This observation highlights the characteristic of DEAEPN as a condensed phase flame retardant, where it interferes with the thermal decomposition process, limiting depolymerisation and promoting the formation of char.

The textile samples treated with co-polymers exhibit in general similar profiles as DEAE PN-treated samples, in that only one major decomposition step is observed (Figure 2.6).

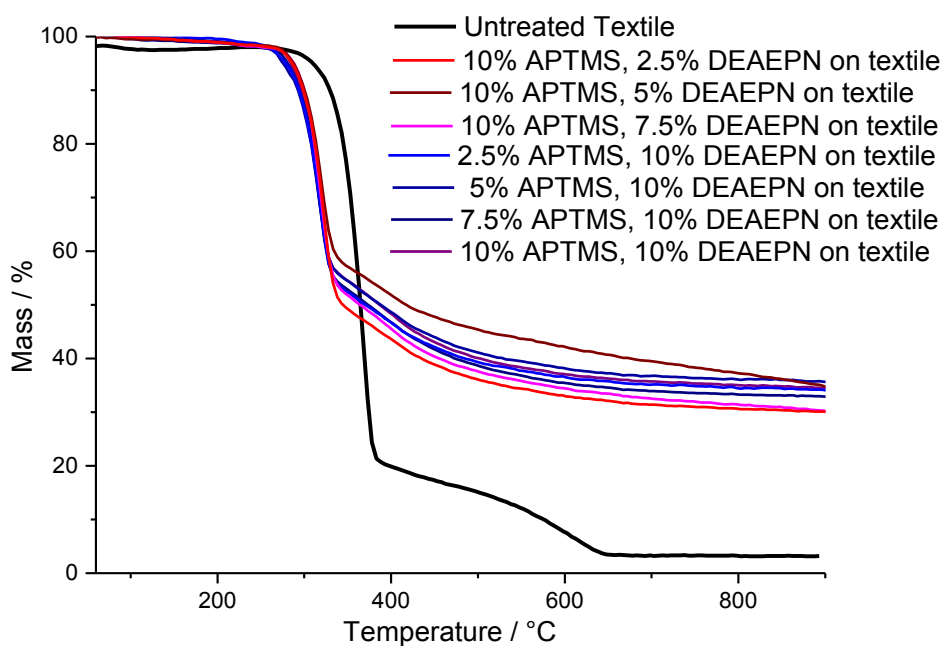


Figure 2.6: TG curves of untreated textile and textiles treated with co-polymers of DEAE PN and APTMS at various amounts.

Regardless of the relative proportion of both monomers, similar temperatures at onset of decomposition is observed for all the treated samples, similar to that of DEAE PN treated textile. Higher ratios of DEAE PN and APTMS seem to give higher residues. However when the DEAE PN loading in the co-polymer is decreased, the mass loss steps generally increase and give less char.

These trends correlate to the previously observed LOI behaviour, where higher LOI and char yields are associated to textiles treated with higher ratios of DEAE PN to APTMS.

Next we proceed to analyse the gaseous species evolved from the thermal decomposition of FR treated cotton textiles. Here, we compare the FTIR spectra of the evolved species during the thermal decomposition of these samples obtained at the end of the major mass loss step (Figure 2.7).

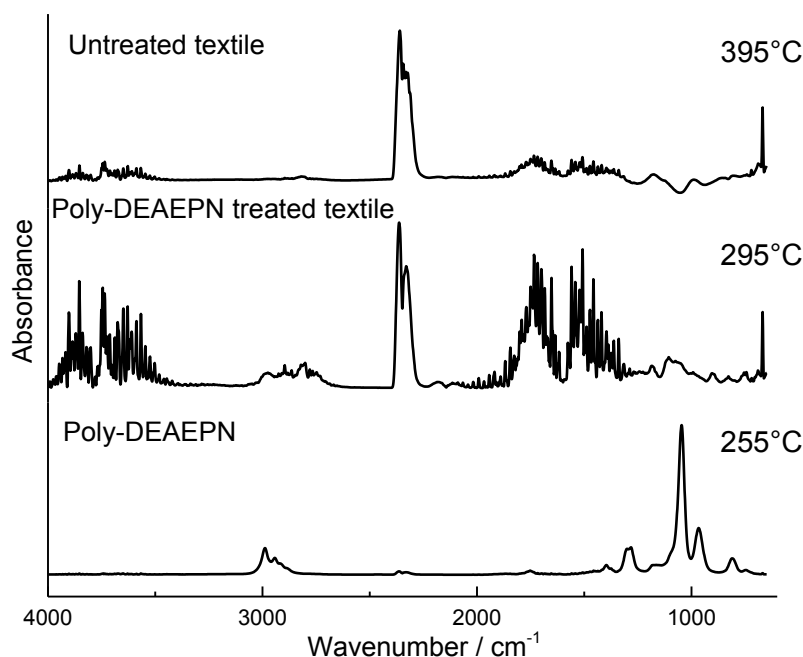


Figure 2.7: FTIR spectra of evolved species obtained at the end of mass loss step during the decomposition of untreated textile, DEAEPN treated textile and poly-DEAEPN.

From the spectrum of the evolved species obtained at the end of largest mass loss step of textile sample treated with 10 wt% DEAEPN, we observe strong absorptions at 4000–3000  $\text{cm}^{-1}$  and 1800–1300  $\text{cm}^{-1}$  originating from water, sharp and intense absorptions at 2300  $\text{cm}^{-1}$  and 668  $\text{cm}^{-1}$  indicating carbon dioxide. The assignment of these absorptions are summarized in the following Table 2.3

Wavenumber / $\text{cm}^{-1}$	Type of Absorption	Assignment
4000–3000	Broad, medium	$\nu$ (H–O–H), water
2300	Sharp, intense	$\nu$ (O=C=O), carbon dioxide
1800–1300	Broad, medium	$\delta$ (H–O–H), water
668	Sharp, medium	$\delta$ (O=C=O), carbon dioxide

Table 2.3: Assignment of absorptions to the respective vibrational modes.

Besides that, additional absorptions at 3000–2800  $\text{cm}^{-1}$  can be attributed to the vibrational modes of  $\text{sp}^3$ -C-H bonds. These absorptions probably originate from the ethyl groups and the alkyl chains of DEAEPN. As a comparison we also present the spectrum from decomposition of DEAEPN sample polymerized by plasma. Here, absorptions at 2990  $\text{cm}^{-1}$ , 1270  $\text{cm}^{-1}$ , 1060  $\text{cm}^{-1}$  and 980  $\text{cm}^{-1}$ , which can be respectively attributed to  $\text{sp}^3$  C-H, P-O-C, C-O-H and O-C-O vibrational modes. Putting these two spectra together, the absorptions from carbon dioxide and water originate from the decomposition of the cotton textiles, while the absorptions in the remaining regions originate from the decomposition of poly-DEAEPN.

A similar observation is made when we compare the FTIR spectra of evolved species obtained during the largest mass loss steps in the thermal decomposition of textiles treated with 10wt% APTMS and poly-APTMS (Figure 2.8).

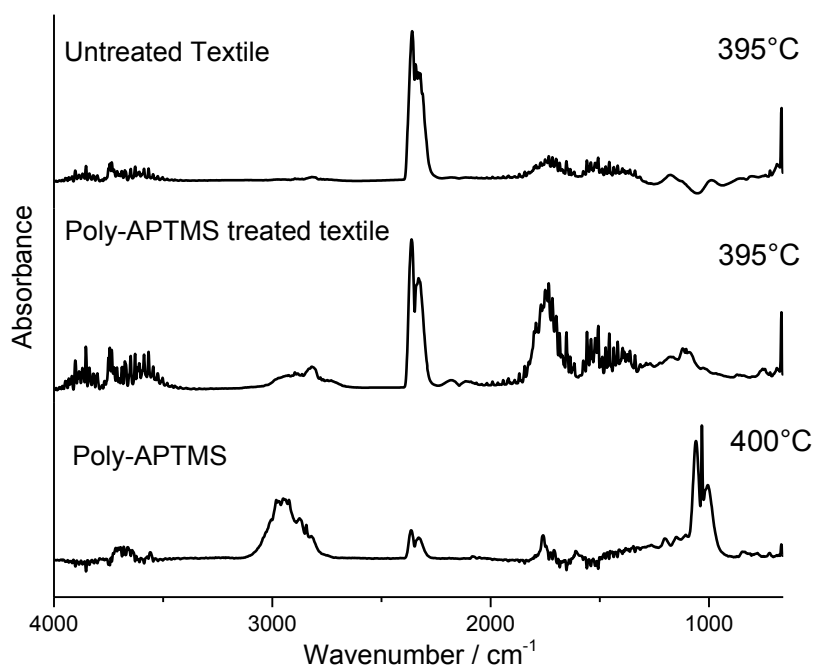


Figure 2.8: FTIR spectra of evolved species obtained from the end of mass loss step for untreated textiles, APTMS-treated textiles and polymerised APTMS.

The spectrum of 10wt% APTMS on textile also shows water and carbon dioxide. Besides that, absorptions at  $3000 - 2800 \text{ cm}^{-1}$ ,  $2300 - 2100 \text{ cm}^{-1}$  and around  $1200 \text{ cm}^{-1} - 980 \text{ cm}^{-1}$  are also observed. This is similar to the spectra for poly-APTMS, where the absorptions are observed, other than those of water and carbon dioxide, at  $2990 \text{ cm}^{-1}$  ( $\nu \text{ sp}^3 \text{ C-H}$ ),  $1770 \text{ cm}^{-1}$  ( $\nu \text{ C=O}$ ),  $1090 \text{ cm}^{-1}$  ( $\nu \text{ C-O-H}$ ) and  $980 \text{ cm}^{-1}$  ( $\nu \text{ O-C-O}$ ). Comparing both spectra we observe that the decomposition of poly-APTMS releases more organic moieties, possibly from the hydrolysis of trimethoxy groups, releasing methanol, which in turn contributed as fuel to the flame which explains the low LOI values. The presence of methanol can be verified with the MID spectra of  $m/z = 31$ , also obtained during the decomposition of poly-APTMS and APTMS treated cotton textiles.

From the thermal decomposition profiles of APTMS on textiles, it is evident that the effect that APTMS has on the thermal decomposition of textile is limited in terms of LOI. However, the more char it produces indicates the formation of a protective coating. Also, as a co-polymer with DEAEPN on cotton textiles, APTMS brings little enhancement to the flame retardant

properties of DEAEPN. This was observed from the similar temperatures at onset of decomposition for the co-polymer treated textiles, and from the LOI measurements.

## ***2.5 Concluding Remarks***

In summary, we observe that APTMS itself contributes to slightly increased LOI and char yield, but the effect on flammability in terms of LOI is not as pronounced compared to DEAEPN on textiles. When co-polymerised with DEAEPN, APTMS improves the overall grafting yield but it does not further enhance the flame retardancy of DEAEPN on cotton textiles.

From the first impression the combination of P, Si and N via the co-polymerisation technique of the two monomers does not exhibit effectiveness in enhancing the flame retardant properties of DEAEPN. As it seems, silicon in the form of APTMS does not intrinsically possess significant flame retardant properties, nor does it, in the form of copolymer, possess the cooperative effect that nitrogen has with phosphorus.

# **Chapter 3**

## **Synthesis of New Flame Retardant Compounds**

### 3.1 Introductory Remarks

In this chapter, we present the chemical synthesis of all the new flame retardants relevant to our investigation of structure-to-property relationships of some structurally related compounds where the environment as well as P/N, P/Si ratios are varied. These include esters and silyl esters of hypophosphates, pyrophosphates and imidodiphosphates, N-silylated phosphoramidates and phosphorohydrazidates, as illustrated in Figure 3.1. Their synthesis procedure, mechanisms and, when appropriate, solid state structures are among the aspects being described and discussed.

R	X	Name
Et	Nothing	Hypophosphate Ester
Et	O	Pyrophosphate Ester
Et	NH	Iminodiphosphate Ester
TMS	Nothing	Hypophosphate Silyl Ester
TMS	O	Pyrophosphate Silyl Ester
TMS	NH	Imidodiphosphate Silyl Ester
Et	NH-NH	Phosphorohydrazidate
		N-silylated Phosphoramidate

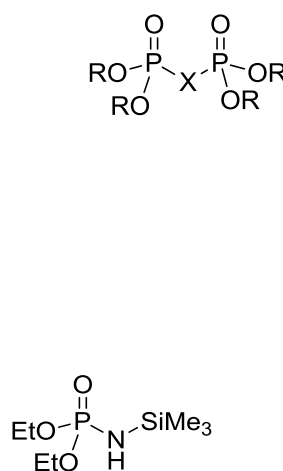


Figure 3.1: Structures of various compounds whose syntheses are presented in this chapter.

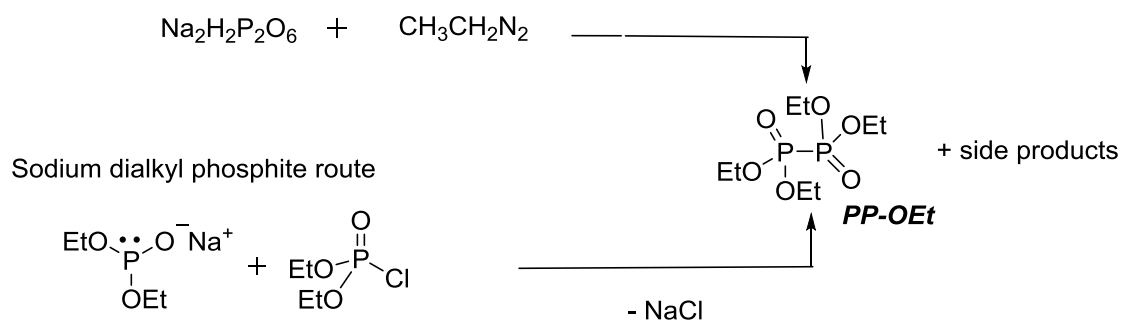
### 3.2 Phosphate Esters

#### 3.2.1 Tetraethyl Hypophosphate (PP-OEt)

The synthesis of **PP-OEt** has been described in various studies<sup>37</sup> (Scheme 3.1). These articles reported on the synthesis of tetraalkyl hypophosphates either via esterification of hypophosphoric acid with diazoalkanes<sup>45</sup>, or by condensation of sodium dialkyl phosphites with dialkyl chlorophosphates. The former process requires a sophisticated experimental setup for the production of hypophosphoric acid<sup>46</sup> and acutely toxic and explosive diazoalkanes<sup>45</sup>, while the latter method requires a very inert condition owing to the use of sodium. It often generates undesired side products<sup>47</sup> such as hypophosphites, pyrophosphates and P<sup>III</sup>-P<sup>IV</sup> mixed anhydrides<sup>48</sup>. These side products are often difficult to separate from the desired hypophosphate products.

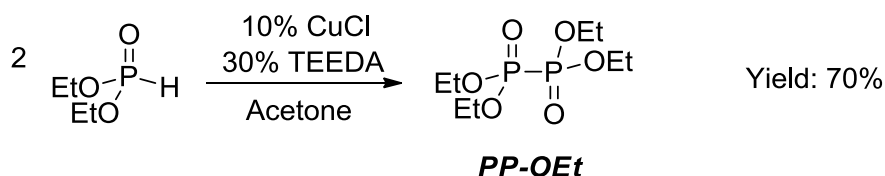


Diazoalkane Route



Scheme 3.1: Two possible routes of generating tetraalkyl hypophosphates

In 2010, Zhou *et al*<sup>49</sup> reported the formation of a direct phosphorus–phosphorus bond through a dehydrogenative coupling reaction in the presence of Cu(I) and N, N, N', N' – tetraethylethylenediamine (TEEDA), a sterically hindered base, in substoichiometric amounts (Scheme 3.2). Because it can take place in air, we attempt to obtain **PP-OEt** using this method.



Scheme 3.2: Zhou's method<sup>49</sup> to obtain **PP-OEt** from diethyl phosphite via a Cu(I)-mediated pathway.

In this procedure, two equivalents of diethyl phosphite are stirred in a small amount of reagent-grade acetone with 10 mol% CuCl and 30 mol% TEEDA. This reaction takes place at room temperature and in air, but water has to be excluded by placing a guard tube filled with calcium chloride as desiccator. As the reaction progresses, the solution mixture slowly changes from yellowish green through green, finally to a deep blue colouration at the end of the reaction. To obtain the final product in one-gram scale, at least 25.5 hours is required for a total completion of the reaction. This is in contrast with the duration reported by Zhou *et al*, which was 1.5 hours for an NMR-tube scale (150 mg).

The reaction progress is followed up using proton-coupled <sup>31</sup>P NMR spectroscopy (Figure 3.2). Initially, a doublet of quintets is observed centering at 7.7 ppm in the proton-decoupled <sup>31</sup>P NMR spectrum. The quintet multiplicity originates from a three bond phosphorus-proton coupling (<sup>3</sup>J<sub>P-H</sub> = 10 Hz), while the doublet splitting centred at 8 ppm can be attributed to the one bond phosphorus-proton coupling (<sup>1</sup>J<sub>P-H</sub> = 685 Hz). As the reaction progresses, the intensity of this signal decreases, with a simultaneous increase in intensity of a quintet (<sup>3</sup>J<sub>P-H</sub> = 4.4 Hz) centred at 7.2 ppm, signifying the consumption of diethyl phosphite to produce tetraethyl hypophosphate.

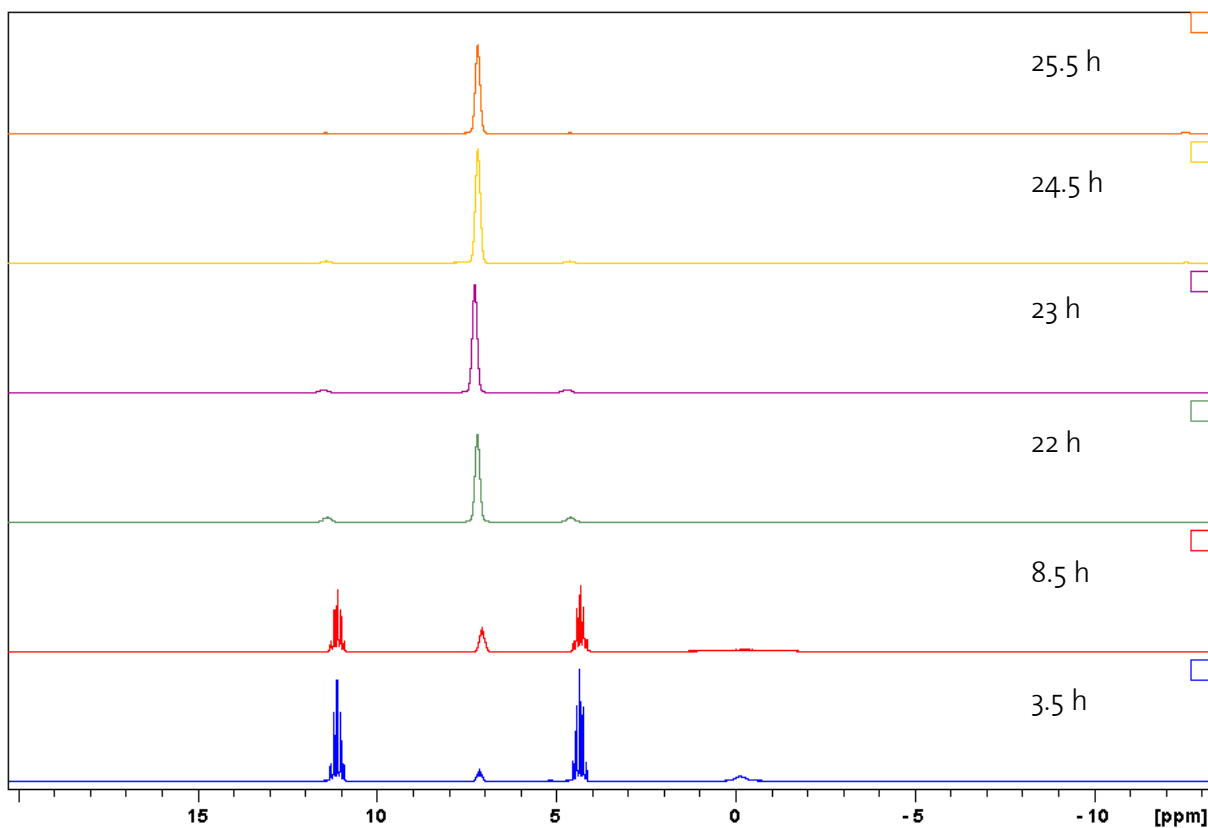
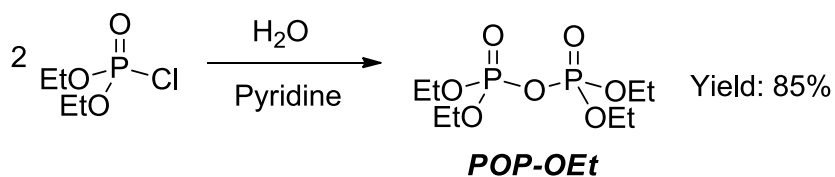


Figure 3.2: The progress of reaction with proton-coupled  $^{31}\text{P}$  NMR spectroscopy.

One advantage of this procedure is that an inert condition is not required for the reaction. However, the reaction should not be allowed to exceed 30 hours to prevent the generation of tetraethyl pyrophosphate as the side product. Furthermore, to remove the copper ions, a work-up procedure using saturated aqueous solution of ammonium chloride is employed. Distillation is then performed to remove remaining TEEDA from the mixture, yielding colourless liquid of **PP-OEt**.

### 3.2.2 Tetraethyl Pyrophosphate (**POP-OEt**)

**POP-OEt** was synthesized in accordance to the published procedure<sup>50</sup> by careful addition of water to diethyl chlorophosphate (Scheme 3.3).



Scheme 3.3: Synthesis of **POP-OEt** via a double hydrolysis reaction

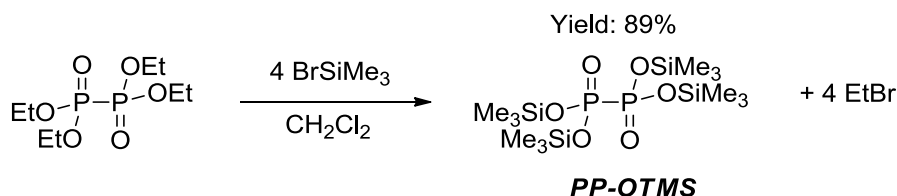
Pyridine serves not only as the solvent but also the acid scavenger to remove HCl generated

from the reaction. The colourless liquid product can then be isolated via a filtration step to remove the salt, followed by the evaporation of pyridine using rotavapor for at least two hours. The  $^{31}\text{P}$  NMR spectrum of the product shows a singlet at -13 ppm while the reactant, diethyl chlorophosphate, has a chemical shift of 8 ppm and is consistent to the published<sup>50</sup> results. In this reaction, the amount of water has to be carefully controlled to achieve the desired stoichiometry of the reaction. To isolate the product, removal of pyridine has to be thorough, as a trace amount of pyridine would catalyze the subsequent hydrolysis of **POP-OEt**. This significantly reduces the shelf life. In this aspect, it has been observed that the liquid slowly turns yellowish brown after a week when **POP-OEt** is stored under room temperature. However, storing the isolated product under -30 °C in the freezer could prolong its shelf life significantly longer (longer than two years).

### 3.3 Synthesis of Phosphate Silyl Esters

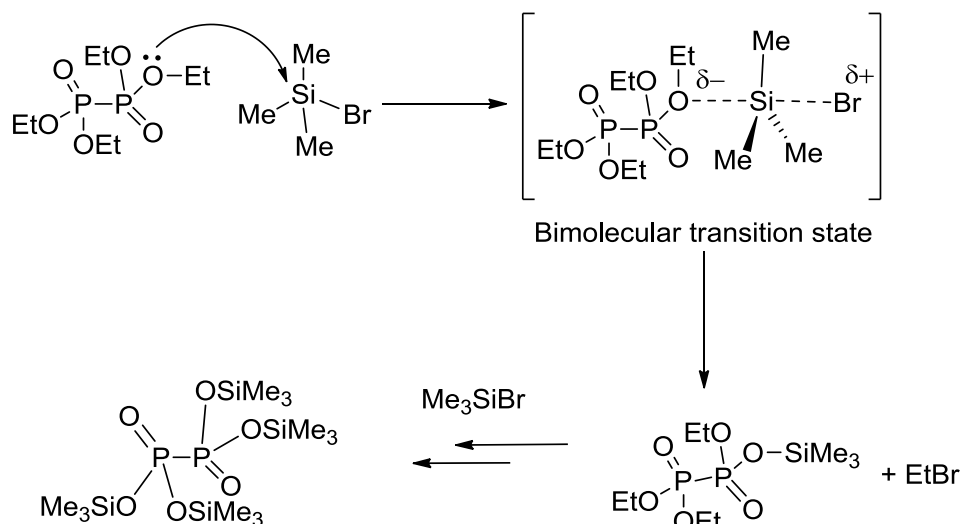
#### 3.3.1 Tetrakis(trimethylsilyl) Hypophosphate (**PP-OTMS**)

This procedure (Scheme 3.4) is analogous to the silylation of phosphinic acid dialkyl ester<sup>37,51</sup>, involving a reaction between one equivalent of **PP-OEt** with an excess of trimethylsilyl bromide to afford **PP-OTMS**.



Scheme 3.4: The synthesis of **PP-OTMS** according to Ruflin et al<sup>37</sup>

Essentially, it is a transesterification of the ethyl ester by trimethylsilyl ester group. The addition of trimethylsilyl bromide onto the  $\text{CH}_2\text{Cl}_2$  solution of **PP-OEt** has to be performed at -5 °C to prevent the reaction from being too exothermic. After at least 15 hours of reaction, **PP-OTMS** is obtained and isolated as white waxy solid or colourless crystal.



Scheme 3.5: A proposed mechanism of silylation through a bimolecular transition state.

Illustrated in Scheme 3.5, the mechanism is understood to be so: acting as the nucleophile, the oxygen at the alcohol group attacks the electron deficient silicon centre of trimethylsilyl chloride. This generates a bimolecular transition state<sup>52</sup>, where the arrangement surrounding the silicon centre has a trigonal bipyramidal geometry. Upon the formation of the silicon-oxygen bond, ethyl bromide is also generated as a by-product, which escapes the system because of its very low boiling point and high volatility at the reaction temperature.

### 3.3.2 Tetrakis(trimethylsilyl) Pyrophosphate (**POP-OTMS**)

This procedure is analogous to the silylation of phosphinic acid dialkyl ester<sup>37,51</sup>, involving a reaction between one equivalent of **PP-OEt** with an excess of trimethylsilyl bromide to afford **PP-OTMS**.

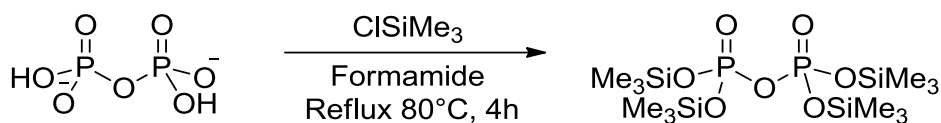


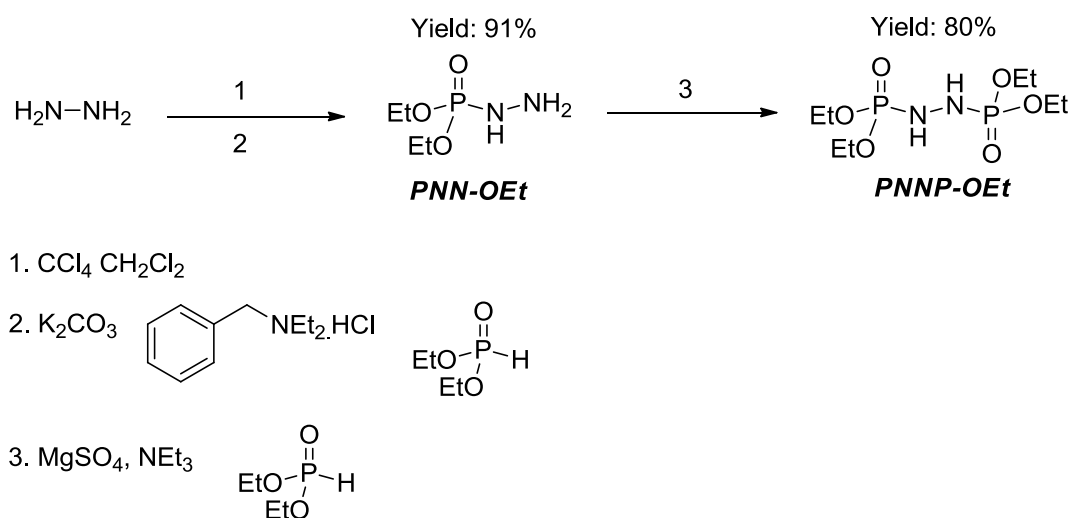
Figure 3.3: The synthesis of **POP-OTMS** in accordance to Wessjohan *et al*<sup>53</sup>.

The synthesis of tetrakis(trimethylsilyl) pyrophosphate (**POP-OTMS**) involves the reaction of one equivalent of disodium dihydrogen pyrophosphate with a 10% excess of chlorotrimethylsilane (TMSCl) in the solution of formamide as both the acid scavenger and the solvent (Figure 3.3). TMSCl is in a 10% excess to ensure complete conversion of  $\text{Na}_2\text{H}_2\text{P}_2\text{O}_5$ . During the course of the reaction, white precipitation of NaCl appeared. After refluxing the reaction mixture for at least four hours, a colourless liquid appears in a separate phase above the white precipitate of NaCl in formamide. The colourless liquid was then collected. The <sup>31</sup>P

NMR spectrum of the product shows a single singlet peak at -26.1 ppm, indicating a very high purity of the final product, **POP-OTMS**, which is a viscous colourless liquid. The product can be obtained at 85% yield and stored over a long period (at least two years) when kept in the freezer under -30°C as either a white solid or a colourless liquid.

### 3.4 Diethyl Phosphorohydrazidate (**PNN-OEt**) and *N, N'*- Bis(diethyl)phosphoryl Hydrazidate (**PNNP-OEt**)

The synthesis of **PNN-OEt** was performed according to the procedure described by Zwierzak et al<sup>54</sup>. In this procedure, one equivalent of diethyl phosphite was first reacted with one equivalent of hydrazine in the presence of tetrachloromethane, dichloromethane, anhydrous potassium carbonate and triethylbenzylammonium chloride. The equivalence of diethyl phosphite and hydrazine is crucial in this step to control the selectivity of the reaction to favour the formation of **PNN-OEt**. This mixture creates a two-phase system allowing solid-liquid phase transfer catalysis to take place. The carbonate anion as an inorganic base is transported directly from the solid phase into the liquid phase by triethylbenzylammonium chloride, which is the phase-transfer catalyst. After two hours of reaction, the reaction mixture was filtered, and the removal of solvent from the filtrate yielded an off-white liquid that shows a signal at 6 ppm in <sup>31</sup>P NMR spectroscopy, revealing the presence of **PNN-OEt**.



Scheme 3.6: Synthesis of **PNN-OEt** and **PNNP-OEt** via a two-step reaction

This reaction is believed to be similar to that of Atherton-Todd reaction<sup>55,56</sup>. While the exact mechanism has been a subject of debate<sup>57-60</sup>, it is believed that this mechanism most probably involves a chlorophosphate intermediate, which subsequently reacts with the base to form a new P–N bond, leading to the phosphorohydrazidate product in this reaction.

**PNNP-OEt** is then synthesized via a similar procedure by reacting one equivalent of **PNN-OEt** reaction mixture with another equivalent of diethyl phosphite in the presence of trimethylamine in stoichiometric amount and anhydrous magnesium sulphate as the desiccator. Prior to the addition, the mixture has to be filtered to remove the potassium carbonate. The product **PNNP-OEt** is isolated as a colourless crystal after two hours of reaction, filtering off the reaction mixture and subsequently removing the solvent from the filtrate. In  $^{31}\text{P}$  NMR spectrum, **PNNP-OEt** presents as a singlet peak at 8 ppm.

In addition to that, we were able to obtain the solid state structure of **PNNP-OEt**, depicted for the first time in Figure 3.4.

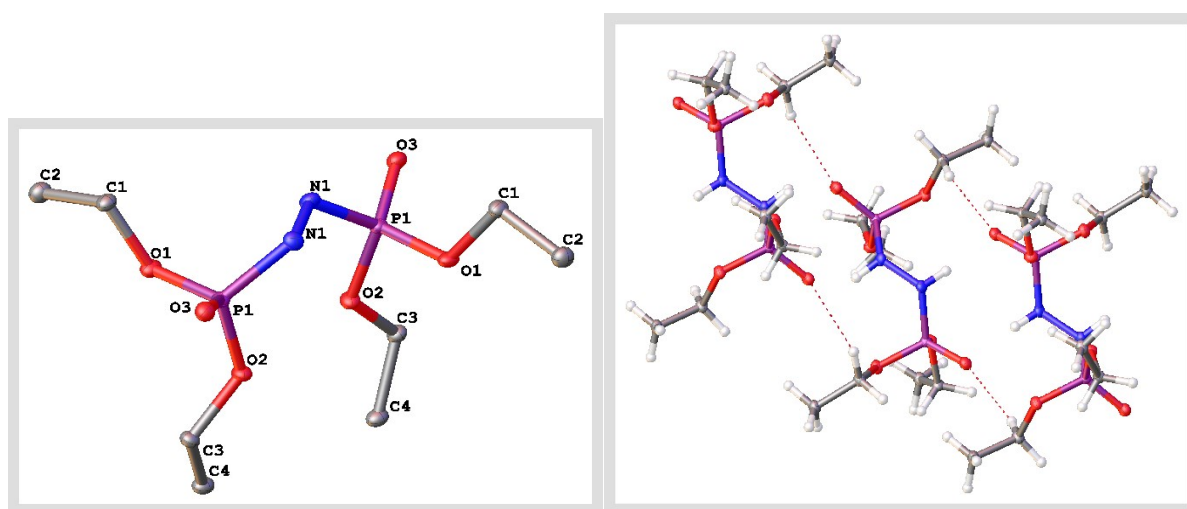


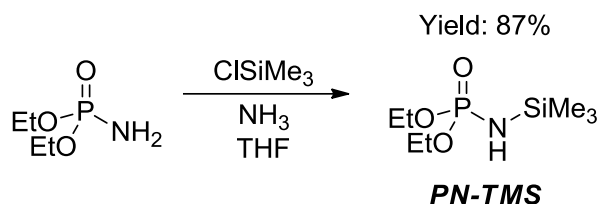
Figure 3.4: The solid state structure of **PNNP-OEt**

In the solid state, this molecule displays a  $C_2$  symmetry. The atoms surrounding phosphorus centre are arranged in tetrahedral manner. The nitrogen-nitrogen bond has a length of 1.402 Å. This length is shorter compared to that of hydrazine at 1.45 Å but still significantly longer than that of azide at 1.2 Å. Also, it is shorter than most of the nitrogen-nitrogen bond found in substituted hydrazines in the literature<sup>61</sup>.

In a single crystal of **PNNP-OEt**, the atoms are arranged in such a way that through intermolecular hydrogen bonds, the molecules form an array of a particular regular pattern, which runs in the direction parallel to the plane b of the crystal, with the C–H  $\cdots$  O=P hydrogen bond at 2.114 Å, and the C–H $\cdots$ O angle at 148.35°.

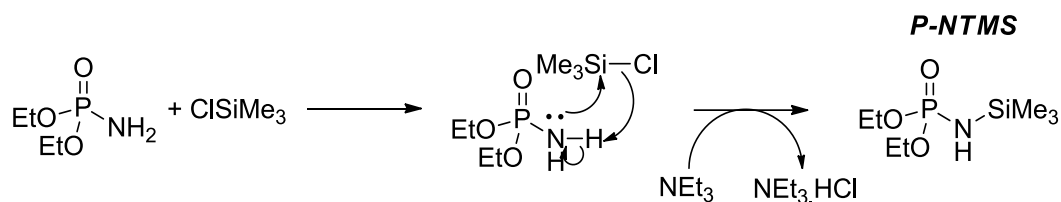
### 3.5 Diethyl N-Trimethylsilyl Phosphoramidate (*P-NTMS*)

The synthesis of *P-NTMS* was achieved by a simple silylation of diethyl phosphoramidate at room temperature using trimethylsilyl chloride as the silylating agent.



Scheme 3.7: Synthesis of *P-NTMS* via N-silylation of diethyl phosphoramidate.

In this reaction, one equivalent of diethyl phosphoramidate is being reacted with one equivalent of trimethylsilyl chloride in the presence of trimethylamine in a solution of THF. Being a better nucleophile than the oxygen atom, the nitrogen centre in the primary amide reacts preferentially with the trimethylsilyl electrophile. As an acid scavenger, triethylamine then traps the HCl generated from the reaction in the form of triethylammonium chloride salt, which is insoluble in THF and easily removed via a filtration step. After one hour of reaction, the product *P-NTMS* can be isolated as colourless crystals and characterized in  $^{31}\text{P}$  NMR spectroscopy in  $\text{CDCl}_3$  by the presence of a singlet peak at 9.3 ppm.



Scheme 3.8: Proposed mechanism of *P-NTMS* formation through silylation

As illustrated by Scheme 3.8, this reaction is believed to proceed through the nucleophilic attack of the nitrogen atom of diethyl phosphoramidate on the electrophilic silicon centre. This generates HCl as a side product, which is quickly trapped by trimethylamine. This maintains the equilibrium of the reaction towards the formation of product.

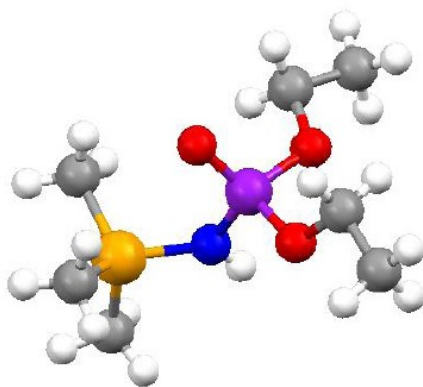


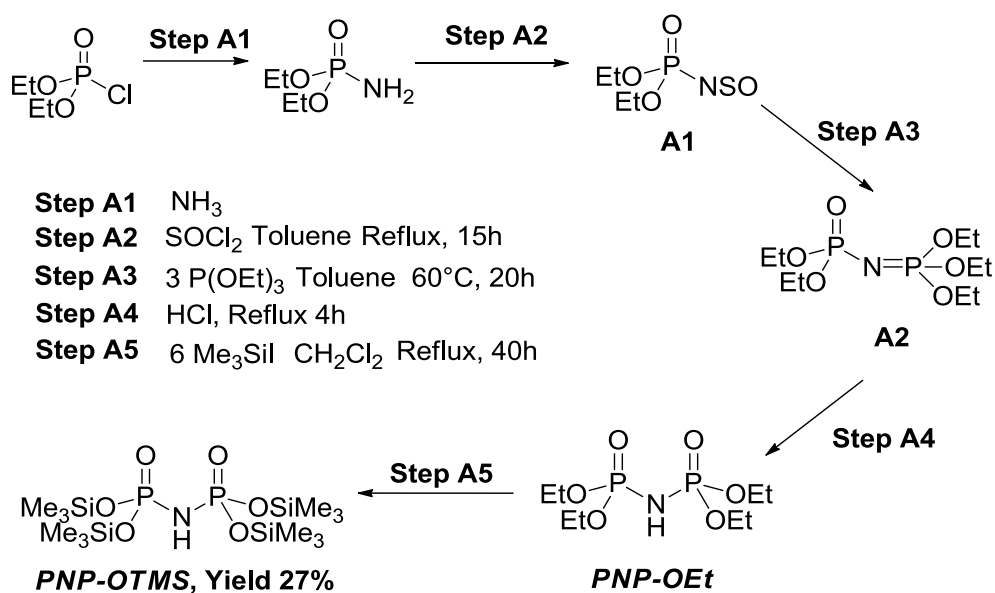
Figure 3.5: The solid state structure of **P-NTMS**

The solid state structure of **P-NTMS** was obtained and reported for the first time in this report. It shows a phosphorus–nitrogen–silicon bond at an angle of 126.3 degrees, with the phosphorus–nitrogen bond at 1.61 Å and nitrogen–silicon bond at 1.75 Å. In comparison, we found a related solid state structure, the diphenyl analogue of **P-NTMS** (CCDC 143828)<sup>62</sup>. In this molecule, the phosphorus–nitrogen–silicon angle is found to be 127.7 degrees, with the phosphorus–nitrogen bond at 1.61 Å and the nitrogen–silicon bond also at 1.75 Å, showing the structural similarity between the diethyl and diphenyl analogues.

### 3.6 Tetrakis(trimethylsilyl) Imidodiphosphate (**PNP-OTMS**)

The synthesis of **PNP-OTMS** was first described as an intermediate<sup>63</sup>. This article reported on an attempt to synthesize a <sup>15</sup>N-enriched phosphorylated DNA, and **PNP-OTMS** was obtained through a five-step reaction starting from diethyl chlorophosphate. In this procedure, diethyl chlorophosphate was first converted to diethyl phosphoramidate by reaction with ammonia, followed by a reflux with SOCl<sub>2</sub> to give diethyl (oxo-λ<sup>4</sup>-sulfanylidene) phosphoramidate, which is subsequently converted to diethyl (triethoxy-λ<sup>5</sup>-phosphanylidene) phosphoramidate via a reaction with three equivalents of triethyl phosphite. Hydrogen chloride gas is then bubbled through the solution to generate tetraethyl imidodiphosphate, which is then converted to tetrakis(trimethylsilyl) imidodiphosphate by trimethylsilyl iodide. This procedure is summarized in Scheme 3.9.





Scheme 3.9: Synthesis of **PNP-OTMS** as reported by Reynolds et al.<sup>63</sup>. (Method A)

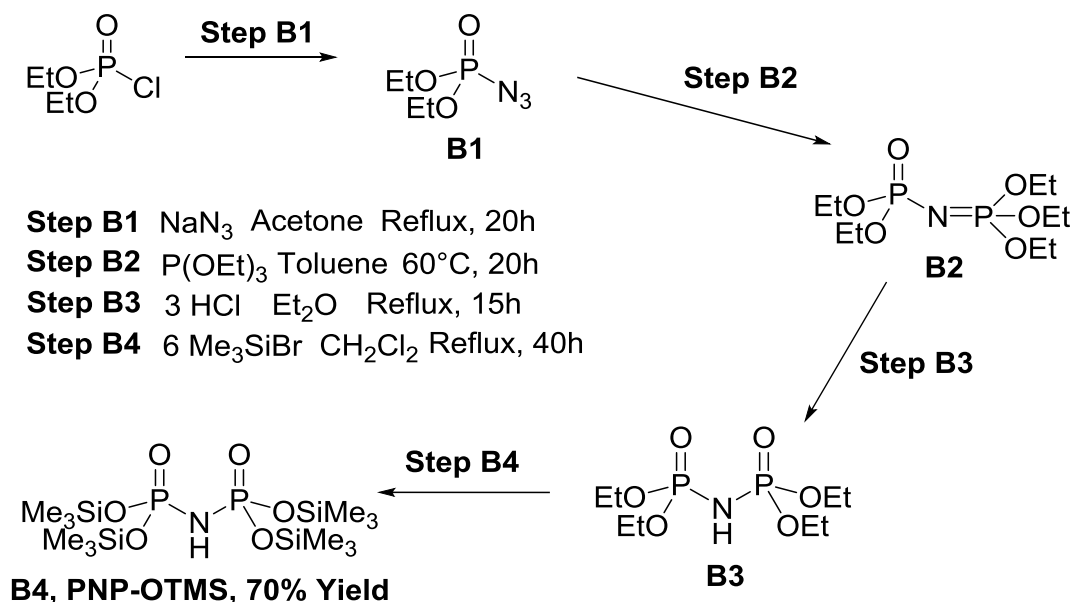
To reproduce this synthesis, we made minor adjustments from the original procedure were made. Firstly, we started directly from diethyl phosphoramidate instead of diethyl chlorophosphate, since the former is now commercially available. This shortens the procedure to a four-step reaction. Secondly, instead of bubbling  $\text{HCl}$  gas through the reaction mixture in step A4, we directly used a purchased solution of 2 mol  $\text{HCl}$  in  $\text{Et}_2\text{O}$ .  $\text{Me}_3\text{SiBr}$  in step A5 was used in place of  $\text{Me}_3\text{SiH}$  because the former is cheaper and the reaction is more selective.

However, this modified procedure has several disadvantages that resulted in a low yield (27%) and purity (51%) of the final product.

First of all, a strongly corrosive acid, thionyl chloride ( $\text{SOCl}_2$ ) was used in step A2. As  $\text{SOCl}_2$  is a very strong electrophile, triethylamine is not suitable to be used as an acid trapping agent. Consequently, one additional equivalent of the diethyl phosphoramidate has to act as the acid scavenger. This significantly reduces the atomic efficiency and becomes the major yield-limiting step of the reaction.

Besides that, this reaction also generates yellow impurities, and can only be separated by a careful vacuum distillation before proceeding to the next step. In step 3, three equivalents of triethyl phosphite have to be added to give the intended intermediate. To isolate this intermediate, vacuum distillation is again necessary. These two distillation steps altogether renders the reaction energetically expensive and both the final yield (27%) and the purity (51%) of the final product do not justify the means.

To circumvent the disadvantages mentioned for the previous method, we report a four-step alternative route (Method B, Scheme 3.10) to obtain **PNP-OTMS** at a quantitative yield and a higher purity of the final product.

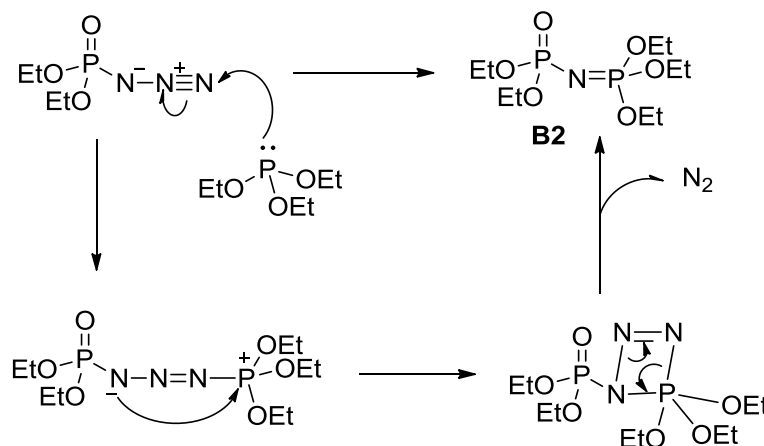


Scheme 3.10: The synthesis of **PNP-OTMS** through Method B.

This route involves using diethyl phosphoramidate as the starting material, converting it to diethyl phosphorazidate (intermediate **B1**) in the first step via a reaction with sodium azide<sup>64</sup>, and then reacting **B1** with one equivalent of triethyl phosphite to yield diethyl (triethoxy- $\lambda^5$ -phosphanylidene)phosphoramidate (intermediate **B2**) in the second step. The two subsequent steps are identical to that we have modified previously.

As illustrated in Scheme 3.10, the first two steps are similar to a procedure published by Riesel *et al* in 1983<sup>65</sup>. However, to avoid the usage of environmentally unfriendly tetrachloromethane via Atherton-Todd reaction, we employ the method reported by C. Timperly<sup>64</sup> which involves only a simple nucleophilic substitution reaction. Here, intermediate **B1** is generated as the first intermediate in place of **A1**. An advantage of this step lies in the generation of sodium chloride as the only side product, which is neutral, insoluble in acetone and can be easily separated by filtration. Contrary to the previous method, the solution mixture in this route remained colourless, and its  $^{31}\text{P}$  NMR spectra shows only a single peak at 0.1 ppm (as opposed to 4.6 ppm for the starting material diethyl chlorophosphate), indicating the formation of only one phosphorus-containing product.

In addition, in the second step of this procedure, only one equivalent triethyl phosphite is required to react with **B1**. This points to a higher atomic efficiency than the corresponding step in the previous method. Here, the subsequent intermediate, **B2** is formed through the Staudinger reaction, involving a rearrangement of the azide group to afford a new phosphorus-nitrogen bond (mechanism in Scheme 3.11). This reaction generates nitrogen gas as a side product, which readily escapes from the reaction mixture at an elevated temperature.



Scheme 3.11: Mechanism of the Staudinger reaction leading to the formation of **B2**.

The formation of intermediate **B2** can be identified by its characteristic “roofing” pattern in  $^{31}\text{P}$  NMR spectrum centred at  $-2.3$  ppm. This arises when the difference in chemical shifts of the phosphorus centers become small compared to the coupling between them.

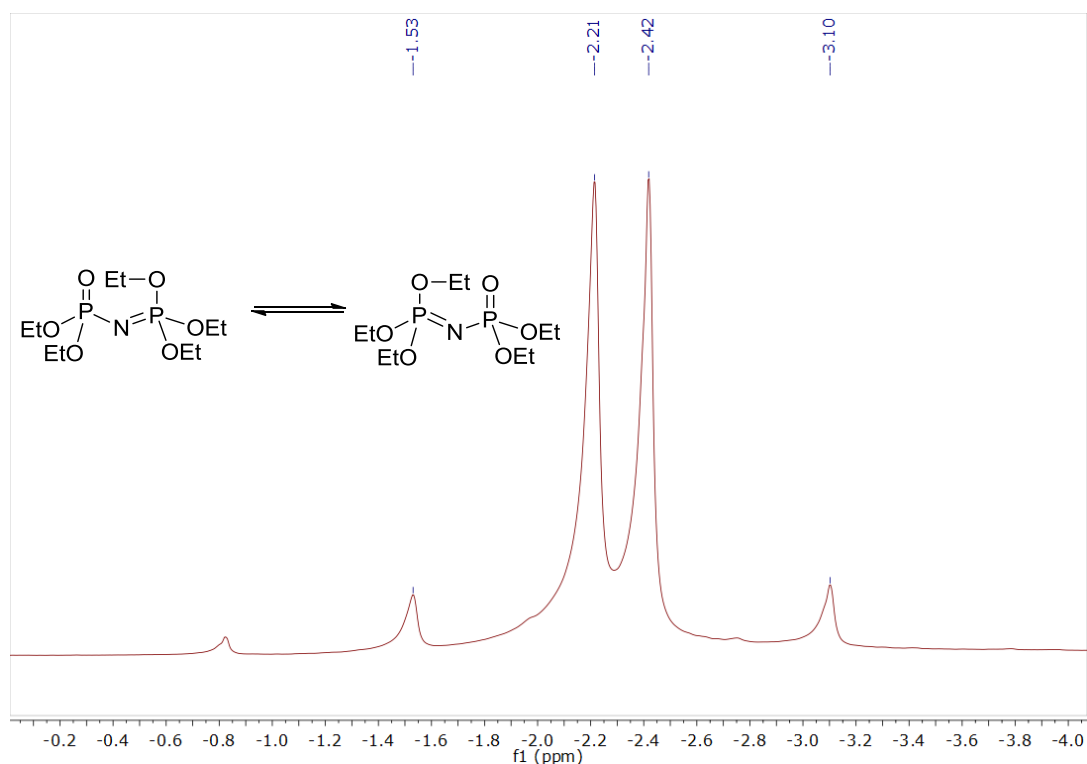


Figure 3.6: The  $^{31}\text{P}$  NMR spectrum of **B2** in its neat liquid obtained at room temperature.

From the spectrum depicted in Figure 3.6, the coupling constant between both phosphorus is 69 Hz, while the difference in the chemical shift of the two phosphorus centres ( $\Delta\delta_{PP}$ ) is 0.57 ppm. The temperature dependence of this phosphorus-phosphorus coupling has been studied and reported in 1979 by Riesel *et al*<sup>66</sup>.

From **B2**, the subsequent steps are carried out just as described previously. One important difference in these two methods lies therein, that prior to step 3, distillation is no longer necessary and excess triethyl phosphite can be removed via reduced pressure. The neat liquid of **B2** can be directly added onto the HCl in Et<sub>2</sub>O solution to give **PNP-OEt**, or intermediate **B3**, which can be identified by a singlet peak at -0.36 ppm in the <sup>31</sup>P NMR spectrum. Further reaction of **B3** with six equivalents of trimethylsilyl bromide then yields the desired final product, **PNP-OTMS**, or **B4**, which presents as a singlet at -17 ppm in its <sup>31</sup>P NMR spectrum. It can be isolated as light brown crystals when cooled in a supersaturated solution of dry hexane.

In summary, through Method B, the final product can be obtained at a better atomic efficiency and a much higher spectroscopic purity without the need for energetically expensive distillation processes.

### 3.7 Concluding Remarks

With insights into the molecular design of the phosphorus-based flame retardant compounds based on previous studies conducted in our laboratory<sup>5,6,31–33,37</sup>, the potentially new flame retardants were successfully synthesized in sufficient yields and purity, and some of their properties are summarized in Table 3.1.

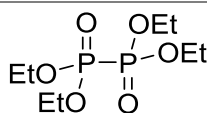
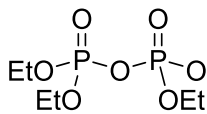
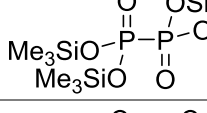
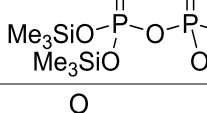
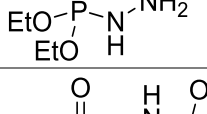
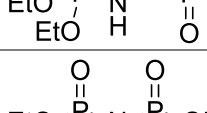
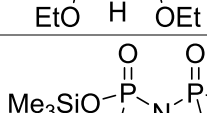
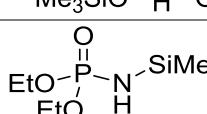
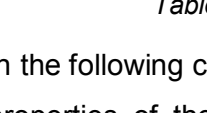
Compound	Abbreviation	MW/ g mol <sup>-1</sup>	Boiling point/ °C	<sup>31</sup> P NMR (δ / ppm)	Physical State
	<b>PP-OEt</b>	274.19	77°C at 1 mmHg	+6.5 (s)	Liquid
	<b>POP-OEt</b>	290.19	135-138°C at 1 mmHg	-13.1 (s)	Liquid
	<b>PP-OTMS</b>	450.70	Melting point 55-57 °C	-10.1 (s)	Solid
	<b>POP-OTMS</b>	466.70	decomposes at 150°C	-30.8 (s)	Liquid
	<b>PNN-OEt</b>	168.13	160 – 162°C	8.4 (s)	Liquid
	<b>PNNP-OEt</b>	304.22	Melting point 99 – 100 °C	6.8 (s)	Solid
	<b>PNP-OEt</b>	289.20	Decomposes at 145°C	-0.36 (s)	Liquid
	<b>PNP-OTMS</b>	465.12	Decomposes at 152°C	-17.3 (s)	Solid
	<b>PN-TMS</b>	304.22	Melting point 53°C	9.3 (s)	Solid

Table 3.1: Table of characterisation of compounds reported in this chapter

In the following chapters, we present the findings of our investigation into the flame retardant properties of these compounds applied onto cotton textiles using various techniques of characterization.



# **Chapter 4**

## **Phosphorus and Silicon - Phosphate Silyl Esters**

## 4.1 Earlier Investigations on Tetrakis(trimethylsilyl) Hypophosphate

In 2006, Ruffin in her thesis<sup>32</sup> reported a loss in weight of the **PP-OTMS** impregnated on cotton textile after the sample was exposed to air (Figure 4.1). The textile sample was first treated with 35.5 wt% of **PP-OTMS**. This loading registered a sharp decrease to 18.9 wt% within 30 minutes of contact with air and remained at 18.9 wt% thereafter.

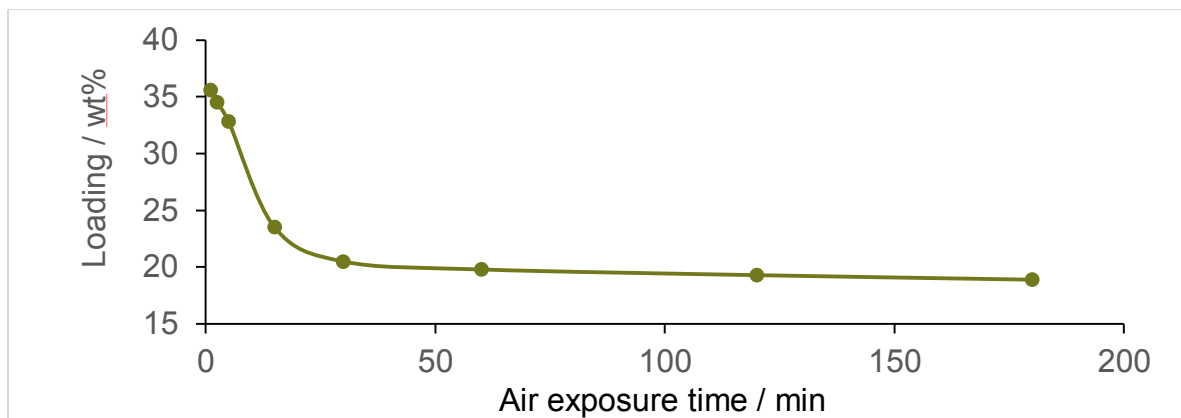


Figure 4.1: The decrease in the wt% loading of a cotton sample treated with **PP-OTMS** after exposure to air.

When the flammability of treated sample was measured after different durations of exposure to air, the LOI which was initially low at 21 at 35.6 wt% significantly increases to 37 at 18.9 wt% loading. The observed decrease in loading is directly correlated to an increase in the LOI (Table 4.1).

Compound on textile	Exposure in air / min	Loading / wt%	LOI
<b>PP-OTMS</b>	1	35.6	21
<b>PP-OTMS</b>	120	18.9	37

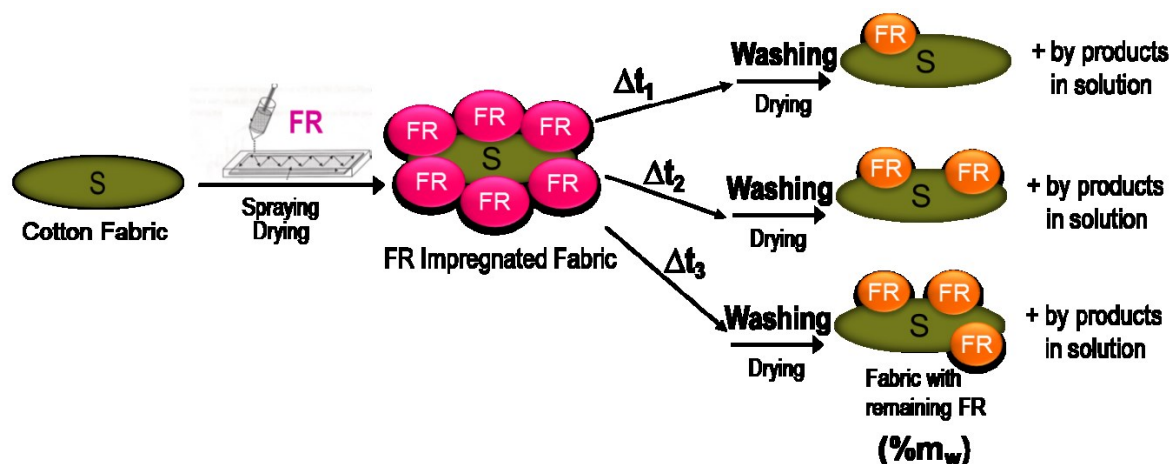
Table 4.1: The loadings of **PP-OTMS** on cotton textile and their corresponding LOI after different durations of exposure to air<sup>32</sup>.

Elemental analyses of the samples show that despite the decrease in loading, the phosphorus content was found to be the same as the initial added amount. Further investigations revealed that the loss of loading, together with the increase of LOI, can be attributed to the loss of trimethylsilyl side groups of the **PP-OTMS** molecule via hydrolysis.

With evidence from IR spectroscopy, Ruffin then proposed that beyond two hours, the active species that is responsible for the increased LOI value for cotton textile has a structure similar to that of hypophosphoric acid  $[P_2O_6]^{2-}$ , resulting from a complete hydrolysis of the initial form, **PP-OTMS**.



Here we performed additional experiments where **PP-OTMS**-treated textiles are washed with dichloromethane (solvent of the PP-OTMS) after increasing intervals (15 to 150 min.) of air exposure. The FR loading is then determined again and its flammability is measured. The content of the washing solution was also analysed.. The scheme of this experiment is illustrated in Scheme 4.1 and the results are tabulated in Table 4.2.



Scheme 4.1: A study to probe the nature of interaction between the FR and the fabrics.

$\Delta t$ (min)	$\%m_w$ (wt%)	LOI	By products in washing solution
15	4.4	22.7	Desilylated FR, HMDSO
30	5.5	23.8	Desilylated FR, HMDSO
120	8.4	31.2	HMDSO ( $\text{Me}_3\text{SiOSiMe}_3$ )

Table 4.2: Loading of FR on washed fabric with corresponding LOI and by products in washing solution.

Table 4.2 shows that when the treatment interval increases from 15 minutes to 2 hours, more FR remains on the surface and they are no longer soluble in the same organic solvent that was used for the impregnation. This suggests that reaction between the FR and surface of cotton textiles could have taken place. The increasing LOI with the loading ( $\%m_w$ ) confirms that the loading is the FR and not something else. In the washing solutions, HMDSO was detected for all durations of FR treatment, and desilylated FR compounds were identified at shorter treatment times. This investigation shows that the loss of loading during the impregnation of **PP-OTMS** is related to the loss of TMS groups. With increasing treatment time, more **PP-OTMS** hydrolyse and interact with the surface of cotton textiles. This leads to the observed LOI increase with longer duration of treatment.

## 4.2 The Objective of our investigation in this Chapter

As an extension to this study<sup>32,37</sup>, we aim to further investigate if this phenomenon could be attributed to the presence of phosphorus-phosphorus bond, or the silyl ester side groups. For this purpose we decide to find out if structurally related compounds behave in similar manner in terms of flame retardancy. An analogue of hypophosphate (direct P–P bond) is pyrophosphate, which contain a bridging oxygen atom between the phosphorus atoms. An analogue of silyl ester would be ester groups. The concept behind this investigation is illustrated in the following Figure 4.2.

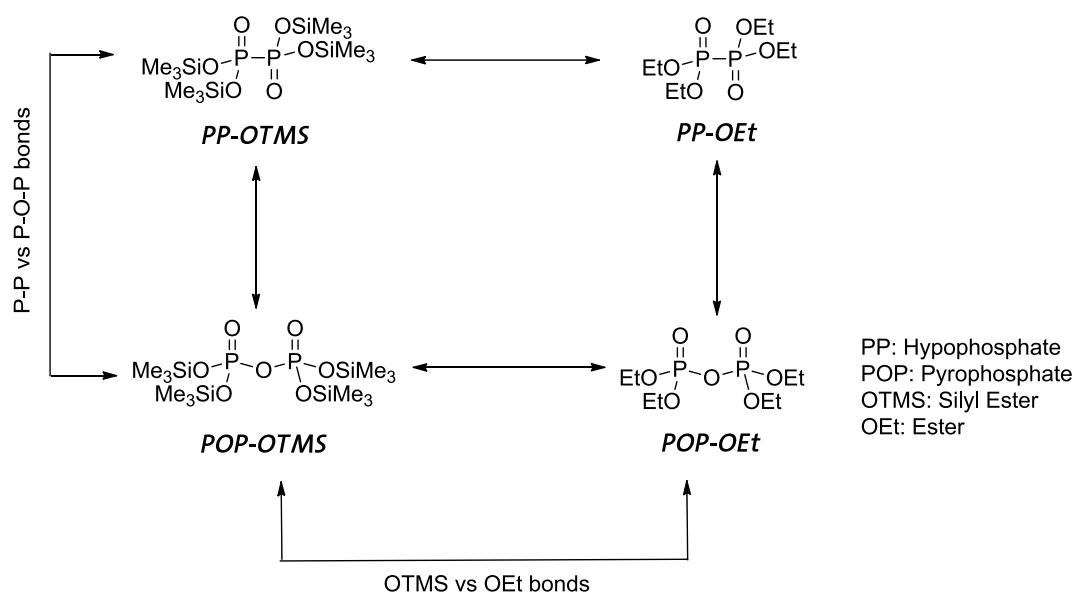


Figure 4.2: Investigation of two possibilities of origin of the LOI behavior discovered in **PP-OTMS** on cotton textiles.

After the synthesis of a series of compounds of similar structures (reported in chapter 3), we then characterized their flame retardant properties via thermogravimetric and evolved gas analyses, heat release studies via PCFC and LOI measurements. Other than that we also analysed the surface of the FR treated cotton textiles.

### 4.3 Impregnation of Flame Retardants onto Cotton Textiles

Prior to the flammability investigation, these compounds are applied via impregnation onto the surface of cotton textiles. Here, textiles are cut into dimensions of 5 cm x 10 cm with weigh ( $0.97 \pm 0.05$ ) g. The FR compounds are weighed from 1% to 5% P to the weight of the textile and then dissolved in THF (due to its volatility) at room temperature in air for a liquor-to-good ratio of 1.3 to 1. This is to ensure that the covering of the entire surface of the textile with just enough volume of the solution. Using a syringe, the solution was then carefully transferred dropwise across the surface of cotton textiles. Thereafter, the samples are left for at least two hours in air at room temperature to allow complete evaporation of THF and treatment of the FR on cotton textiles.

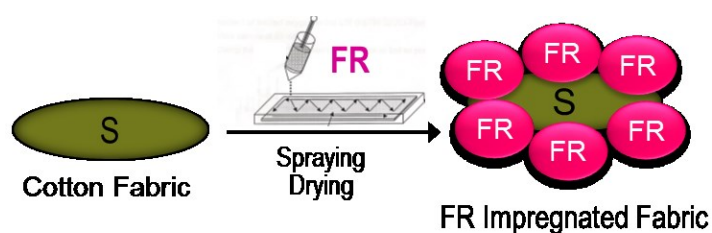


Figure 4.3: Impregnation of FR compounds onto the surface of cotton textiles

Considering the loss in FR loading on the textiles during the initial period of impregnation, the weight of the FRs on cotton textile is monitored before and after at least 2 hours of impregnation in air at room temperature. For the phosphate silyl esters, **PP-OTMS** and **POP-OTMS**, the final and initial phosphorus content on the textile samples remains similar despite an approximately 50% decrease in the loading after impregnation (Table 4.3). This is unlike their corresponding phosphate esters, **PP-OEt** and **POP-OEt**, where the initial and final loadings and phosphorus contents remain relatively constant after impregnation. The same behavior of **PP-OTMS** has been observed by Ruffin, and **POP-OTMS** behaves similarly to **PP-OTMS**.

Compound on textile	Feed loading (wt%)		% Phosphorus	
	Initial	Final	Initial (Calc)	Final (EA)
<b>PP-OTMS</b>	10.2	3.4	1.3	1.1
<b>PP-OTMS</b>	15.0	7.4	2.0	2.0
<b>POP-OTMS</b>	7.8	3.6	1.0	1.0
<b>POP-OTMS</b>	16.2	7.7	2.2	2.1
<b>PP-OEt</b>	4.6	3.9	1.2	1.0
<b>PP-OEt</b>	9.1	8.0	2.4	2.3
<b>POP-OEt</b>	10.1	9.7	1.0	0.9
<b>POP-OEt</b>	19.1	18.9	2.1	1.9

Table 4.3: The initial and final loadings of FR on cotton based on wt% and P content.

## **4.4 Flammability Studies of the FR-treated Cotton Textiles**

After the impregnation of the textiles with FR compounds, we then investigated the flammability of these samples. Because of the loss of weight after impregnation, it is important to note that unless otherwise mentioned, the flammability studies for all samples were performed on FR-treated textile samples more than two hours after their impregnation step.

We employ three techniques to study the flammability of the FR-treated cotton textiles. Firstly, LOI measurements provide us a first and direct indication of their performance as flame retardants. Secondly, TGA-FTIR-MS analyses supply information on the decomposition profile of the cotton textiles, as well as on the identities of evolved gases from the decomposition of the FR-treated textile samples. PCFC, on the other hand, would enable us to obtain a better understanding on how these FR species affect the heat release during the decomposition of the flame retarded cotton textiles.

### **4.4.1 LOI measurements**

Untreated cotton textiles of density 210 g/m<sup>2</sup> burns at an LOI of 17.5 ± 0.3. This value should increase if phosphorus-based flame retardants are present on the textiles. A flame retardant is considered good if its treated substrate has an LOI of 26 at 3% P. The following Figure 4.4 depicts how the LOI values of the FR-treated textiles vary with increasing content of **PP-OEt** and **POP-OEt** on the textiles.

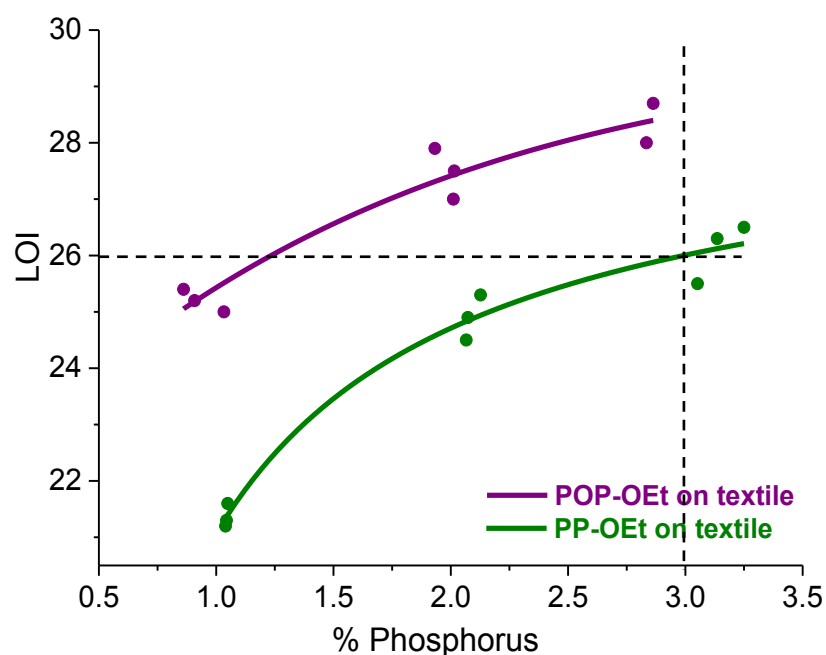


Figure 4.4: The variation of LOI with increasing phosphorus content for cotton textiles treated with **PP-OEt** and with **POP-OEt**.

In general, the LOI of **PP-OEt**- and **POP-OEt**- treated textiles increase with increasing phosphorus content, but the increase is non-linear and the evolution tends to reach a plateau value beyond 3% P. While textiles treated with **PP-OEt** achieves LOI 26 at 3% P, those with **POP-OEt** register the same LOI already at 1.25% P. Across all the loadings, textiles with **POP-OEt** display on average at least 2 LOI units higher than textiles treated with **PP-OEt**. This indicates a better performance of **POP-OEt** compared to **PP-OEt** on cotton textiles.

Unlike phosphate esters, textiles treated with the corresponding silyl esters show remarkably different LOI behavior: the LOI increases linearly with the increase in phosphorus content (Figure 4.5).

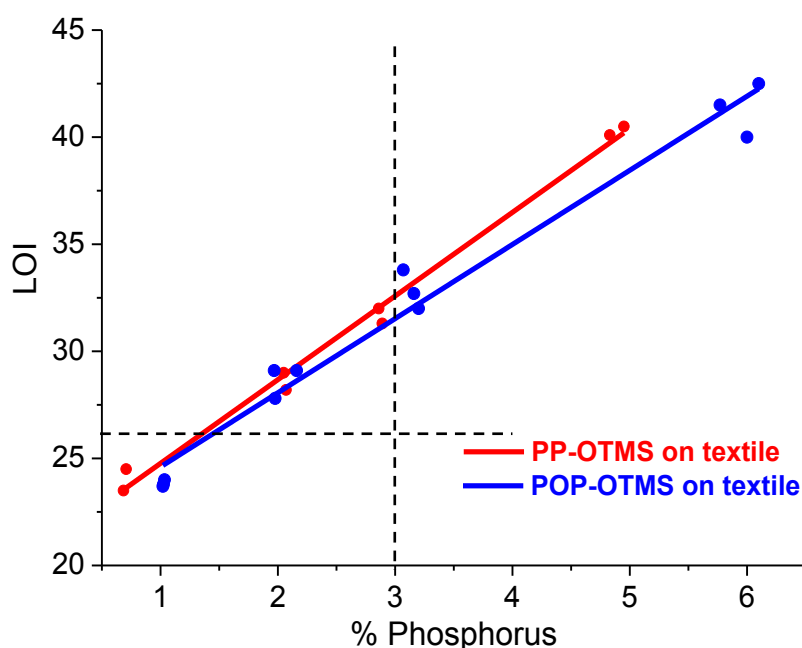


Figure 4.5: The variation of LOI with increasing phosphorus content for cotton textiles treated with **PP-OTMS** and with **POP-OTMS**.

This linear trend is observed in both textiles treated with **PP-OTMS** and with **POP-OTMS**. At as low as 1.5% P, the LOI for both FR-treated textiles reached 26. Compared to textiles treated with **POP-OTMS**, those treated with **PP-OTMS** show higher LOI beyond 1.5% P, indicating its slightly better performance at higher phosphorus loadings.

Relative to textiles treated with phosphate esters, those treated with phosphate silyl esters in general display higher LOI values, exceeding 30 at 2% P and still increases linearly with FR content. The above observations show that textiles treated with **POP-OEt** perform better than those treated with **PP-OEt**, but the difference in the performance of silyl ester-treated textiles (**POP-OTMS** and **PP-OTMS**) is much larger than those treated with esters (**PP-OEt** and **POP-OEt**).

### **Molecular Size and Phosphorylation**

Here it is important to note that the LOI values of textiles treated with **POP-OEt** and those treated with **POP-OTMS** are similar at 1.5% P. This is because at lower FR concentration, regardless of molecular size and temperature, the cellulose phosphorylation is similar in terms of the amount of sites being phosphorylated. At higher FR contents, **POP-OEt** is bigger in size

than **POP-OTMS**, which has lost its TMS groups. Therefore phosphorylation by the latter becomes more efficient under heat or at room temperature.

If it is indeed the loss of TMS groups in silyl ester which leads to an enhancement in its flammability, we would expect similar flammability behavior from textiles treated with tris(trimethylsilyl) phosphate (herein denoted as **P-OTMS**) and textiles treated with ortho-phosphoric acid (**H<sub>3</sub>PO<sub>4</sub>**). The following Figure 4.6 depicts the LOI behavior of the FR-treated textiles with increasing phosphorus content.

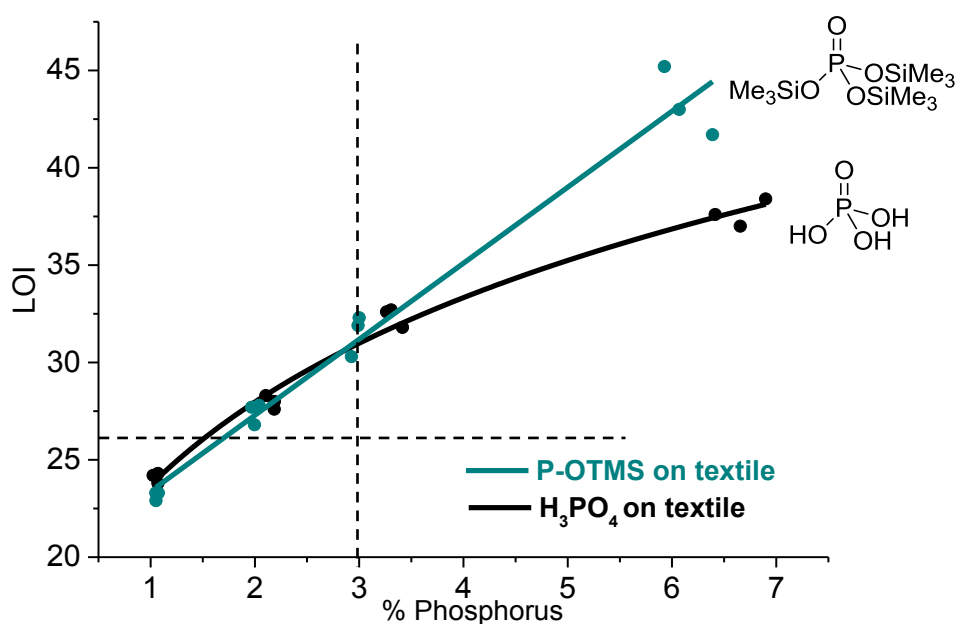
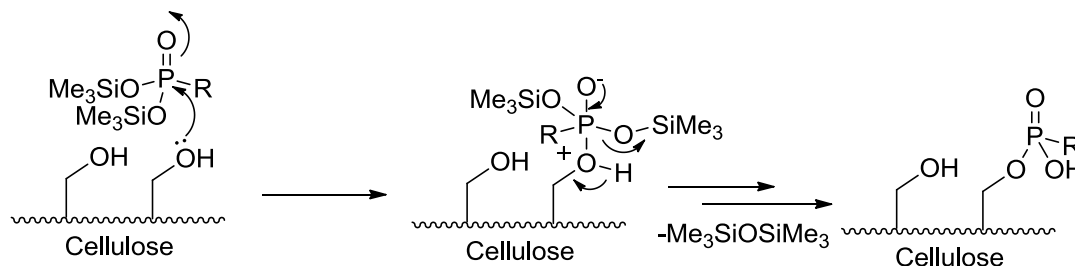


Figure 4.6: The variation of LOI with increasing phosphorus content for cotton textiles treated with **P-OTMS** and with **H<sub>3</sub>PO<sub>4</sub>**.

From this graph, both textiles with **P-OTMS** and **H<sub>3</sub>PO<sub>4</sub>** exhibit similar LOIs lower P contents up to 3%. Beyond this point, the LOI for textiles with **H<sub>3</sub>PO<sub>4</sub>** do not increase as fast as those treated with **P-OTMS**. As for textiles treated with **P-OTMS**, the linearity in LOI with the increase in P content is more pronounced. This is similar to what we previously observed for textiles treated with **PP-OTMS** and **POP-OTMS**.

As textiles with **P-OTMS** exhibit a similar LOI behavior to those of **PP-OTMS** and **POP-OTMS**, we could see that the OTMS groups, or silyl esters, are in common for all the three species, and we have found that these groups are lost through hydrolysis on cotton textiles. It is apparent here that the loss of silyl ester groups has a stronger influence on the flame retardant performance, as opposed to how the phosphorus atoms are surrounded in the molecular

structures. As  $H_3PO_4$  is the product of complete hydrolysis of **P-OTMS**, one would expect the LOI behavior of **P-OTMS** treated textiles, and by extrapolation the other silyl ester-treated textiles, to be similar to that those treated with  $H_3PO_4$ . However, the slower increase in LOI with P content in the textiles treated with  $H_3PO_4$  contradicts this argument. Therefore, some processes must have taken place on the cotton textile during the hydrolysis of the silyl esters. Since phosphorylation of cellulose is crucial to the flame retardant property, it is likely that this has taken place during the hydrolysis of the silyl esters on cotton textiles at room temperature. This explains the release of hexamethyldisiloxane as illustrated in the following Scheme 4.2.



Scheme 4.2: A possible phosphorylation of cellulose by phosphate silyl esters at RT.

With the observed differences in the LOI behavior, we are interested to find out if the thermal decomposition and heat release behavior of the textiles with these investigated FR species are also different from each other. Parallel to our observations in LOI behavior, we expect to see significant differences in the thermal degradation behavior between the phosphate esters and silyl esters, and less between pyrophosphates and hypophosphates.

#### 4.4.2 Thermal Decomposition Studies of various compounds on textiles

In this technique, about 2 mg samples from the textiles are cut out and heated in a crucible at  $10\text{ K min}^{-1}$  heating rate from  $40\text{ }^\circ\text{C}$  to  $900\text{ }^\circ\text{C}$  under an argon flow of  $50\text{ cm}^3\text{ min}^{-1}$ . The change in sample mass in relation to the temperature is determined. The presence of flame retardants should lower both the onset temperature of decomposition as well as the mass loss step of the FR-treated textiles. To compare the efficiency between different FR compounds at their conventionally used maximum P content, we performed measurements for the samples treated with 3% P of the FR.

In the following Figure 4.7, the TGA curves of **PP-OEt**, **POP-OEt**, textiles treated with **PP-OEt** and with **POP-OEt** are illustrated, together with their respective first derivative (DTG) curves.



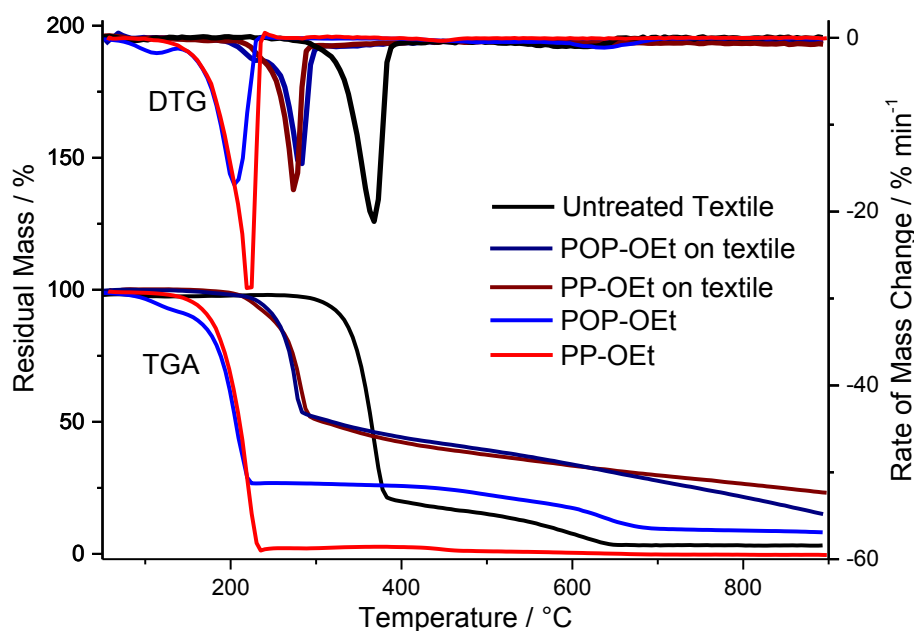


Figure 4.7: TGA and DTG curves of **PP-OEt**, **POP-OEt**, untreated textiles and textiles impregnated with phosphate esters, **PP-OEt** and **POP-OEt**.

From Figure 4.7, **PP-OEt** shows rapid evaporation starting at 192°C, evident from its intense weight loss of 98%. The low residue of 1.5% at 900°C confirms that its vaporisation. In contrast, **POP-OEt** degrades in a three-step process. The onset temperature of decomposition occurs at a much lower temperature of 91°C, but the main decomposition step takes place at similar temperature to **PP-OEt** at 193°C. Between 193°C and 205°C registers the highest mass loss of 63% and can be attributed to the loss of ethanol. This can be confirmed by the MID spectrum which detected in this temperature range intense ion currents for  $m/z = 29$  ( $[C_2H_5]^+$ ) and for  $m/z = 45$  ( $[C_2H_5O]^+$ ). As the remaining 40% of the mass are stable in the range of temperature between 205°C and 500°C, this suggests that **POP-OEt** could exist as a polymeric form carrying a repeating unit of  $[P_2O_7]$ .

The fabric treated with **POP-OEt** decomposes in a two-step process. **PP-OEt**-treated textile gives a similar TGA curve. The decomposition of textile with **POP-OEt** begins at 263°C, 10°C higher than that for textiles with **PP-OEt**. In both cases, these temperatures are lower than that of untreated cotton textile, which starts to decompose 357°C. Compared to **PP-OEt**-treated textile, which loses 46% mass in the major decomposition step, the textile with **POP-OEt** loses a smaller amount by 4%. At the end of measurement at 900°C, textiles with **POP-OEt** leaves behind 24% residue, 9% more than that from textiles with **PP-OEt**. The smaller loss of mass and the higher residue suggest that **POP-OEt** performs better than **PP-OEt** when

applied on cotton textiles.

The smaller mass loss step and higher residue displayed by the decomposition of textiles treated with **POP-OEt** suggests that it retains more char compared to **PP-OEt**. From the vaporization of **PP-OEt** at 192°C, there is a possible competition between the vaporization of **PP-OEt** and the phosphorylation the cellulose chains at elevated temperatures. This results in some of the **PP-OEt** vaporizing and being lost as fuel, evident in the lower LOI values of textiles treated by **PP-OEt** at all P contents. In contrast, the degradation of **POP-OEt** that releases ethyl groups could have contributed to its reactivity, favouring the phosphorylation of cellulose and leading to better LOI values in **POP-OEt** treated fabrics.

For **PP-OTMS**, **POP-OTMS** and the textiles treated with **PP-OTMS** and **POP-OTMS** show slightly different TGA and DTG profiles, as presented in the following Figure 4.8.

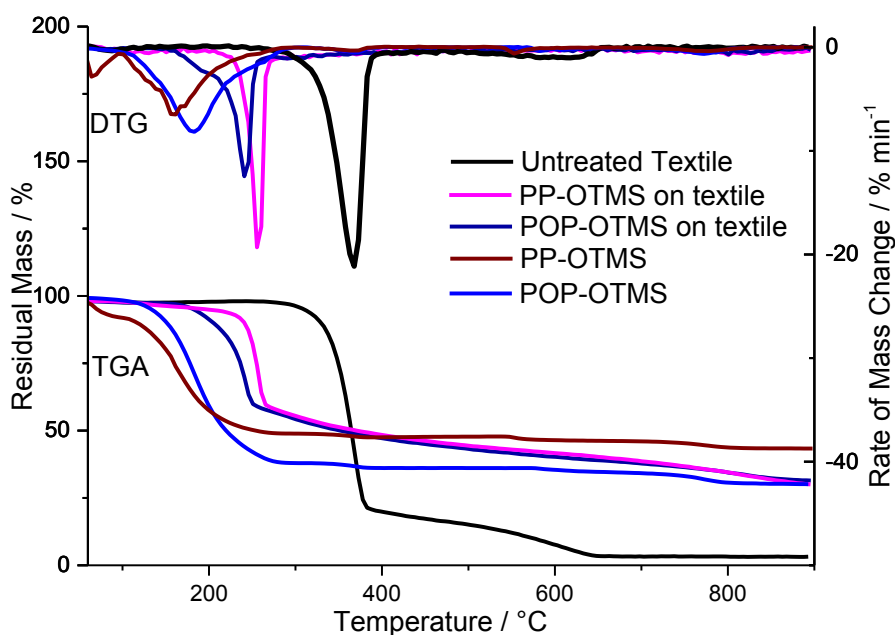


Figure 4.8: TGA and DTG curves of **PP-OTMS**, **POP-OTMS**, untreated textiles and textiles impregnated with phosphate silyl esters, **PP-OTMS** and **POP-OTMS**.

**POP-OTMS** decomposes in a two-step process, beginning at 150°C and loses 61% of its original mass between 150°C and 220°C. This corresponds to the loss of four trimethylsilyl (TMS) groups, and can be confirmed by the MID spectrum which detected in this temperature range ion current for  $m/z = 73$  ( $\text{SiMe}_3$ ). At 900°C, 30% residue is left at the end of degradation. This corresponds to a molecular weight of 140, suggesting that the residue could likely be in the polymeric form of  $[\text{P}_2\text{O}_7]^{4-}$ .

**PP-OTMS** also degrades in a two-step process, which begins at 60°C. Between 60°C to 90°C it loses 6.6% mass. The MID spectrum detected ion currents for  $m/z = 74$  ( $[\text{SiMe}_3]^+$ ) and  $m/z = 147$  ( $[\text{Me}_3\text{Si-SiMe}_3+\text{H}]^+$ ). This indicates a substoichiometric release of TMS groups at this stage. The following stage between 120°C to 290°C registers a mass loss of 43%, indicating the loss of about 2 TMS groups. At 900°C, 43% residue is left at the end of the thermal decomposition. Corresponds to a molecular weight of 194 and signifies a net loss of 3.5 TMS groups.

In the presence of the silyl ester species, the TGA curve of textile treated with **POP-OTMS** shows that it degrades in a two-step process, unlike that treated with **PP-OTMS** which degrades in a single mass-loss step. While the onset temperature of decomposition is higher for textiles treated with **PP-OTMS** (263°C) than those with **POP-OTMS** (186°C), the total mass loss steps are very similar at 37%. At the end of measurement at 900°C, both samples also leave 31% residue.

The lower onset temperature of decomposition of **PP-OTMS** shows that the loss of TMS groups occurs at a lower temperature, allowing more efficient phosphorylation of cellulose to take place. As a result, **PP-OTMS** appears to exhibit slightly better flame retardant properties compared to **POP-OTMS**. This explains the previous observation the slightly higher LOI of textiles treated with **PP-OTMS** compared to those treated with **POP-OTMS**.

Presented in Figure 4.9, we next analyze the thermal decomposition behavior of textiles treated with **P-OTMS** and **H<sub>3</sub>PO<sub>4</sub>**.

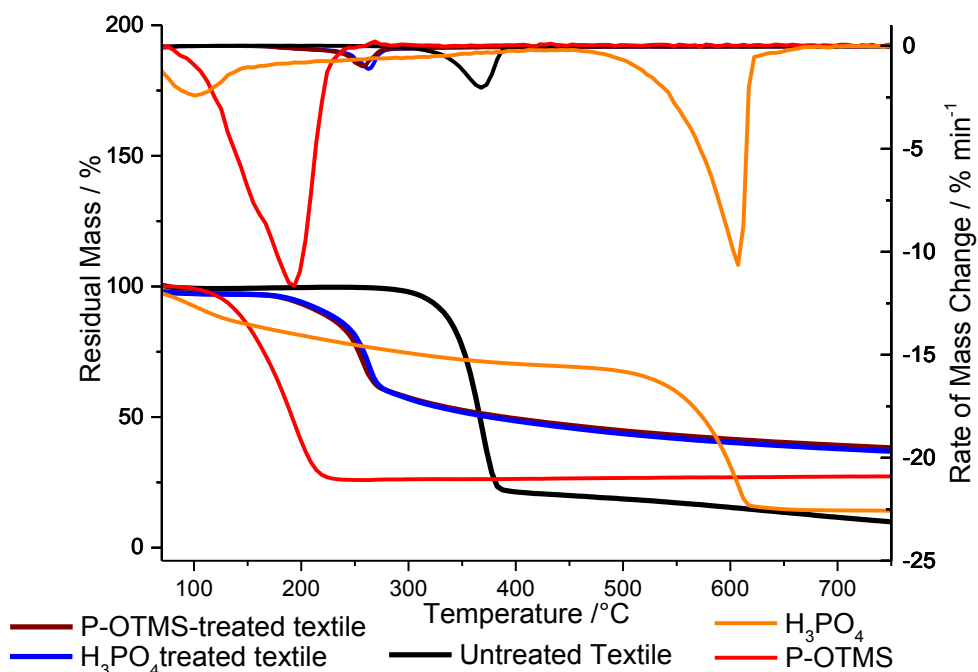


Figure 4.9: TGA and DTG curves of untreated textiles and textiles impregnated with **P-OTMS** and **H<sub>3</sub>PO<sub>4</sub>**.

The TG curves of textiles treated with **P-OTMS** and **H<sub>3</sub>PO<sub>4</sub>** show similar thermal decomposition profiles to the fabrics impregnated with **PP-OTMS** and **POP-OTMS**, with one slower mass loss step beginning at a lower temperature of 168°C, similar to the fabrics treated with **POP-OTMS**. The mass loss step is 26%, 9% smaller than those of textiles treated with **PP-OTMS** and **POP-OTMS**. At 900°C, these treated textiles both give 34% residue. The mass loss step of **P-OTMS** begins at 135°C and occurs through 220°C, and **H<sub>3</sub>PO<sub>4</sub>** is already releasing water from 60°C. This suggests the possibility for phosphorylation to take place at temperatures before the cotton textile begins to decompose.

In the TG curve of **H<sub>3</sub>PO<sub>4</sub>**, the residual mass of 75% that remains over a broad temperature range between 300°C and 544°C suggests that the initial mass loss is related to the polycondensation reaction that generates polyphosphoric acid. This in turn introduces a competition between condensation reaction and cellulose phosphorylation. This effect becomes stronger at higher concentrations of **H<sub>3</sub>PO<sub>4</sub>** and explains the previous observation that the LOI of **H<sub>3</sub>PO<sub>4</sub>**-treated textiles increases relatively slower than fabrics treated with **P-OTMS** at higher P content.

#### 4.4.3 Heat Release Studies on the Flame Retardants on Cotton Textiles

The heat release profile of pyrolysis products of relevant materials provides another key understanding of its flame retardant properties. This profile can be measured via PCFC, where the rate of heat release with increasing temperature can be charted through the amount of oxygen consumed during the combustion of pyrolysis products of the materials. A typical sample of 2 mg is obtained from the FR-treated textiles, and heated on an alumina crucible at the rate of  $1 \text{ Ks}^{-1}$  from  $120^\circ\text{C}$  to  $750^\circ\text{C}$ . The consumption of oxygen from the combustion of pyrolysis products are measured during the heating and converted to the rate of heat release via oxygen consumption calorimetry. For the purpose of comparison between different

Figure 4.10 illustrates the heat release (HR) curves of **POP-OEt**, untreated cotton textiles and textiles treated with **PP-OEt** and **POP-OEt** at 2% P.

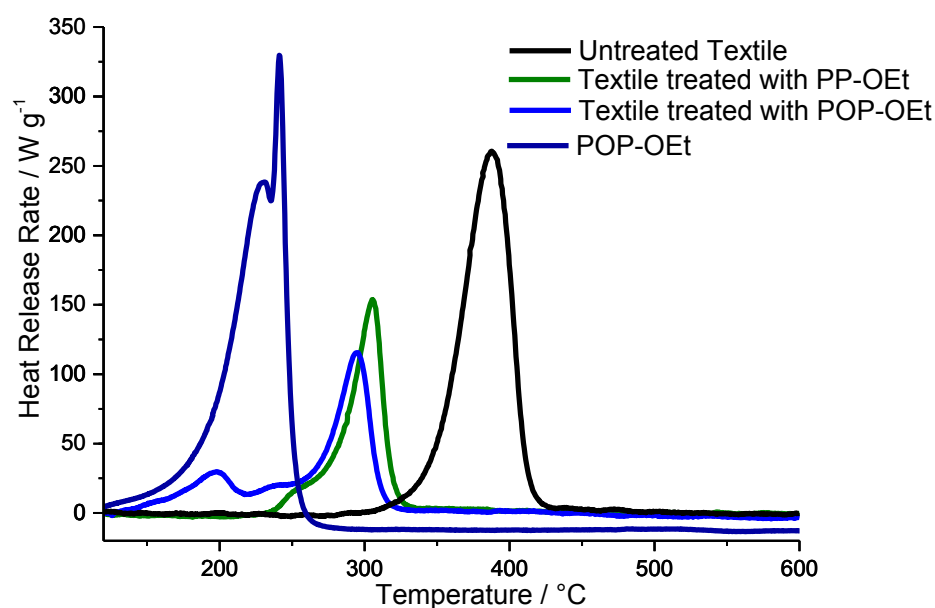


Figure 4.10: Heat release profiles of untreated textiles and textiles treated with **PP-OEt** and **POP-OEt**.

The HR curve of **POP-OEt** shows two heat release events, with one maximum occurring at  $225^\circ\text{C}$  and the other at  $240^\circ\text{C}$ . Although the temperature of these maxima shifted to slightly lower temperatures on the HR curve of textile treated with **POP-OEt**, it is evident that the two minor peaks at  $193^\circ\text{C}$  and at  $235^\circ\text{C}$  originated from the pyrolysis of **POP-OEt** molecules. The major heat release event with the maximum heat release rate at  $295^\circ\text{C}$  is associated with the cotton fabrics that are flame retarded with **POP-OEt**. In contrast to this, the HR curves of textiles treated with **PP-OEt** shows only one major heat release event with the maximum heat

release rate occurring at 297°C and a bump at 266°C. As the onset of decomposition of textiles treated with **PP-OEt** occurs at 253°C, the bump at 266°C can be associated to the vaporization of **PP-OEt** from the fabric sample. In both cases, we observe reductions in the THR and HRC values. This indicates the flame retardant characteristics of **PP-OEt** and **POP-OEt**.

In contrast to the multiple heat release events observed in the HR curves of textiles treated with **PP-OEt** and **POP-OEt**, the HR curves of textiles treated with **PP-OTMS** and **POP-OTMS** exhibit only a single heat release event. This is despite the two heat release events in the pyrolysis of **POP-OTMS** (Figure 4.11). Owing to the difference in the heating rates in PCFC and in TGA, it is probably a coincidence that the maximum heat release occurs at similar temperatures for **POP-OTMS** and the fabrics treated therewith.

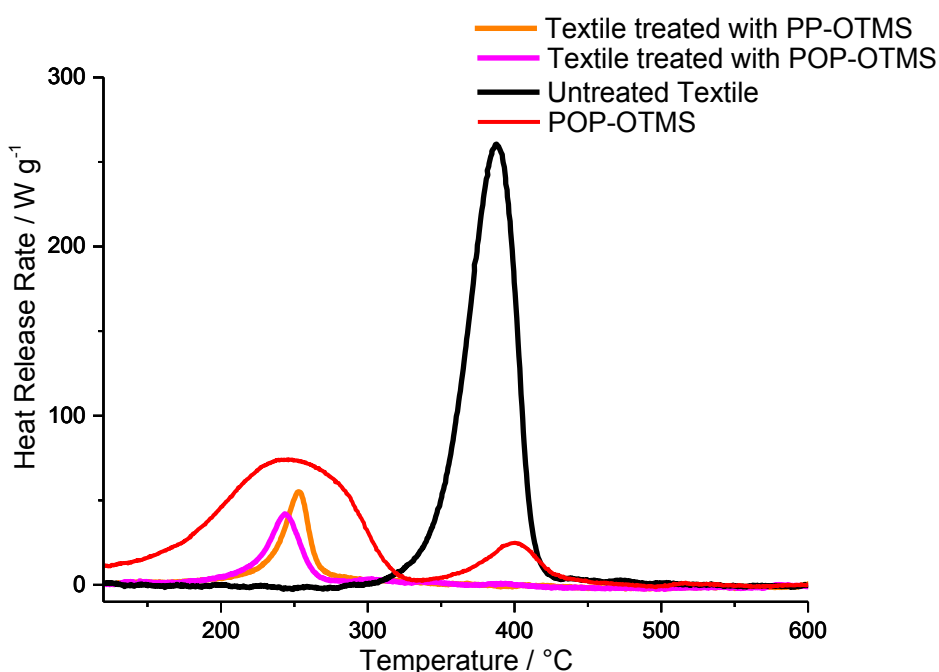


Figure 4.11: Heat release profiles of untreated textile and textiles treated with **PP-OTMS** and **POP-OTMS**.

Similar to the one-step mass loss in their respective TGA curves, the single heat release events in the pyrolysis of fabrics treated with **POP-OTMS** and **PP-OTMS** corresponds to the flame retarded fabrics. Their flame retardant efficiencies are particularly highlighted in their THR and HRC values, where reductions of more than 85% is observed for THR and more than 76% is observed in HRC. These suggest that most of them have been trapped in the condensed phase, which subsequently interferes strongly with the pyrolysis of the cellulose chains. These again suggest that these silyl esters have a higher efficiency in cellulose phosphorylation, as thereby contributing to the much better flame retardant properties relative

to **PP-OEt** and **POP-OEt** observed in the LOI and TGA measurements.

Similar to those of textiles treated with **PP-OTMS** and **POP-OTMS**, the HR curves for fabrics treated with **P-OTMS** and **H<sub>3</sub>PO<sub>4</sub>** also exhibit single heat release events (Figure 4.12). Again, this indicates that much of these FRs are trapped in the condensed phase which inhibits pyrolysis of the cotton textiles.

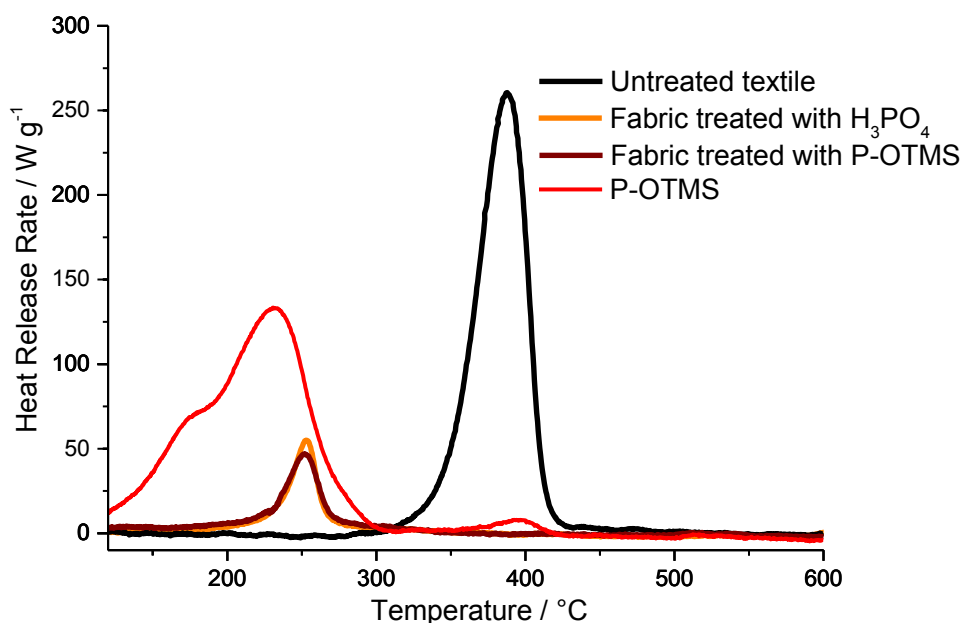


Figure 4.12: Heat release profiles of untreated textile and textile samples treated with **H<sub>3</sub>PO<sub>4</sub>** and **P-OTMS**.

While the temperature at maximum heat release for **P-OTMS** occurs at 230°C, those for cotton textiles treated with **P-OTMS** and **H<sub>3</sub>PO<sub>4</sub>** occurs at just slightly higher temperatures at 250 °C. The THR values reduced by more than 80%, and the HRC reduce by at least 85%. All these observations exhibit close similarities to the textiles treated with **PP-OTMS** and **POP-OTMS**, hence their similar efficiencies in the phosphorylation of cellulose.

The following Table 4.4 illustrates how each of the PCFC parameters varies with the P contents of each FR species on cotton textiles.

Compound on Textile	P content / %	$T_{pHRR} / ^\circ\text{C}$		avg HRC <sub>sum</sub> / $\text{kJ g}^{-1} \text{K}^{-1}$	avg THR / $\text{W g}^{-1}$
		$T_1$	$T_2$		
None (Untreated)		392 (4)		330 (4)	10.9 (1)
<b>PP-OEt</b>	1	141 (2)	305 (5)	240 (5)	7.1 (3)
	2	266 (6)	295 (2)	188 (2)	4.77 (4)
	3	164 (4)	282 (4)	159 (2)	3.7 (9)
<b>POP-OEt</b>	1	300 (1)		151 (4)	6.3 (1)
	2	193 (3)	297 (2)	138 (11)	5.6 (3)
	3	204 (6)	288 (2)	120 (9)	5.17 (4)
<b>PP-OTMS</b>	1	266 (5)		95 (7)	2.33 (2)
	2	262 (3)		76 (6)	1.6 (5)
	3	247 (11)		92 (8)	1.56 (2)
<b>POP-OTMS</b>	1	260 (12)		61 (7)	2.0 (4)
	2	244 (1)		44 (1)	1.33 (4)
	3	249(2)		51 (1)	1.27 (4)
<b>P-OTMS</b>	1	284 (3)		94 (5)	2.7 (2)
	2	253 (2)		54 (2)	1.43 (5)
	3	240 (1)		44 (1)	1.27 (4)
<b>H<sub>3</sub>PO<sub>4</sub></b>	1	272 (2)		78 (2)	2.4 (1)
	2	249 (2)		49 (1)	1.65 (2)
	3	242 (1)		46 (1)	1.31 (1)

Table 4.4: PCFC parameters for phosphate esters and phosphate silyl esters of various phosphorus content on cotton textiles. The errors are indicated in parentheses.

In general, treated with silyl esters and phosphoric acid, the cotton textiles exhibit only one heat release event, with THR values decrease by at least 85%, and the HRC values remain below  $100 \text{ kJ g}^{-1} \text{K}^{-1}$  from 1% P to 3% P. These values indicate the self-extinguishing properties of the flame retarded textiles in ambient air.

With increasing P content, the average **THR** values increase for textiles treated with **PP-OEt** and **POP-OEt**, but decrease for the fabrics treated with **PP-OTMS**, **POP-OTMS**, **P-OTMS** and **H<sub>3</sub>PO<sub>4</sub>**. Also, except for textiles treated with **POP-OEt** at 1% P, at least two heat release events have been observed in the textiles treated with **PP-OEt** and **POP-OEt** from 1% P to 3% P. This highlights the competing events of decomposition of the FRs and their efficiencies in the



phosphorylation of cellulose. At higher P contents more FRs decompose without phosphorylation, giving rise to the multiple heat release events in PCFC, the multiple mass loss steps in TGA, and the slower increase on LOI at higher P contents because more FRs are lost as fuels.

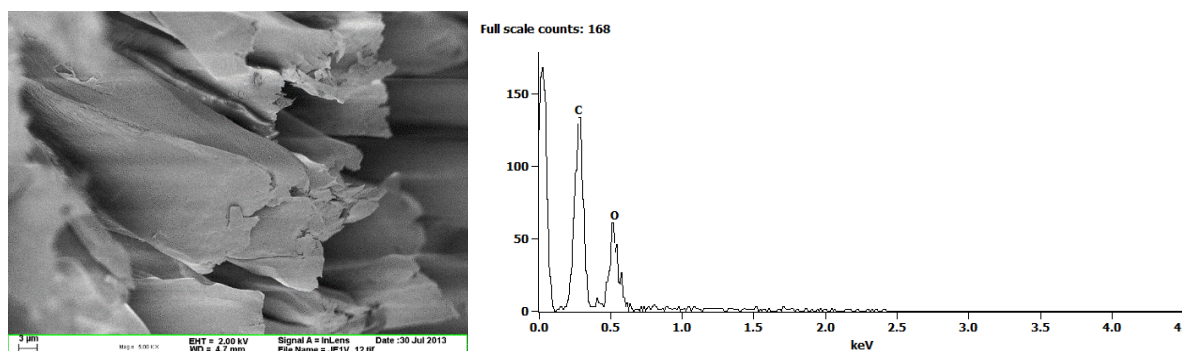
From analyses via PCFC, TGA and LOI, we learned that the phosphate silyl esters have similar efficiencies in the phosphorylation of cellulose. This explains their excellent flame retardant behavior compared to those of phosphate esters. However the flammability measurements do not indicate at which temperature phosphorylation occurs. Since we have found from earlier investigations that the phosphate part of the silyl ester FRs remain on the fabric surface after rinsing with THF, there is a possibility that the phosphorylation is taking place already at room temperature during the impregnation step. It is therefore of our interest to proceed with surface analyses of FR-treated fabrics to study deeper into the interaction between the silyl ester FRs and the surface of cotton textiles.

## 4.5 Surface Analyses of Cotton Textiles treated with Phosphate Silyl Esters

### 4.5.1 Surface Morphology and Profiling of Elemental Distribution via EDX Spectroscopy

The SEM images in Figure 4.13 show the surface of the cotton textile under different scales of magnification after impregnation with **PP-OTMS**. We could observe here that the structure and morphology of the fabric surface remains similar to that of untreated cotton fabric. This indicates that impregnation of phosphate silyl esters does not cause observable changes to the surface morphology of the cotton fabrics.

(i)



(ii)

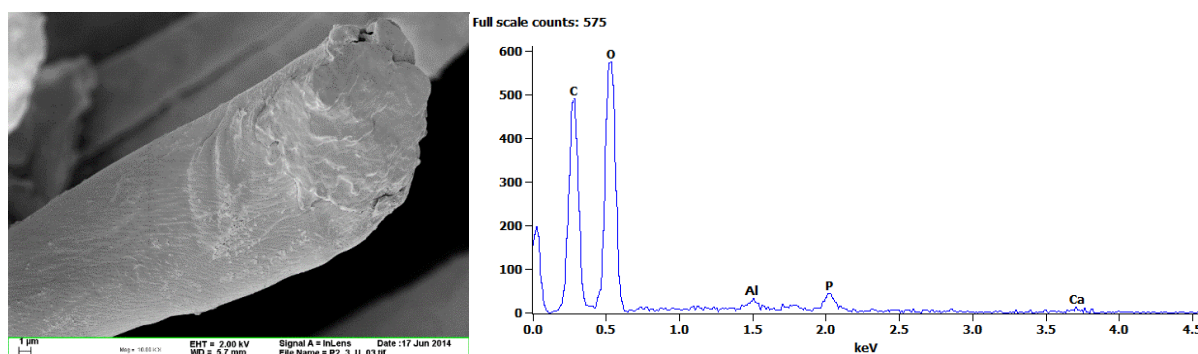


Figure 4.13: **SEM** Images and the corresponding **EDX** spectra of (i) untreated cotton textile; (ii) cotton textile treated with **PP-OTMS**.

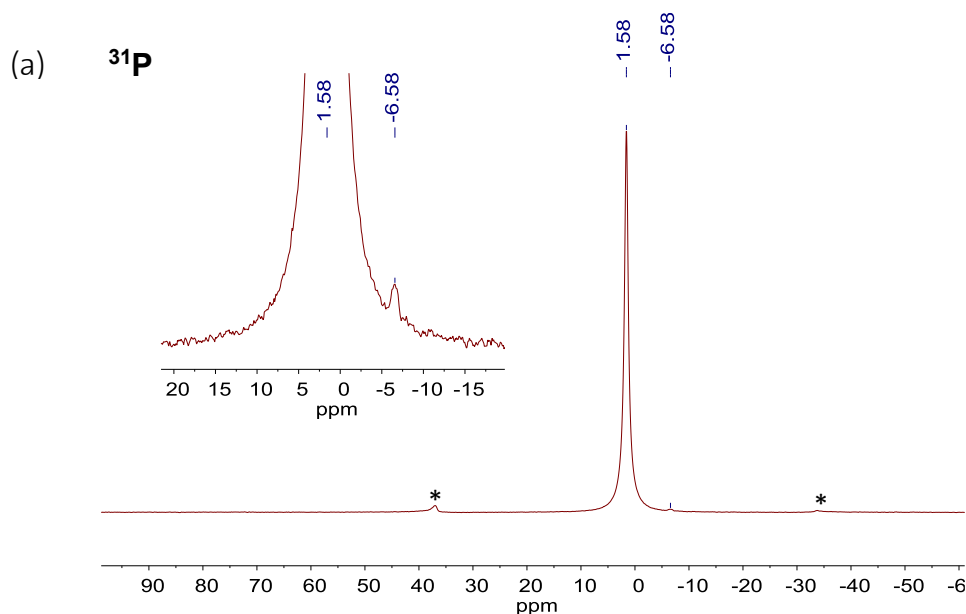
The EDX spectra (Figure 4.13) indicate some residual phosphorus on the surface of the untreated textile. This phosphorus likely originates from the processing of the textile since they are used as purchased. It is also evident here that silicon is absent after the impregnation. This also further complements our earlier observation on the absence of silicon via XPS analysis, confirming the loss of TMS moieties from the original phosphate silyl ester molecules.

All in all, through the above mentioned characterization methods we could deduce that the active form of phosphate silyl ester FRs no longer contain the silyl groups. This allows the reduction in size of the FRs, giving them access to higher number of OH groups for cellulose phosphorylation to take place. In this way, the much improved flame retardancy of phosphate silyl ester FRs is directly related to the chemical modification of the cellulose fibers coupled with the loss of TMS groups.

#### 4.5.2 Characterization of FR-treated textiles by Solid-state NMR Spectroscopy

In attempt to better understand the nature of the interaction between the phosphate silyl ester and cotton textiles, we performed solid-state NMR measurements of the FR impregnated textile samples. The most direct observation would be to obtain through solid-state NMR spectroscopy an evidence of a P–O–C bond. For the ease of spectral interpretation we performed the measurement on cotton textiles treated with the simplest phosphate silyl ester, ***P-OTMS***.

The NMR experiment is performed using cotton textiles treated with ***P-OTMS*** at 5% P placed in a zirconia rotor of 4.0 mm under a MAS frequency of 10,000 rpm. The spectra are displayed in the following Figure 4.14.



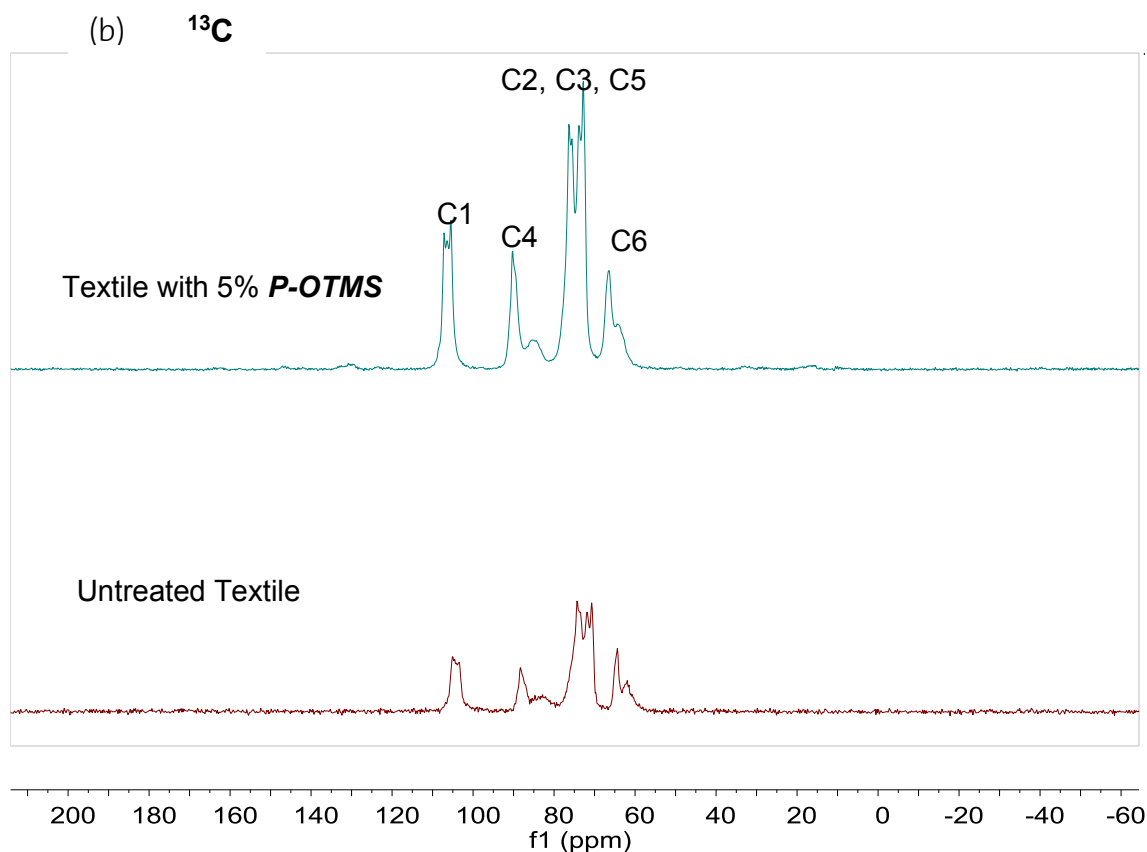


Figure 4.14: Solid-state CP-MAS (a)  $^{31}\text{P}$  (b)  $^{13}\text{C}$  NMR spectra of textiles treated with **P-OTMS** at 5% **P**. The asterisks (\*) denote spinning sidebands.

The solid-state CP-MAS  $^{31}\text{P}$  NMR spectrum of **P-OTMS** treated textile reveals 2 peaks at 1.7 ppm and at -6.1 ppm. Both of these two  $^{31}\text{P}$  peaks have chemical shifts which are significantly distinct from that of **P-OTMS**, which resonates at -26 ppm. The major peak at 1.7 ppm shows that the **P-OTMS** on the fabric surface have lost their silyl ester groups, since this chemical shift is nearest to that of the triply desilylated phosphate silyl ester. The resonance at -6.1 ppm most likely arises from the incomplete hydrolysis of a very small amount of **P-OTMS** on the cotton surface.

Figure 4.14(b) displays the CP-MAS  $^{13}\text{C}$  spectrum of the same FR impregnated fabric. The observed peaks could be assigned to the respective carbons on the cellulose subunits<sup>67</sup>. However, these peaks appear to be similar to that of the untreated cotton fabric. In other words, we could not observe with confidence any changes to the chemical environment of the carbons. Because of issues of sensitivity (relative low natural abundance of  $^{13}\text{C}$  and hence, the concentration of  $^{13}\text{C}-\text{O}-^{31}\text{P}$  will be below the limit of detection of NMR) and resolution, no further conclusive confirmation on room temperature phosphorylation could be made. We henceforth proceed to perform the XPS analysis of the FR impregnated fabric surface.

### 4.5.3 X-Ray Photoelectron Spectroscopy (XPS) Analysis

XPS is a surface analysis technique that measures the elemental composition, giving information on chemical state and electronic state of the elements that exist on the surface of a material. To obtain more information on whether phosphorylation has taken place at room temperature on the FR-treated cotton textiles, we performed XPS measurements on various FR-treated samples.

As XPS instrument operates in ultra-high vacuum ( $10^{-9}$  mbar) and are highly sensitive to moisture, our FR-treated samples have to be subjected to reduced pressure ( $10^{-3}$  mbar) at room temperature for at least 20 days to remove all moisture before measurements can take place. Typically, a low resolution spectrum is first obtained for a survey of the different elements on the surface, followed by the measurement of high resolution spectra for more accurate values of the chemical shifts of each element.

The chemical shifts of the spectra are then compared to those found in the literature listed in Table 4.5.

Compound / Substrate	C1s / eV			P2p / eV
	C-C-H	C-O-H	C-O-C	P-O-C/ $PO_4^{3-}$
<i>Urea/H<sub>3</sub>PO<sub>4</sub>/Cotton Textile</i> <sup>68</sup>	285	Not mentioned	Not mentioned	133.7
<i>Urea/H<sub>3</sub>PO<sub>4</sub>/Chitosan</i> <sup>69</sup>	285	286.6	288.3	133.8
<i>Urea/H<sub>3</sub>PO<sub>4</sub>/Cellulose Nanofibrils</i> <sup>70</sup>	285	286.8	288.2	134.7
<i>Urea/H<sub>3</sub>PO<sub>4</sub>/Kraft fibres</i> <sup>71</sup>	285	286.7	288.1	134.6

Table 4.5: Chemical shifts of the various bonds found in the literature.

### Low Resolution spectra

The following Figure 4.15 depicts the XPS survey spectra of untreated and **P-OTMS** treated cotton textiles.

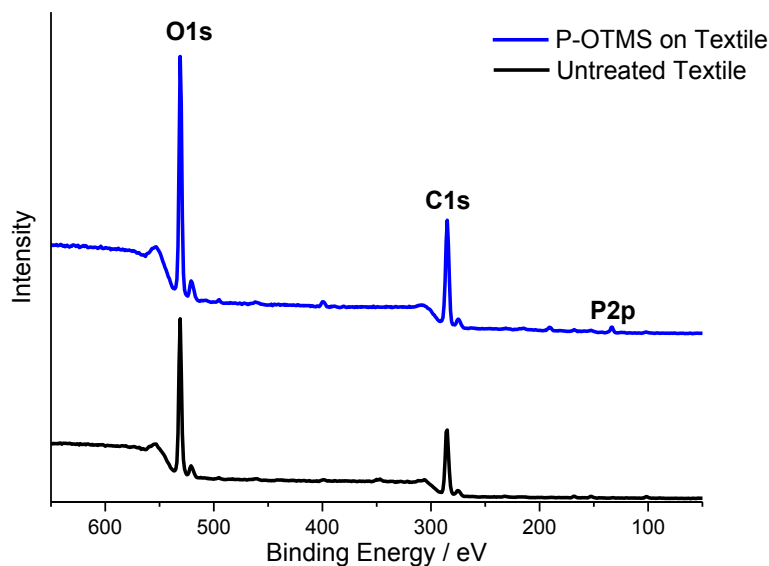


Figure 4.15: XPS Spectra of untreated and cotton fabrics treated with **P-OTMS**.

In untreated cotton textile, two distinct peaks can be observed at binding energies of 285 eV and at 328 eV. They can be respectively attributed to elemental C 1s and O 1s. For the **P-OTMS** impregnated fabrics, additional peaks are also observed at 133 eV and at 190 eV. These peaks are assigned respectively to P 2p and P 1s, indicating the presence of the FR on the textile surface.

It is important to highlight here that no peaks were detected in the range of 100 – 104 eV<sup>72</sup>. As this binding energy is characteristic of Si 2p, this signifies the absence of silicon in the treated samples. Also, in the O1s spectrum, a peak at 534.4 eV<sup>73</sup> was not observed. This is further evidence that TMS groups have been lost from the surface of the phosphate silyl ester after treatment on the textile samples.

### High resolution spectra

In Figure 4.16, the high-resolution scans of the elemental C 1s and P 2p regions are presented for cotton textiles treated with **P-OTMS**.

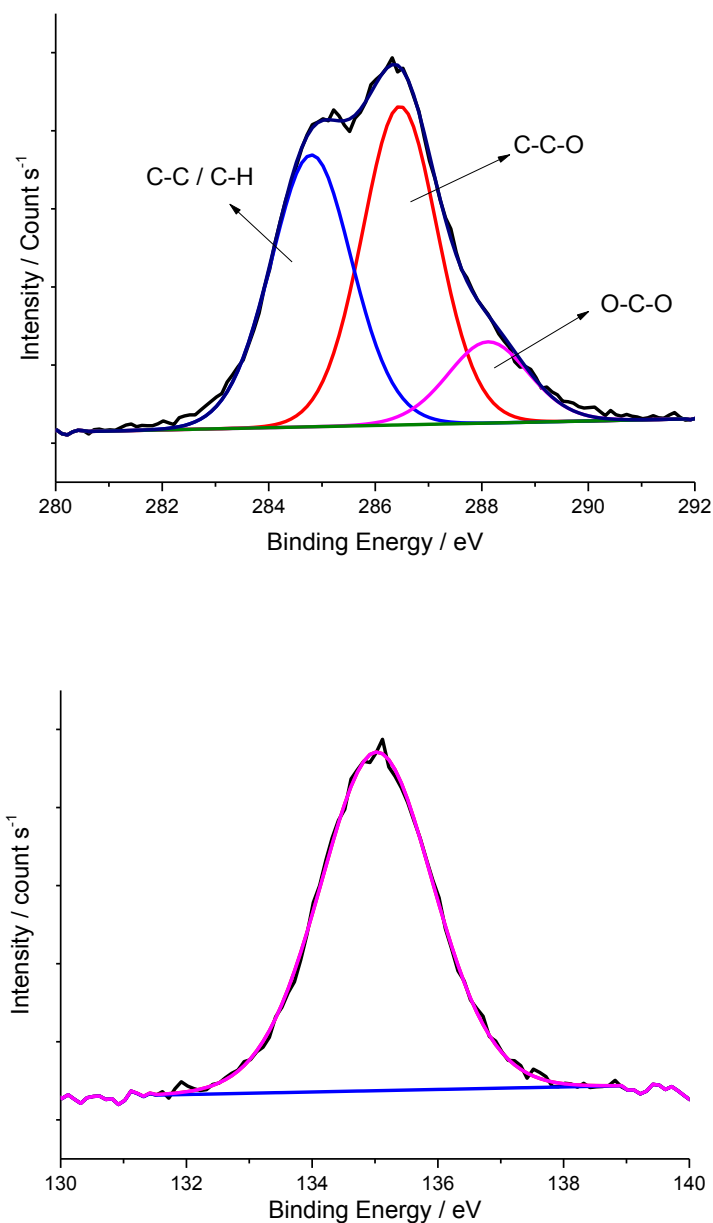


Figure 4.16: High-resolution scans of (i) C 1s; (ii) P 2p for **P-OTMS** treated cotton textiles.

The C 1s spectrum of the untreated cotton textile could be deconvoluted into 3 component peaks: The first component peak centered at 285 eV is attributed to C–C or C–H bonds; the second component centered at 286.5 eV can be attributed to C–C–O bonds; the third component peak at 288 eV is associated with O–C–O bonds. The corresponding values of the FR-treated textile samples are presented in Table 4.6.

	Compound / Substrate	C1s / eV			P2p / eV
		C-C-H	C-O-H	C-O-C	P-O-C/PO <sub>4</sub> <sup>3-</sup>
1	Untreated Cotton Textile	285	286.7	288.4	-
2	<b>H<sub>3</sub>PO<sub>4</sub></b> / Cotton Textile	285	286.6	288.2	135.4
3	<b>P-OTMS</b> / Cotton Textile	285	286.4	287.5	134.9
4	<b>PP-OEt</b> / Cotton Textile	285	286.5	288.3	134.7
5	<b>POP-OEt</b> / Cotton Textile	285	286.3	286.5	135.0
6	<b>POP-OTMS</b> /Cotton Textile	285	286.6	288.2	134.9
7	<b>Urea/H<sub>3</sub>PO<sub>4</sub></b> /Cotton Textile <sup>68</sup>	285	Not mentioned	Not mentioned	133.7
8	<b>Urea/H<sub>3</sub>PO<sub>4</sub></b> /Chitosan <sup>69</sup>	285	286.6	288.3	133.8
9	<b>Urea/H<sub>3</sub>PO<sub>4</sub></b> /Cellulose Nanofibrils <sup>70</sup>	285	286.8	288.2	134.7
10	<b>Urea/H<sub>3</sub>PO<sub>4</sub></b> / Kraft fibres <sup>71</sup>	285	286.7	288.1	134.6

Table 4.6: The binding energies of C1s and P2p of various samples. Values from selected literature are included for the purpose of comparison.

Here, we can see that in the presence of the phosphorus-based FRs, the C 1s component peaks remain within a similar range relative to that of untreated cotton textile and the reported literature values. As peaks from C-O-P bonds have typically at 286.4 eV and could overlap with peaks from C-C-O bonds, no definite conclusion can be drawn here about the presence of C-O-P bonds in these investigated samples.

From Entries 2 and 9 it appears that in the presence of urea, the chemical shift of P 2p moves 1.7 eV towards a lower binding energy. Comparing Entries 2 and 3 it appears that the presence of **P-OTMS**, the chemical shift of P 2p also moves 0.5 eV to a lower binding energy but to a lesser extent than when urea is present. With fabrics treated with **PP-OEt** (Entry 4) and with **POP-OEt** (Entry 5), the P 2p peaks are observed in a similar range of 134.7 to 135.0 eV. As we know that it is unlikely that **PP-OEt** and **POP-OEt** phosphorylates cellulose at room temperature, its chemical shift corresponds to the P-O-C bond within **PP-OEt** or **POP-OEt**. Comparing entries 5 and 6, we observe almost identical chemical shifts (difference of only 0.1 eV) between textiles treated with **POP-OEt** and those treated with **POP-OTMS**. As we know that the TMS groups are lost during the treatment of cotton fabrics with phosphate silyl esters, this gives a strong indication that the P2p chemical shift for textiles treated with **POP-OTMS** arises also from P-O-C bond, and a P-O-C bond in a fabric sample treated with **POP-OTMS** shows that the cellulose has been phosphorylated at room temperature.



All in all, from the evidence from the different P 2p binding energies, coupled with the absence of silicon, and in view of the similarities in the flame retardant properties in phosphate silyl esters, we believe that the above interpretation can be extrapolated that in other phosphate silyl ester-treated cellulosic fabrics, phosphorylation of cellulose took place at room temperature (Figure 4.17).

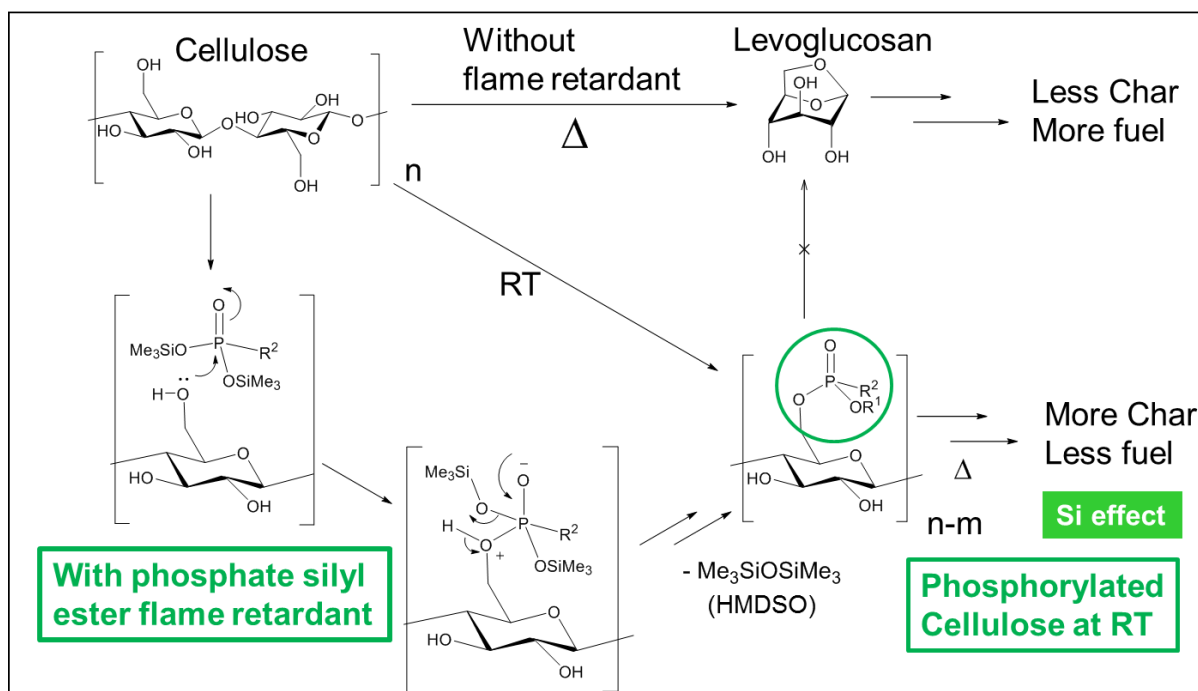


Figure 4.17: Room temperature phosphorylation of the cellulose with the proposed mechanism.

## 4.6 Concluding Remarks

We have presented in this chapter the characterization of the FR properties of four structurally related FR species, namely **PP-OEt**, **POP-OEt**, **PP-OTMS** and **POP-OTMS** on cotton textiles.

From the investigation of the structure-to-property relationship, we conclude that the cleavage of P-O-Si bonds leading to desilylation in phosphate silyl esters allows for a reduction in FR molecular size. The smaller size of 'naked' phosphates allows not only denser packing across the same surface area (depicted in Figure 4.18), but also access to more OH sites for cellulose phosphorylation. This is reflected in the linear increase of LOI observed with increasing phosphorus content when the cellulosic fabrics are treated with **PP-OTMS** and **POP-OTMS**.

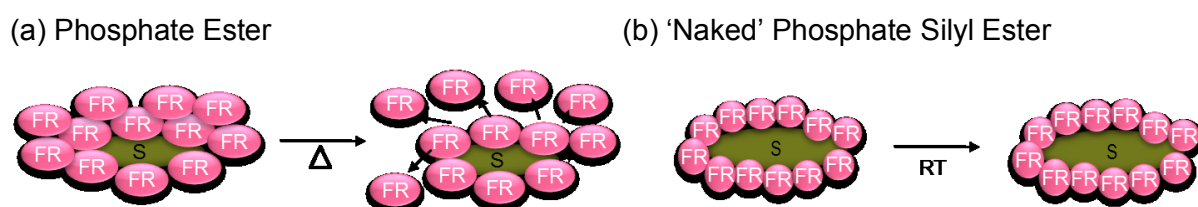


Figure 4.18: The influence of molecular sizes in phosphate ester and 'naked' phosphates (denoted as FR) on the packing density and access to more OH sites for phosphorylation.

For **PP-OEt** and **POP-OEt**, since the cleavage of phosphate ester and subsequent phosphorylation take place at elevated temperatures, desorption of FR molecules with minimal interaction with the cellulose will take place than before they can interfere with the cellulose degradation. In this case, the LOI values will tend towards a maximum value. This is the case observed for textiles treated with **POP-OEt** at higher P contents.

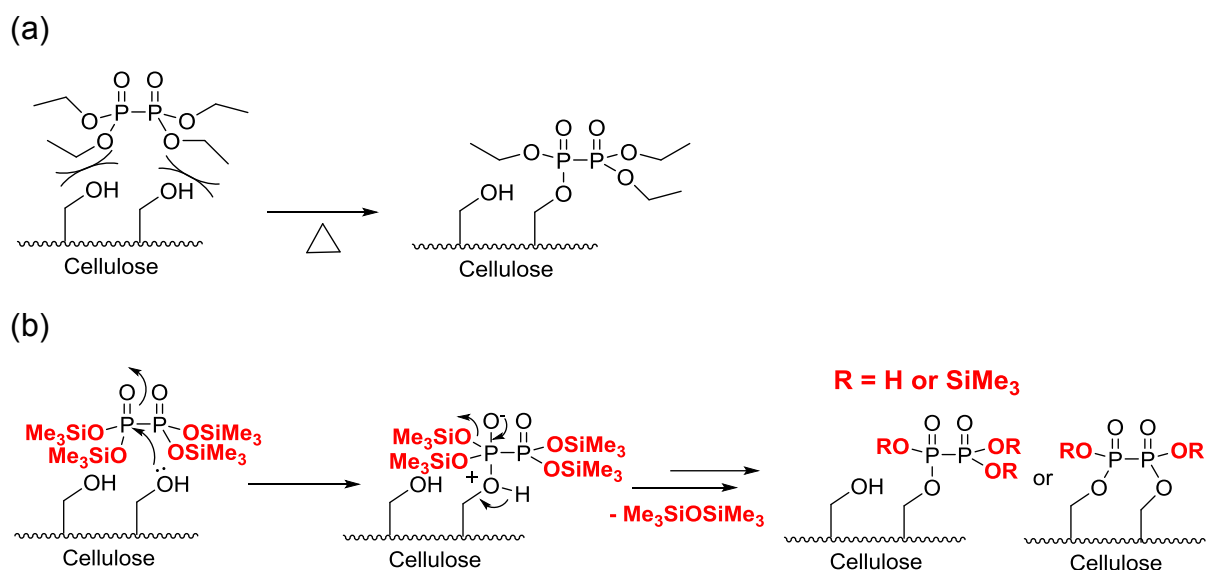


Figure 4.19: For phosphorylation to occur, (a) the ester groups in phosphate esters are less easily cleaved, hence requires an additional step with heat before phosphorylation; (b) since desilylation of phosphate silyl ester FRs takes place readily at room temperature facilitating phosphorylation of cellulose to take place.

Here we would like to emphasize on the direct correlation among the molecular size, room temperature phosphorylation and FR efficiency with phosphate silyl esters as flame retardant compounds. It is important to point out that to the best of our knowledge, this is the first time that such correlation has been drawn in the study of FR efficiencies. This is one of the most important findings of this thesis.

It is interesting to note that from the behavior of phosphate silyl esters, it appears that silicon does enhance the flame retardancy of phosphate-based compounds. Ironically, in the case of phosphate silyl esters, this enhancement is achieved by silicon leaving the condensed phase in the form of TMS groups. This is in sharp contrast to the well-known phosphorus-nitrogen synergism, where nitrogen improves the flame retardancy of phosphorus-based compounds by its participation in the condensed phase action inhibiting the thermal decomposition of cellulose.

It is therefore of interest if we could combine both of these effects to achieve an even greater enhancement in the flame retardant properties of the FR compound on cotton textile. The results of these findings are reported in the following Chapter 5.



## **Chapter 5**

**Phosphorus, Nitrogen and Silicon: Combination  
Possible for enhanced FR properties?**

## 5.1 Introductory Remarks

In the previous chapter, we have demonstrated that the hydrolytic instability of phosphate silyl ester bonds contributed to their much better phosphorylation efficiency, leading to excellent flame retardant properties observed in various flammability measurements. This overshadows the difference in flame retardancy observed between hypophosphates (direct P-P bond) and pyrophosphates (P-O-P bond).

Extrapolating from here, we would like to explore the possibility to combine the well-known phosphorus-nitrogen synergism<sup>28,35,74,75</sup> with the phosphate silyl ester bonds to further improve efficiency of the FR. The molecule with the simplest structure which would fulfil both of these criteria would be the tetrakis(trimethylsilyl) imidodiphosphate, or **PNP-OTMS** (Figure 5.1).

For comparison purposes we also present here the characterization of its phosphate ester analogue, tetraethyl iminodiphosphate (**PNP-OEt**). Besides that, there exists another alternative in attempt to combine phosphorus, nitrogen and silicon in a compound, namely diethyl (N-trimethylsilyl) phosphoramidate (**P-NTMS**) by silylation of the amide group in phosphoramidate (**P-NH<sub>2</sub>**).

All the compounds involved in this investigation has been summarized in Figure 5.1.

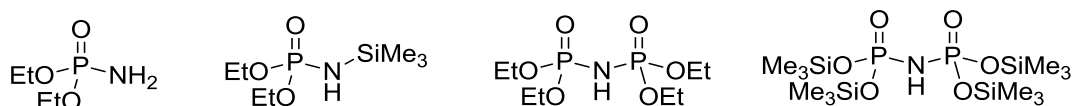


Figure 5.1: Structure of (from left to right) **P-NH<sub>2</sub>**, **P-NTMS**, **PNP-OEt**, **PNP-OTMS** under investigation in this chapter.

## 5.2 Impregnation of FRs onto cotton textile

Similar to the phosphate silyl esters, the FRs are added onto cotton textile via the impregnation with THF in air at room temperature for at least two hours.

Tracing the weight of the textile we found out that after impregnation with **PNP-OTMS**, the final increase in weight on the textile is 60% lower than that of the amount of FR that was added onto the textile surface. For textiles treated with **P-NTMS** the loading also decreases, but in a smaller percentage than those treated with **PNP-OTMS** (12%). However the P content is found to be relatively constant. This observation resembles those made for the phosphate

silyl esters in the previous chapter. When the textiles are treated with *P-NH<sub>2</sub>* and *PNP-OEt*, the loadings and corresponding phosphorus contents remain relatively consistent. This is also similar to that observed previously for the textiles treated with *PP-OEt* and *POP-OEt*.

Compound on textile	Feed loading (wt%)		% P	
	Initial	Final	Initial (Calc)	Final (EA)
<i>PNP-OTMS</i>	7.6	2.5	1.0	0.8
<i>PNP-OTMS</i>	15.3	5.5	2.0	1.8
<i>PNP-OEt</i>	5.0	4.6	1.1	1.0
<i>PNP-OEt</i>	9.2	8.9	2.0	1.9
<i>P-NTMS</i>	6.2	5.6	1.2	1.0
<i>P-NTMS</i>	15.1	13.3	2.2	2.1
<i>P-NH<sub>2</sub></i>	5.2	5.1	1.1	1.0
<i>P-NH<sub>2</sub></i>	10.2	9.4	2.1	1.9

Table 5.1: The initial and final loadings of FR on cotton based on wt% and P content

### 5.3 Flammability of the FR treated cotton textiles (LOI)

Figure 5.2 illustrates the variation of LOI with the FR loading on cotton textiles with increasing phosphorus content.

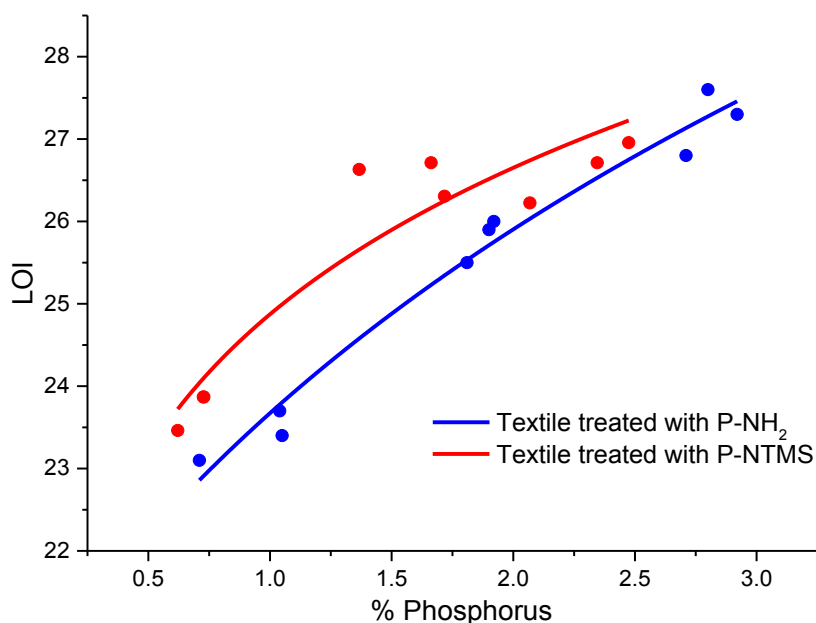


Figure 5.2: Variation of LOI to increasing phosphorus contents for textiles treated with *P-NH<sub>2</sub>* and *PN-TMS*.

Here we observe that for textiles treated with ***P-NH<sub>2</sub>***, the LOI values increase from 23 at 1% P to 27 at 3% P. At all loadings, textiles with ***P-NTMS*** give higher LOI values than those with ***P-NH<sub>2</sub>*** at the same phosphorus content. This suggests that ***P-NTMS*** performs better than ***P-NH<sub>2</sub>*** as a flame retardant on cotton textile. With the increase in P content, the rate of increase of LOI decreases faster in textiles treated with ***P-NTMS*** relative to those treated with ***P-NH<sub>2</sub>***.

We present in Figure 5.3 the LOI behaviour with increasing phosphorus content of ***PNP-OTMS*** and ***POP-OTMS*** on cotton textiles.

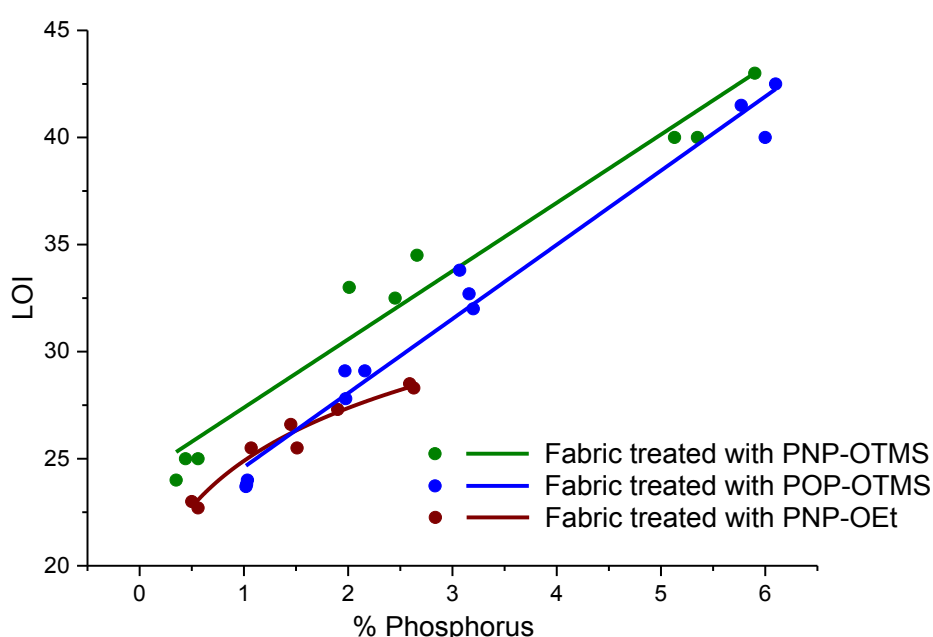


Figure 5.3: The variation of LOI with increasing phosphorus content for cotton textiles treated with ***PNP-OEt***, ***PNP-OTMS*** and ***POP-OTMS***.

From Figure 5.3, textiles treated with ***PNP-OEt*** shows increasing LOI with increasing P content, but the rate of increase reduces and approaches a maximum value of 28 at 2.7% P. Remarkably, textiles treated with ***PNP-OTMS*** exhibit a roughly linear LOI behaviour within the range of investigated phosphorus loading. Compared to ***PNP-OEt***, the difference in behaviour is analogous to that described in the previous chapter between ***PP-OTMS***, ***POP-OTMS*** and ***PP-OEt***, ***POP-OEt***.

Besides that, textiles with ***PNP-OTMS*** also have higher LOI relative to those with ***POP-OTMS*** at the same phosphorus content. At about 2.3% P, the difference in LOI is as much as 3 units.



This suggests that the replacing the oxygen with a nitrogen bridge has further enhanced the LOI behaviour. Compared to all other related phosphate silyl ester FRs (*P-OTMS*, *PP-OTMS* and *POP-OTMS*), the measured LOI values for textiles with *PNP-OTMS* give the highest values across the range of investigation. This lends support to the much discussed synergistic effects of phosphorus and nitrogen<sup>10,26,74</sup> in their flame retardant action on cotton fabrics.

#### 5.4 Thermal Decomposition and Evolved Gas Analyses of the FR-treated cotton textiles

To understand the thermal decomposition profiles of the FR-treated textiles, we present in the following Figure 5.4, the TGA and DTG curves of textiles treated with *P-NH<sub>2</sub>* and *P-NTMS*.

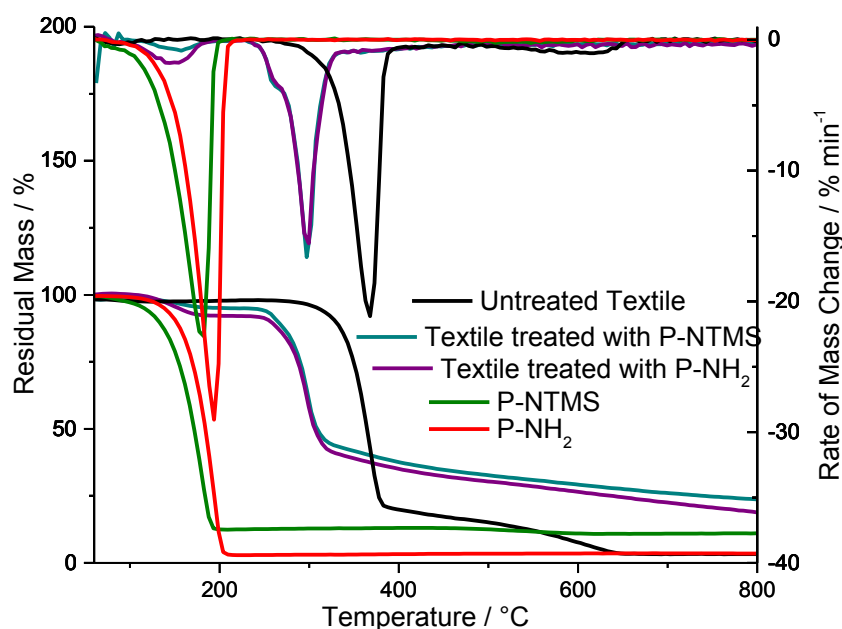


Figure 5.4: TGA and DTG curves of *P-NH<sub>2</sub>*, *PN-TMS*, untreated cotton textiles and textiles treated with *P-NH<sub>2</sub>* and *P-NTMS*.

The TGA curve of *P-NH<sub>2</sub>* consists of a one-step mass loss beginning at 145°C. Between 145°C and 205°C, 96% mass loss is registered. This signifies vaporization of *P-NH<sub>2</sub>*, similar to that observed for *PP-OEt* in the previous chapter. *P-NTMS* also shows a similar behavior, with one mass loss step of 75% beginning at 130°C. The decomposition of textiles with *P-NH<sub>2</sub>* and *P-NTMS* consists of two major steps with similar onset temperatures:  $T_1$  at 150 °C and  $T_2$  at 275°C. A closer look at the DTG curves reveal a minor decomposition step which begins at 253°C for textiles with both of the FR species. The major mass loss step for both samples are about 50%, with the textile treated with *P-NTMS* giving 6% more char than that with *P-NH<sub>2</sub>*.

These similarities suggest their similar interaction with the textiles during thermal decomposition.

By comparison, the first mass loss step can be associated with the vaporization of a small amount of FRs from the surface of cotton textiles. This reveals that at elevated temperatures, there is a competition between the vaporization of the FRs into the gas phase, and phosphorylation of the cellulose by the FRs in condensed phase. At higher FR contents, more FRs are lost as fuels instead of FRs for the cellulose-based substrate. This explains why the LOI increase in textiles treated with ***P-NH<sub>2</sub>*** and ***P-NTMS*** are nonlinear and the rate of LOI increase decreases with increasing P content.

We next look at the thermal decomposition profiles of textiles treated with ***PNP-OTMS***, ***PNP-OEt*** and ***POP-OTMS*** in Figure 5.5.

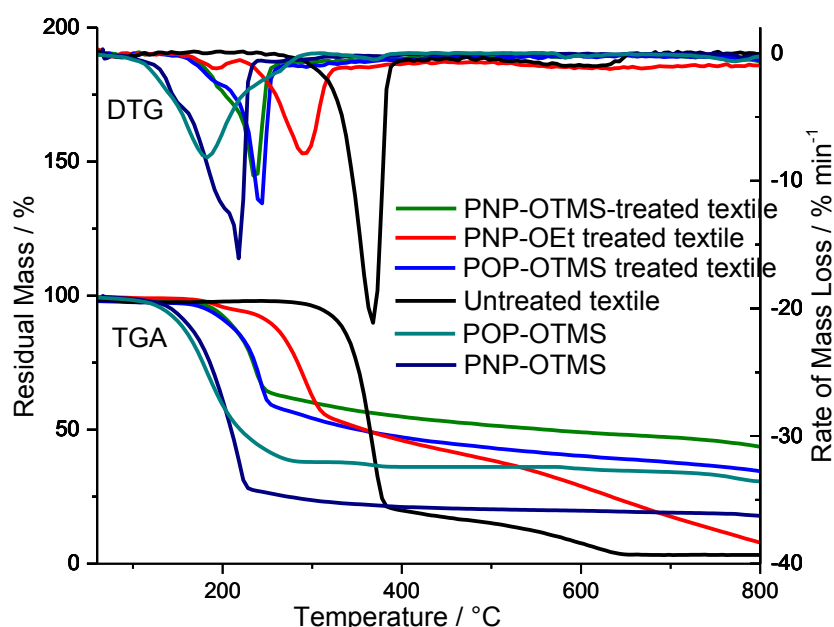


Figure 5.5: TGA and DTG curves of ***PNP-OTMS***, ***PNP-OEt*** and ***POP-OTMS*** on cotton textiles.

The TGA curves of ***PNP-OTMS*** and ***POP-OTMS*** shows that they begin to decompose at similar temperatures of 150°C, but the mass loss is about 13% greater in ***PNP-OTMS*** than in ***POP-OTMS***. As the mass loss step is associated to the loss of TMS groups (confirmed by ion currents of  $m/z$  73 and 146 in the MID spectra), this shows that ***PNP-OTMS*** releases more TMS groups than ***POP-OTMS***.

Relative to ***PNP-OTMS*** treated textiles, the textiles treated with ***PNP-OEt*** begin to degrade similarly at 208°C. However, the major mass loss step occurs at much higher temperatures between 298°C and 315°C. The gradual mass loss with increase in temperature leads to a

very low amount of residue of 9% at 900°C. This indicates that **PNP-OEt** does not remain in the condensed phase at higher temperatures.

The textiles treated with **PNP-OTMS** exhibits a similar decomposition profile to those treated with **POP-OTMS**. The decomposition temperatures begin at similar temperatures of 208°C but the mass loss is less in textiles treated with **PNP-OTMS**, giving 9% more residue at 900°C. This highlights the superior flame retardant property of **PNP-OTMS** to **POP-OTMS** and could be related to the extent of desilylation during the decomposition step of the respective compounds. As **PNP-OTMS** is more desilylated, the smaller size allows it access to more OH sites on the cellulose chains, hence increased efficiency in the phosphorylation of cellulose. This corresponds to our previous observation in the higher LOI values for textiles treated with **PNP-OTMS** relative to those treated with **POP-OTMS** in the range of investigated P contents.

### 5.5 Heat Release Analyses of FR-treated cotton textiles

In Figure 5.6 the HR curves for cotton textiles treated with **P-NH<sub>2</sub>** and **P-NTMS** are presented. Same as presented in the previous chapter, these samples are measured under the heating rate of 1 Ks<sup>-1</sup>.

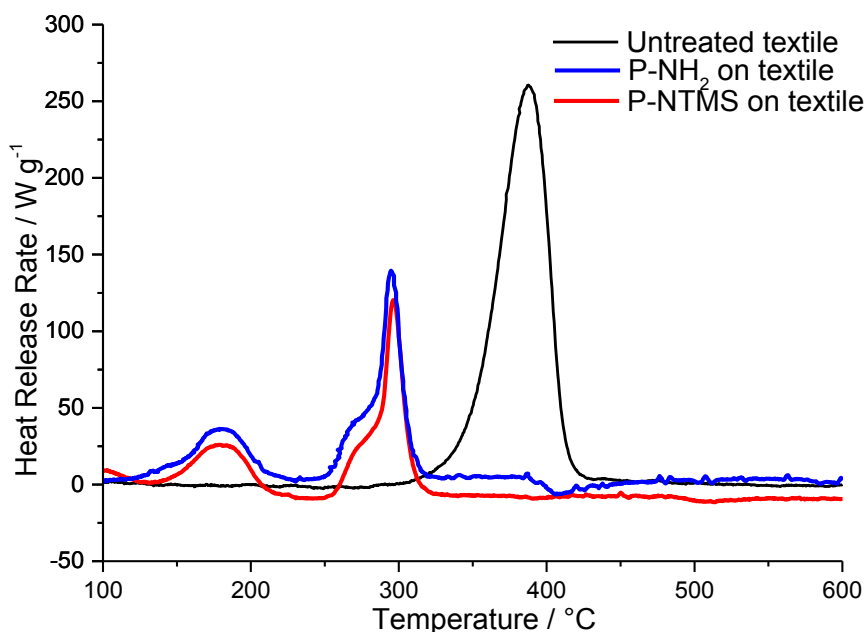


Figure 5.6: Heat release curves of textiles treated with **P-NH<sub>2</sub>** and **P-NTMS**.

When the textiles are treated with **P-NH<sub>2</sub>** and **P-NTMS**, the HR curves show one major heat release event with the maximum HRR occurring at 298°C, and a bump at 255°C and a minor

HR events with the maximum occurring at 180°C. The minor HR event can be attributed to the vaporization of the FRs from the fabrics, since we learned earlier in the TGA curves that **P-NH<sub>2</sub>** vaporizes at 145°C and **P-NTMS** at 130°C. The heat release events observed for textiles treated with **P-NH<sub>2</sub>** and those with **P-NTMS** reflects resemblance to their DTG curves, in which a major peak with a bump and a minor peak were also observed. These explain their lower FR efficiency at 3% P because some of the FR vaporizes at relatively low temperature (130°C to 145°C), too quickly to react with cellulose to act as flame retardant.

In contrast, textiles with **POP-OTMS** and **PNP-OTMS** show only one heat release event, as illustrated in the following Figure 5.7.

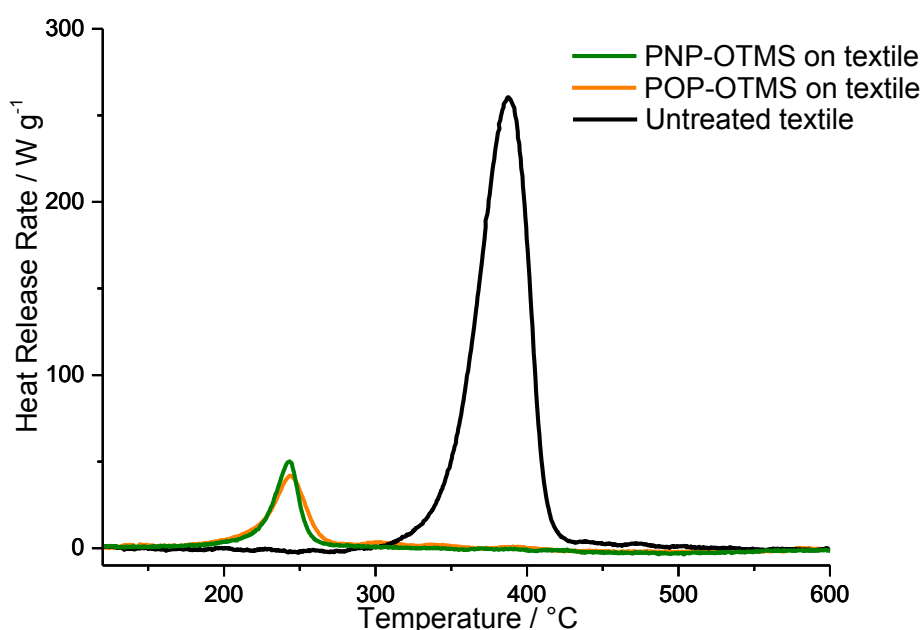


Figure 5.7: Heat release curves of cotton textiles treated with **PNP-OTMS** and that with **POP-OTMS**.

Similar to the textiles treated with **P-OTMS**, **PP-OTMS** and **POP-OTMS**, textiles impregnated with **PNP-OTMS** also exhibit a single HR event. Not only that, the temperature of peak HRR, THR and HRC are also similar at the same P content. This again suggest the similar reactivity of **PNP-OTMS** with the other silyl esters in the phosphorylation of cellulose, therefore explains the observed similarities in their heat releast profiles.

By comparing the PCFC parameters given in the following Table 5.2, one sees the extent of reduction in the various PCFC parameters is generally larger for **PNP-OTMS** at the same phosphorus content on cotton textiles.

Compound Textile	on P content / %	$T_{pHRR} / ^\circ\text{C}$		avg HRC <sub>sum</sub> / $\text{kJ g}^{-1} \text{K}^{-1}$	avg THR / $\text{kJ g}^{-1}$
		$T_1$	$T_2$		
<b><i>P-NH<sub>2</sub></i></b>	1	158 (2)	300 (1)	255 (6)	5.2 (4)
	2	181 (7)	298 (2)	151 (4)	4.5 (2)
	3	161 (4)	278 (3)	140 (3)	4.9 (2)
<b><i>P-NTMS</i></b>	1	290 (2)	310 (4)	312 (3)	8.7 (1)
	2	181 (9)	297 (2)	138 (11)	5.6 (3)
	3	156 (3)	272 (3)	150 (4)	5.1 (2)
<b><i>PNP-OEt</i></b>	1	216 (1)	304 (1)	120 (1)	5.2 (5)
	2	216 (3)	291(1)	100 (2)	3.6 (1)
	3	219 (5)	265 (12)	102 (7)	3.7 (4)
<b><i>POP-OTMS</i></b>	1	260 (12)		61 (7)	2.0 (4)
	2	244 (1)		44 (1)	1.33 (4)
	3	249(2)		51 (1)	1.27 (4)
<b><i>PNP-OTMS</i></b>	1	273 (2)		50 (1)	2.37 (4)
	2	239 (3)		51(4)	1.23 (1)
	3	239 (6)		43 (2)	1.13 (5)
<b>None (Untreated)</b>		392 (4)		330 (4)	10.9 (1)

Table 5.2. Heat release parameters of the investigated FRs at various loadings on cotton textiles.

From the PCFC parameters presented in this table, we observe more than one heat release events in textiles treated with ***P-NH<sub>2</sub>***, ***P-NTMS*** and ***PNP-OEt***. All three of these FR compounds contain diethyl phosphate ester bonds, therefore the observed similarity in FR behavior compared to the phosphate esters in the previous chapter. Similar to those treated with ***POP-OTMS***, fabrics impregnated with ***PNP-OTMS*** display HRC values of less than  $100 \text{ kJ g}^{-1} \text{K}^{-1}$ , highlighting its self-extinguishing properties in ambient conditions. Also, the THR remained below  $2.5 \text{ kJ g}^{-1}$ , indicating the excellent flame retardant efficiency similar to the other silyl ester species.

## 5.6 Concluding Remarks

In this chapter we presented the results of our investigation into the flame retardant properties of *P-NH<sub>2</sub>*, *P-NTMS*, *PNP-OEt* and *PNP-OTMS*.

Amongst these FR species, *PNP-OTMS* has proven to have a flame retardant performance superior to *POP-OTMS* on cotton textiles. This exemplifies the possibility of combining two aspects of flame retardancy study on the structural design of a phosphorus-based compound for application of cotton textiles, namely phosphorus nitrogen synergism with phosphate silyl ester bonds. While we learned from TGA that *PNP-OTMS* undergoes more desilylation than *POP-OTMS*, this allows the smaller size of the desilylated phosphate molecule to access more OH sites on the cellulose chains. Therefore more extensive phosphorylation of cellulose at room temperature can take place and hence this contributes to our observation in the LOI measurements. Another reason could stem from the relative thermal stability of the oxygen and nitrogen bridges, whereby the P-N-P bridge are more thermally stable than P-O-P bridge, therefore allowing double phosphorylation to take place. However, this remains a hypothesis and requires more evidence.

By comparing the flame retardant behavior of *P-NTMS* and *P-NH<sub>2</sub>* we can deduce that the silylation of phosphate ester into phosphate silyl ester has a much significant effect than the silylation of the amide side chain of phosphoramidate in enhancing its flame retardancy on cotton textiles.

## **Chapter 6**

### **Phosphorohydrazidates as Flame Retardants on Cotton textiles**

## 6.1 Introductory Remarks

This chapter details our exploration into using phosphorohydrazidates as potential flame retardants, since their molecular structure are analogous to phosphazenes<sup>76</sup> and phosphoramidates but never been tested as flame retardants on cotton textiles.

In chapter 3, we reported on the synthesis based on published procedures detailed by Zwierzak *et al* in 1976<sup>54</sup> and reported the first crystal structure of a phosphorohydrazidate in Chapter 3. Then we proceed to discuss the flame retardant properties of this class of compounds and then compare them to the other groups as reported in the previous chapters.



Figure 6.1: Diethyl Phosphorohydrazidate (**PNN-OEt**) and *N,N'*-bis(diethyl) phosphoryl hydrazidate (**PNNP-OEt**)

## 6.2 Impregnation of the FR species on cotton textiles

The FR species, **PNN-OEt** and **PNNP-OEt**, are applied onto cotton textiles using the impregnation method described in the previous chapters, using THF as the solvent in air and under room temperature for at least two hours. The loadings of FR and the % phosphorus are found to be consistent to the fed amount after the treatment step. This is similar to the behavior of the other phosphate ester species in the previous chapters.

Compound on textile	Feed loading (wt%)		% P	
	Initial	Final	Initial (Calc)	Final (EA)*
<b>PNN-OEt</b>	5.6	4.3	1.3	1.0
<b>PNN-OEt</b>	10.9	10.5	2.1	1.9
<b>PNNP-OEt</b>	4.8	4.6	1.1	1.0
<b>PNNP-OEt</b>	8.2	7.1	1.8	1.6

\*measured by elemental analyses

Table 6.1: The initial and final loadings of FR on cotton based on wt% and P content.

## 6.3 Flammability Measurements for FR impregnated cotton textiles with LOI

We next proceed to characterize the flammability behavior of **PNN-OEt** and **PNNP-OEt** on cotton textiles. Figure 6.2 illustrates the LOI behavior of textiles treated with these two FR species with increasing phosphorus content.



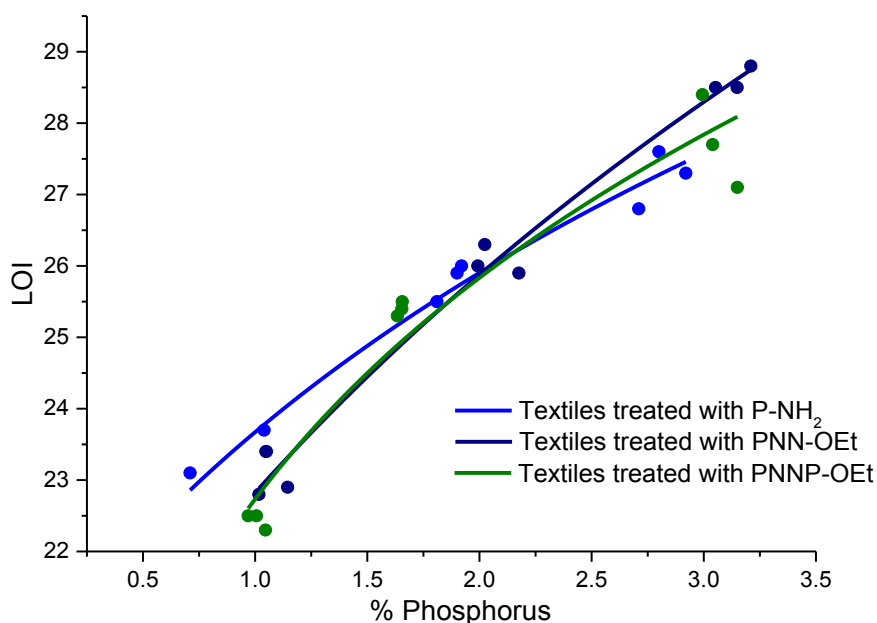


Figure 6.2: The variation of LOI with FRs of various phosphorus content on cotton textile.

Figure 6.2 illustrates that textiles with **PNN-OEt** and **PNNP-OEt** exhibit similar LOI behaviour at lower P contents below 1.75% P. Beyond this concentration, the increase in LOI becomes slower in textiles treated with **PNNP-OEt** compared to those of textiles treated with **PNN-OEt**. Compared to textiles with **P-NH<sub>2</sub>**, their LOI behaviour is lower at lower P contents. This is because **P-NH<sub>2</sub>** is relatively smaller in size, therefore has access to greater density of cellulose primary OH sites for phosphorylation. At only beyond 2.2% P, the textiles treated with phosphorhydrazidates display higher LOI values compared to those with **P-NH<sub>2</sub>**.

However, comparing the two phosphorhydrazidates, **PNN-OEt** performs better than **PNNP-OEt** as a flame retardant at P contents higher than 2% P. This is possibly because of the higher nitrogen-to-phosphorus ratio and the presence of a primary amine group in **PNN-OEt**, resulting in its higher polarity (as suggested by Salimova<sup>5</sup> in her thesis), hence the ability to form a wider network of hydrogen bonds at higher P content with the surface of cotton textiles.

Next we proceed to analyse the thermal decomposition profiles of textiles treated with these phosphorhydrazidate species.

## 6.4 Thermal Decomposition Analysis of Cotton Fabrics Impregnated by *PNN-OEt* and *PNNP-OEt*

The thermal decomposition profiles of textiles treated with *PNN-OEt* and *PNNP-OEt* are presented in the following Figure 6.3.

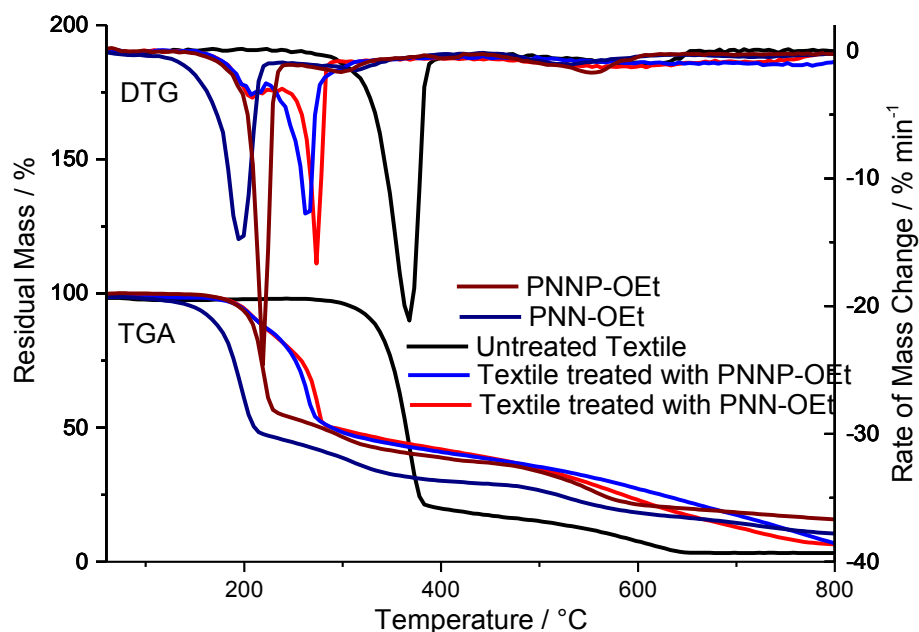


Figure 6.3: TGA and DTG curves of cotton textile and textiles impregnated with *PNN-OEt* and *PNNP-OEt* at 3% P.

The TG curve of *PNN-OEt* shows that it begins to decompose at 170°C, 30°C lower than that of *PNNP-OEt*. Together with the greater mass loss of 50% (vs 45% in textiles treated with *PNNP-OEt*) in the first step, this implies a slightly better phosphorylation efficiency in *PNN-OEt* compared to *PNNP-OEt*. However, the bumps on the DTG curve of textiles treated with *PNN-OEt* and *PNNP-OEt* can be attributed to the decomposition of the FRs on the cotton textiles alone, without further interaction in the condensed phase. Similar to what has been observed for *PNP-OEt* in chapter 5, the mass loss continued gradually after the major step at around 280°C to give less than 10% residue at 900°C. This observation indicates that at 550°C (where a slight mass loss is observed), the FRs do not remain in the condensed phase, removing the inhibition towards the formation of char II.

## 6.5 Heat Release Studies of Phosphorohydrazidates on Cotton textiles

Measured by PCFC, we present the heat release profiles of **PNN-OEt** and **PNNP-OEt** in Figure 6.4.

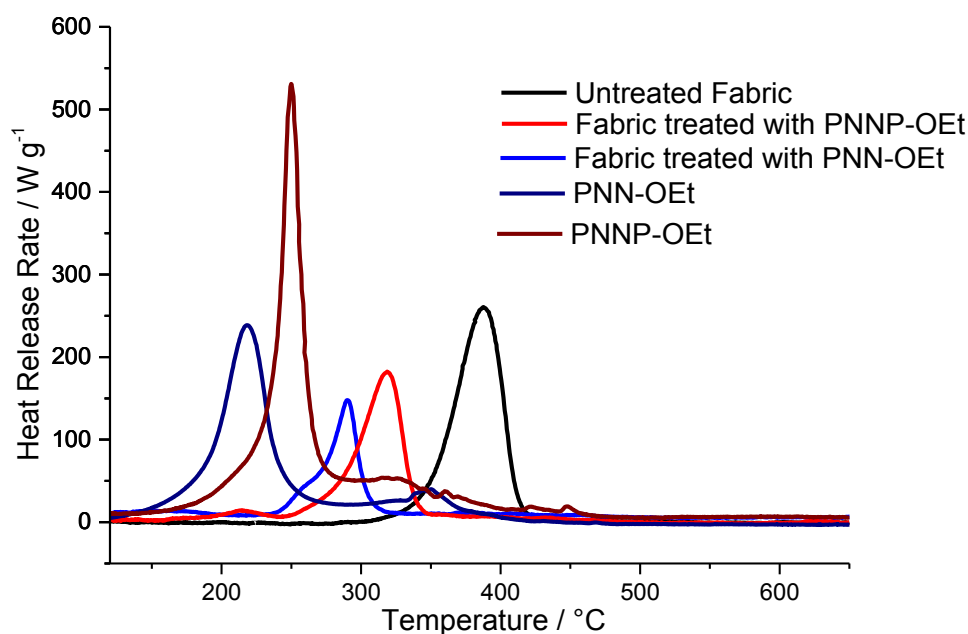


Figure 6.4: The HR curves of untreated textile and textiles treated with **PNN-OEt** and **PNNP-OEt**.

The HR curves of **PNN-OEt** and **PNNP-OEt** treated textiles show that they undergo pyrolysis at much lower temperatures (215°C and 256°C respectively) than that for untreated cotton textiles (395°C). Relative to **PNN-OEt**, **PNNP-OEt** releases much more heat in pyrolysis, with its THR almost twice the value of **PNN-OEt**. This explains why textiles treated with **PNNP-OEt** also releases more heat than textiles treated with **PNN-OEt** per unit gram of sample.

The HR curve of textile treated with **PNN-OEt** shows that the maximum HRR has shifted to a lower temperature compared to textiles treated with **PNNP-OEt**. Also the THR is relatively lower for textiles treated with **PNN-OEt**. Both suggests the superiority in FR properties of **PNN-OEt** over **PNNP-OEt** for cotton textiles.

## 6.6 Concluding Remarks

We reported in this chapter for the first time the study of phosphorohydrazidates as FR on cotton textiles.

While ***PNN-OEt*** and ***PNNP-OEt*** show better FR efficiency than ***P-NH<sub>2</sub>*** for cotton textiles only at higher P contents (> 2% P), the advantages they possess over ***P-NH<sub>2</sub>*** is not as pronounced as those of ***PNP-OTMS*** over ***P-NH<sub>2</sub>*** as mentioned in the previous chapter. The better FR efficiency in ***PNN-OEt*** can be attributed to its smaller size. Being smaller allows the FR access to higher number of OH sites of the cellulose chains within the vicinity. This explains its higher FR efficiency in terms of LOI relative to that of ***PNNP-OEt***. The second reason is that ***PNN-OEt*** contains a primary and a secondary amide group, ***PNNP-OEt*** has two secondary amide groups, and ***P-NH<sub>2</sub>*** has only one secondary amide group. With a primary amide group, more extensive network of hydrogen bonds could be formed among the FR compounds and between the FR and the cellulose chains on the surface of cotton textiles. This explains why, at higher FR concentrations, the observed FR efficiency is in this order: ***PNN-OEt*** > ***PNNP-OEt*** > ***P-NH<sub>2</sub>***.

Once again this highlights the greater influence of the phosphate silyl ester bond over the FR efficiency compared to those of phosphate esters, since all three of these compounds also possess diethyl ester groups.

## **Chapter 7**

### **Protection of Phosphate Silyl Ester Treated Cotton Textiles**

In this chapter we report our attempt to protect the flame retarded cotton textiles by grafting and polymerizing a fluorine-rich monomer<sup>27,33</sup> on the surface of the textile. The energy for the polymerization and grafting is provided by cold argon plasma, and the fluorine-rich functionality would render the surface-modified cotton textiles water repellent. In this way, the partially phosphorylated cotton textiles could be protected from being rinsed away by water.

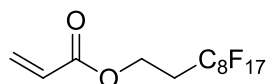


Figure 7.1: The structure of 1,1,2,2, tetrahydroperfluorodecyl acrylate (AC8) monomer

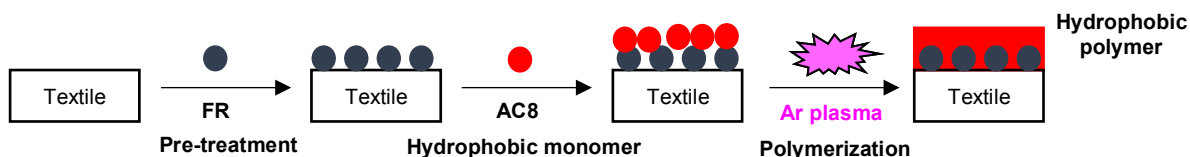
## 7.1 Plasma as a Source of Energy for Polymerization

Defined as the fourth state of matter, plasma consist of a fluid mixture of excited gas particles, including cations and electrons. Over 99% of the matter in space is believed to be made of plasma (gas and stars)<sup>77</sup>. This type of plasma is generated at very high temperatures (more than  $10^6$  K) and are in a state of equilibrium.

In the laboratory, non-equilibrium plasma could be generated at low temperature<sup>77,78</sup> and pressure with an external source of energy input, for example irradiation with radio frequency at a certain energy.

In our laboratory, we employ the radio frequency as an energy source to generate plasma from argon gas at low pressure. In this way the plasma can be generated at room temperature at 90 Pa (500 mTorr), and is energetically sufficient to generate radicals and induce grafting and polymerization reactions, but not too much to cause the degradation of the polymers and the cotton textiles.

## 7.2 Monomer Impregnation and the Plasma-Induced Graft Polymerization (PIGP) Process



Scheme 7.1: Illustration of PIGP process from impregnation (pre-treatment of FR and addition of AC8 monomer) to low pressure argon plasma treatment.

In summary, the surface modification process of the cotton textiles consists of the following phases: The textile first undergoes pre-treatment with flame retardant compounds, typically up to 3% P or 20 % to the weight of the textile, via impregnation in air at room temperature. The AC8 monomer is then added, ranging from 5% to 15% to the weight of the textile, also via impregnation in air at room temperature. Thereafter, the FR-impregnated textile and AC8 monomer is transferred into a plasma chamber and treated by argon plasma for 10 minutes.

The pre-treatment step of the cotton textiles with flame retardant is conducted identically as described in the previous chapters. Being commercially available and having the simplest structure of the phosphate silyl ester compounds, tris(trimethylsilyl) phosphate, **P-OTMS** is used as the first test FR. Here, a sample of cotton textile was first subjected to a pre-treatment of **P-OTMS** by via impregnation through a solution in THF. The solution is then transferred via a syringe dropwise across the area of the textile. After that, the textile is left for at least 2 hours for the treatment under air at room temperature.

### **7.2.1 Impregnation of AC8 monomer on the FR pre-treated textiles**

Subsequently, the **P-OTMS** pre-treated textile was impregnated with the AC8 monomer (10 or 15 % to the weight of textile) through a solution mixture with ethylene glycol diacrylate (EGDA) as the cross-linking agent (10% to the weight of AC8 monomer), and bis-acyl phosphine oxide (BAPO) as the photoinitiator (5% to the weight of the AC8 monomer).

Owing to its high volatility and quick evaporation, we chose dichloromethane as the impregnating solvent. The reason therein lies the observation that within two hours of impregnation process, the monomer-treated cotton textile samples reveal very low increase in weight (ca. 1 wt%) despite an initial addition of 10 wt% of AC8 monomer by weight of the textile sample. This suggests that the presence of FR decreases the affinity of AC8 on the cotton textile.

Further investigations have shown that a 10-minute period is long enough for DCM to completely evaporate, before the loss of AC8 monomers from a textile sample of dimension 10cm x 10cm. As our system involves a low pressure plasma, the pressure of the internal chamber cannot be too low as this could lead to the loss of more AC8 monomers.

### **7.2.2 PIGP Process**

Through a series of optimization experiments, the following conditions are found to be the most conducive for the eventual grafting and polymerization of AC8 polymers on the surface of the cotton textile:

- |                                       |            |
|---------------------------------------|------------|
| 1. Treatment duration                 | : 10 min   |
| 2. Working pressure of plasma chamber | : 90 Pa    |
| 3. Argon flow                         | : 130 sccm |
| 4. Energy from radio frequency        | : 105 W    |

The following Figure 7.2 shows the repellence of the poly-AC8 grafted cotton textiles towards water and oil droplets after the plasma treatment.

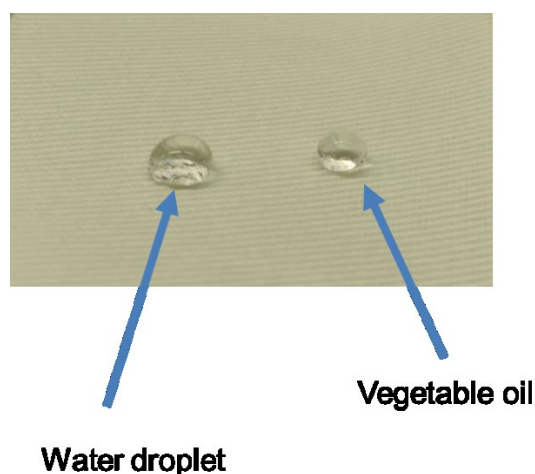


*Figure 7.2: Repellent properties of poly-AC8 grafted cotton textiles towards water and oil.*

The resulting textiles, treated under the abovementioned conditions, all display the hydro- and oleophobic properties after the argon plasma treatment.

### **7.2.3 Water Repellence Measurement (Schmerber Pressure)**

After treating the textiles under the argon plasma, the weight increase remains constant with time. This is a first indication of successful grafting and polymerization of AC8 on the surface of cotton textiles. We then observed that these samples repel water and oil, suggesting that hydro- and oleophobicity has been conferred onto the samples.

To quantify the hydrophobicity of the textile samples, the Schmerber pressure, or the hydrostatic pressure required to force a column of water through a sample of substrate, was measured. This is achieved by using a water column instrument which is set at an increasing hydrostatic pressure gradient of 10 mbar per minute. The Schmerber pressure is determined as the hydrostatic pressure at which three water droplets are observed on the non-exposed side of the textile sample with an area of 100 cm<sup>2</sup> (10cm x 10cm dimension). Figure 7.3 illustrates the results of the different Schmerber pressures ( $P_s$ ) measured when the textile samples are treated under various conditions.



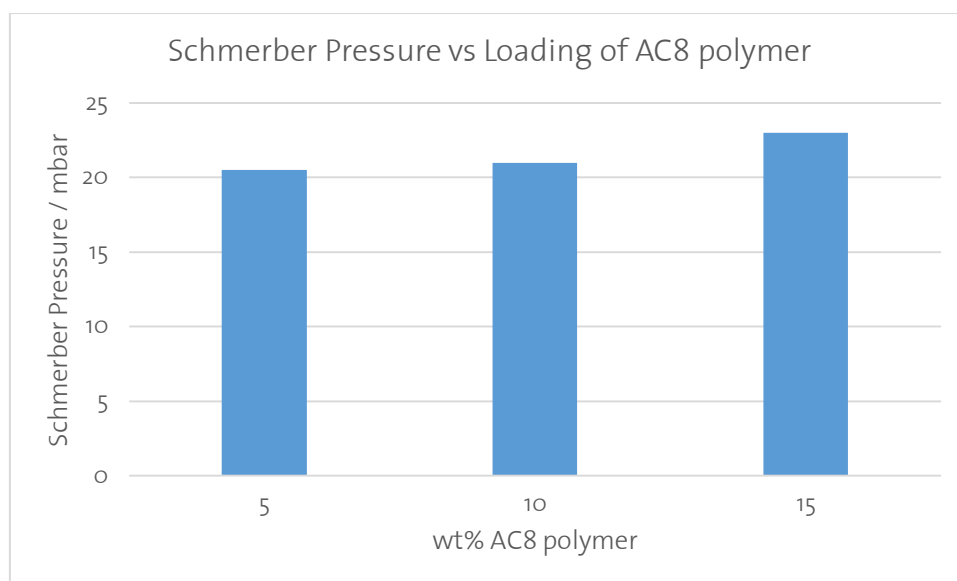


Figure 7.3: Schmerber pressures of virgin cotton fabric after plasma treatment under various conditions.

Untreated cotton textiles do not have a measurable Schmerber pressure because water column easily penetrates through the textile owing to its hydrophilic nature. After the plasma treatment of virgin textile samples impregnated with 5 wt% AC8, the Schmerber pressure is registered at  $20.5 \pm 0.5$  mbar. Higher loadings of AC8 (10 wt% and 15 wt% show only slight increase in Schmerber pressures, an indication of saturation on the surface of textiles. This phenomenon has been observed by Tsafack *et al*<sup>7</sup> in the treatment of PAN fabrics with the same perfluorinated monomer. Therefore, 10 wt% is the optimal amount of AC8 for the best water repellent property to be conferred onto the surface of cotton textiles.

In the following Table 7.1, one can see that with 10wt% AC8 on the FR-treated textile sample, the Schmerber pressure measures  $21.0 \pm 0.3$  mbar (Sample 1, Table 7.1). Further increase in the AC8 loading does not result in a significant increase in the Schmerber pressure. At 15 wt% the Schmerber pressure registered  $23.0 \pm 0.2$  mbar. The measured Schmerber pressures are consistent to those obtained in the absence of flame retardant at the same loadings of AC8, as can be seen from Table 7.1. This observation indicates that the flame retardant does not interfere with the water and oil repellence on the surface of cotton textile. This shows that the LOI behavior of the flame retarded textile is unaffected by both the presence and the loadings of the AC8 polymer on the textile surface.

Textile Sample	1	2	Only FR Control 1	Only Poly-AC8 Control 2	Untreated Control 3
wt% FR	9.7	9.5	9.5	-	-
Wt% AC8 feed	10	15	-	16	-
Total wt% gain*	10.8	20.2	-	12.5	-
P <sub>s</sub> / mbar	21.0	23.0	-	21.2	-
LOI	30.2	29.6	30.5	17.6	17.5
Char yield / %	31	28	30	4	3.5

Table 7.1: Schmerber pressures of the FR pre-treated textiles with AC8 polymer at various loadings. \*Total weight gain of the treated textile relative to that of untreated sample.

In the subsequent step, we then subjected the textile samples to water rinsing to qualitatively determine its resistance towards simple washing steps.

#### 7.2.4 Water Rinsing Test

For the water rinsing test, a plasma-treated cotton textile samples containing **P-OTMS** and AC8 is placed on a glass petri dish containing 10 mL distilled water. The dish is then placed on a shaker for 15 seconds to stir the mixture. The textile sample is then removed from the system and allowed to dry.

During the rinsing, we observed that the water droplets run off the surface quickly without wetting the surface. This indicates that textile surface has acquired water repellence after the plasma treatment. Thereafter we also measured the Schmerber pressures and the results are listed in Table 7.2.

Textile sample	1	2
wt% FR	9.7	9.5
Wt% feed	10	15
Before Rinsing		
Total wt% gain*	10.8	20.2
P / mbar	21.0	23.0
LOI	30.8	29.8
After Rinsing		
Total wt% gain*	10.7	20.2
P/ mbar	20.5	22.8
LOI	30.1	29.4
Char yield / %	32	25

Table 7.2: The LOI value and char yield of the textile samples after rinsing with water. \*Total weight gain of the treated textile relative to that of untreated sample

Table 7.2 shows the corresponding LOI values of the textile samples after rinsing with water. From the table of values obtained we could infer that the water rinsing process caused a decrease in the Schmerber pressures, but does not affect the LOI values of the textile samples

as compared to those before rinsing. This indicates that the FR species are not washed away during the rinsing step.

The obtained results suggest we have conferred oil and water repellence to the FR-treated textiles by the graft polymerization of a perfluorinated AC8 monomer on the surface using the PIGP process.

In other words, through graft polymerization of AC8 on the surface of textiles, we have managed to achieve our objective of protecting the flame retardants against immediate rinsing from water. As washing durability of the silyl ester FR-treated textiles is an important criterion for possible industrial application, our results points to the possibility for this project to eventually move to a larger scale.

### ***7.3 Treatment of Cotton Textiles with Atmospheric Pressure Plasma***

An alternative to low pressure plasma systems, atmospheric plasma systems are, in contrast, open systems and therefore potentially allows a large scale treatment of textiles to confer various properties on their surfaces. One such system (as designed and built in Luxembourg Institute of Science and Technology) even combines the plasma treatment and a simultaneous deposition of a desired chemical for the surface modification and functionalization. The following Figure 7.4 illustrates the setup of the atmospheric plasma device, allowing treatment of materials of maximum 2.5 mm thickness, including cotton textiles.

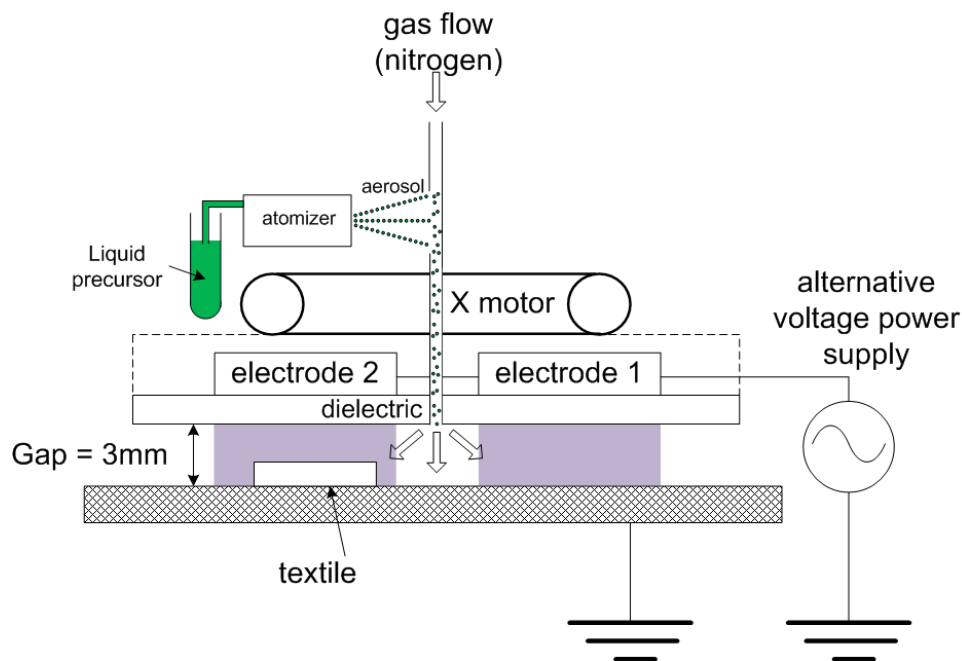


Figure 7.4: The experimental setup of the atmospheric argon plasma coupled with deposition capabilities. (With permission from Dr. Julien Bardon, Luxembourg Institute of Science and Technology, LIST)

It is known in the literature that organosilicon materials<sup>79</sup> can be coated onto the metal surfaces to protect them from corrosion. As we wish to protect our FR-treated textiles against washing, we aim to utilize a similar process to confer wash resistance to our FRs on textiles. To this end, Mahltig *et al*<sup>60,81</sup> coated silicates on cotton textiles using sol-gel process to confer water repellence to cotton textiles. Hoefnagels *et al*<sup>62</sup> modified the surface of cotton textiles with in situ silica generation on the surface to achieve surface superhydrophobicity. Using a milder and controllable method, we aim in a collaboration with LIST to deposit a silicate material on the surface of the cotton textile pre-treated with **P-OTMS**. The precursor for this silicate material is hexamethyldisiloxane or HMDSO, and it is atomized before being introduced into the gas flow column. The gas flow, which contains mainly nitrogen and 4.5 vol% oxygen, transports the precursor into the plasma region and hence, allowing its deposition on the cotton textile surface as the substrate passes through. After the plasma treatment, the textiles are subjected to surface analyses and flammability tests to study more in depth the effects of the plasma treatment on textile.

### 7.3.1 Surface Analyses and Flammability Test of the HMDSO-Deposited FR Cotton Textiles

Figure 7.5 illustrates the surface composition of the textiles after the atmospheric plasma treatment with HMDSO deposition.

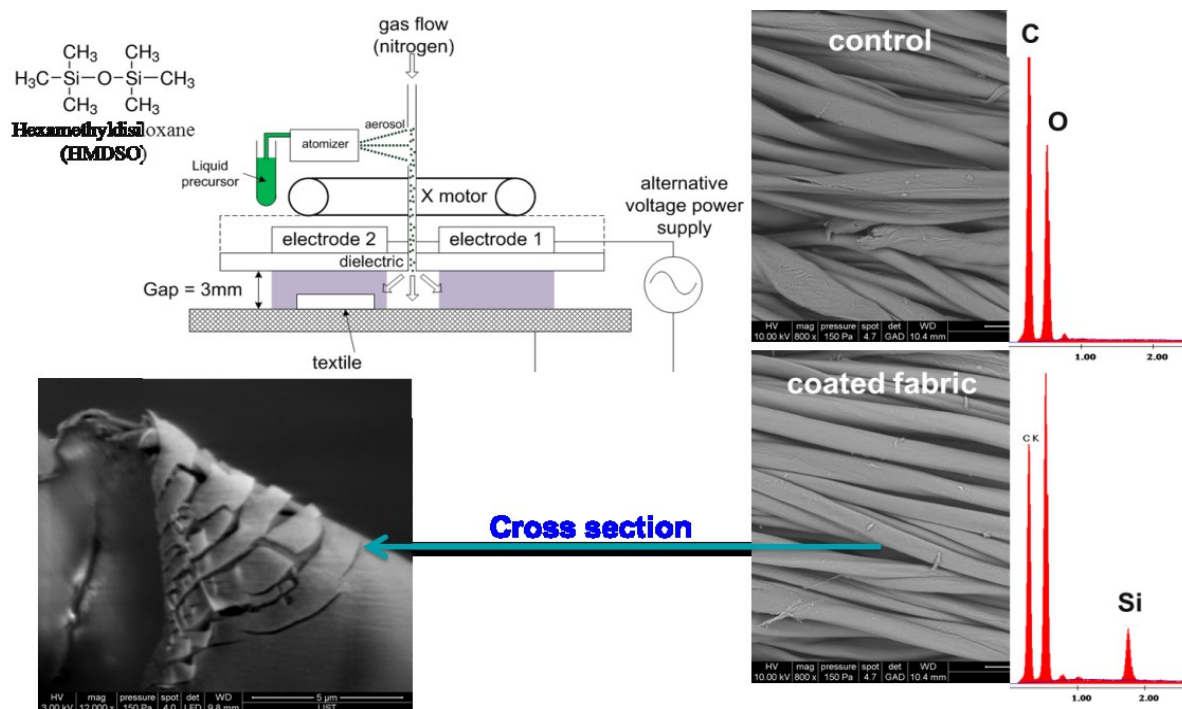


Figure 7.5: The SEM micrograph (left bottom) and EDX images with the elemental spectra (right) for control (top right) and coated fabric samples (bottom right).

From the EDX spectra we see a spike of the silicon peak after treatment, indicating that Si-based material has been deposited on the surface of the cotton textiles. Indeed, this is consistent to the subsequent observation in the SEM image, where the layers of silicate coating the surface of the cotton textiles. As a first indication, we observed a deposition of silicon-rich material on the surface of cotton textile after the atmospheric plasma treatment. After that, the coated samples register an increase in weight by 1 % (results summarized in Table 7.3).

Textile sample	Wt% increase after FR treatment	Wt% increase after plasma treatment	LOI	Char Yield (%)
FR and Plasma	8.0	1.1	30.5	32.0
FR only	8.6	-	30.6	33.0
Plasma only	-	1.1	17.6	3.8
Untreated	-	-	17.5	3.5

Table 7.3: The properties of FR-pretreated cotton textiles after treatment with atmospheric pressure plasma coupled with deposition of HMDSO.

When the textile sample is treated only with plasma, 1.1 wt% increase is measured, but the LOI and char yield does not show significant difference from those of untreated textiles. This shows that the plasma treatment does not affect the LOI behavior and char yield when the treated textiles are burned. In the presence of FR species, the plasma treatment also does

not alter the LOI and char yield of the treated textile samples. This suggests that this atmospheric plasma treatment does not degrade or affect the structural properties of the FR.

### 7.3.2 Thermal Degradation and Heat Release Profile of Plasma treated FR textiles

The thermal decomposition curves of the textiles treated under various conditions are presented in the following Figure 7.6.

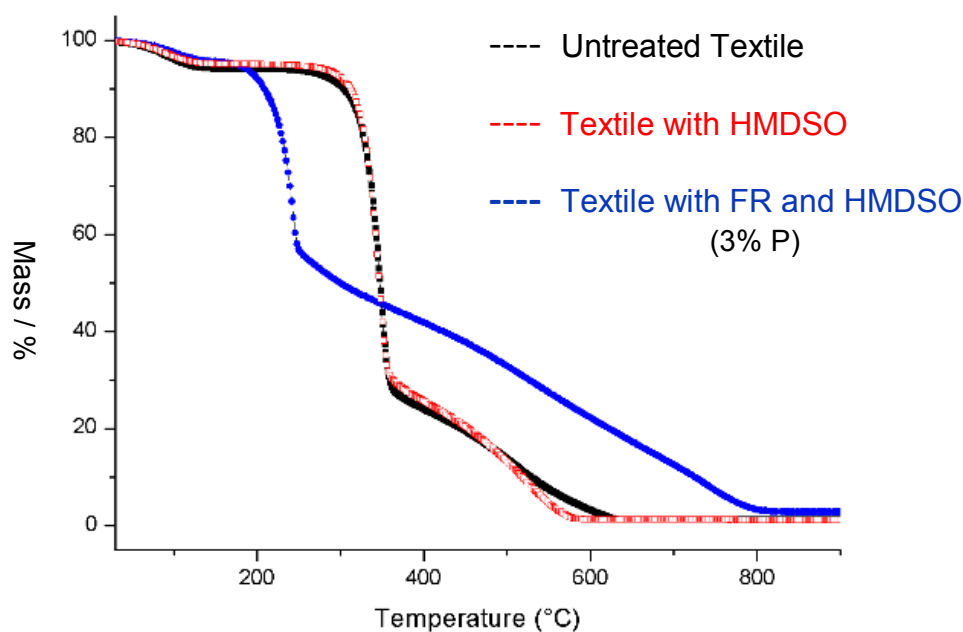


Figure 7.6: TGA spectra of untreated textile and textiles treated under various conditions.

From Figure 7.6, one observes a decrease in the temperature at onset of decomposition only in the textiles where the FR species is present. The thermal degradation profiles of untreated textiles and textiles treated with only HMDSO are almost identical to each other. This shows firstly, the flame retardant efficiency is contributed only by **P-OTMS**. Both the atmospheric plasma treatment and HMDSO deposition does not affect the flammability of the virgin textile. While it seems that the flame retardancy of the FR-treated textile is not altered after the plasma treatment and HMDSO deposition, the gradual mass loss step that occurs between 230°C and 800°C seems to suggest that the FR is gradually lost from the condensed phase within this temperature range. This could possibly be an effect of the deposition and plasma treatment.

Unsurprisingly, the differences in the behaviour of these samples are also observed in their heat release profiles, shown in the following Figure 7.7.

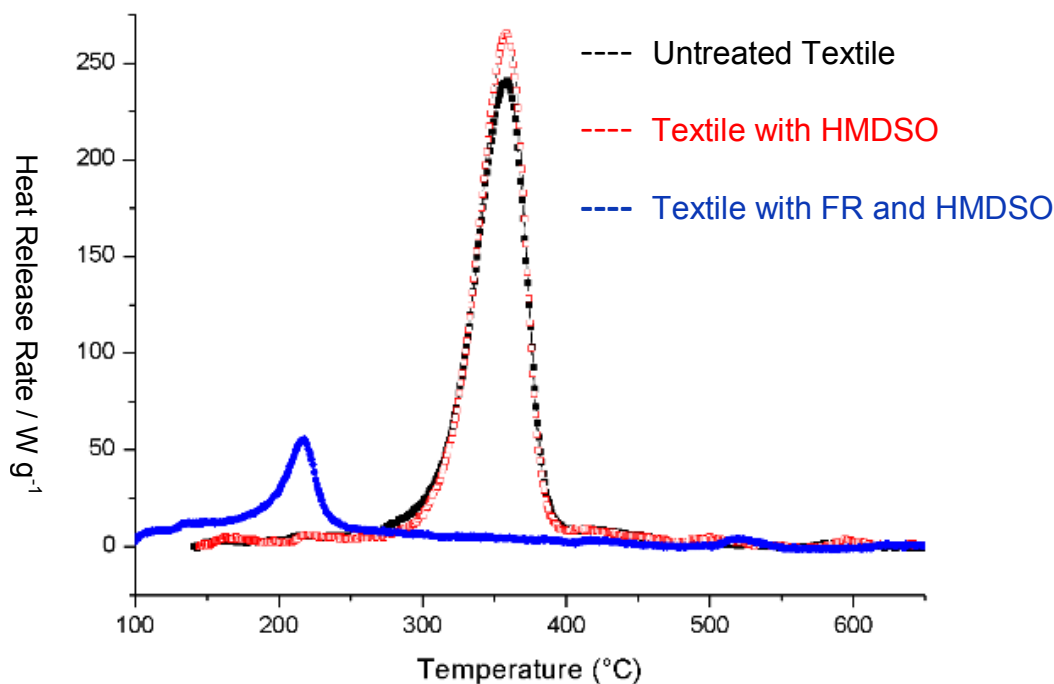


Figure 7.7: Heat release curves of untreated textile and textile sample treated under various conditions.

The virgin textile which has undergone HMDSO and plasma treatment show an almost identical HR profile with textile which has not undergone any treatment. The HR profile of FR-treated textile which underwent deposition and plasma treatment shows a major heat release event with the peak HRR occurring at a much lower temperature (205°C), although there are some heat already being released between 125°C and 180°C. This shows, again that the plasma and HMDSO treatment does not affect the flammability of cotton textiles, but shows some influence to the HR of textiles pre-treated with FR. This indicates that the Si-based material could have some interference to the interaction between the FR and the cellulose moieties.

However, one must take note that the Si content here is relatively low – 0.27% Si based on the weight increase after the deposition and plasma treatment. With only a 1.2% increase in HRR in the presence of Si-based material, it is perhaps acceptable, and the deposition rate could be further increased to observe how the HRR is affected by the amount of Si added to the surface of textiles.

## **7.4 Concluding Remarks**

Summarizing the results from this chapter, the following conclusions could be drawn:

1. In the presence of cross-linking agents and photoinitiator, the simultaneous grafting and polymerization of AC8 polymer across the surface of cotton textiles through the PIGP process has been achieved.
2. The presence of AC8 on the textile surface does not affect the flame retardant properties of the FR-impregnated textile.
3. The presence of FR does not alter the water repellence properties of the surface modified textile.
4. The surface grafted AC8 polymer not only confers hydro- and oleophobicity, but it also protects the FR pre-treated textiles against rinsing by water.
5. With the HDMSO deposition coupled with atmospheric plasma treatment, we found that the Si-based materials are deposited on the surface. Preliminary flammability measurements suggest that they could interfere with the interaction between FR and cellulose during thermal decomposition, however given their relatively low content (0.3% in general) on textiles, this effect can be neglected. We could next attempt at higher deposition rates to observe how the flammability can be affected by thicker Si-based coatings on FR-treated textiles.



# **Chapter 8**

## **Conclusions and Outlook**

## 8.1 Conclusions from this thesis by chapter

These are what we have learned so far from the results of our investigations in each of the chapter:

In chapter 2, we learned that the presence of Si does not affect the flammability of the cotton textile, with or without the presence of P-based FR. However, APTMS does improve the grafting yield of DEAEPN with its higher affinity to cellulose.

In chapter 3, we reported in quantitative yields the syntheses of 8 compounds whose FR properties were investigated for the first time. While only **PNP-OTMS** was synthesized with a new procedure, the application of the other compounds as FRs have never been reported.

In chapter 4 and 5, we learned that the phosphate silyl esters have much better FR efficiency compared to the phosphate esters. This can be attributed to their smaller sizes after losing their TMS groups, hence allowing access to greater density of primary OH sites on the cellulose chain for phosphorylation to take place. Not only that, phosphorylation of the cellulose for phosphate silyl esters takes place at room temperature.

In chapter 5, we also demonstrated the possibility to combine phosphorus-nitrogen cooperativity, containing phosphate silyl ester bonds to achieve an enhanced flame retardant properties on cotton textiles.

In chapter 6 we learned that with **PNN-OEt** and **PNNP-OEt** as examples, the modification of the amide side chain by addition of a nitrogen-nitrogen bond have limited effect in improving the flame retardant properties of the phosphoramidate on cotton textiles. **P-NH<sub>2</sub>** performs better than the phosphorohydrazidates at low P content because of its smaller molecular size, and **PNN-OEt** performs better than **PNNP-OEt** and **P-NH<sub>2</sub>** at higher P contents because of its higher nitrogen-to-phosphorus ratio and its possession of a primary amide group.

In Chapter 7, we presented our achievement of the objective to render the FR pre-treated textiles water repellent and rinse resistant. This was done by the modification of the surface of textiles with an AC8 monomer, followed by its simultaneous graft and polymerization onto the textile surface through an argon plasma treatment via the PIGP process. Preliminary studies with PeCVD of HDMSO on FR-treated textile using atmospheric plasma have shown that the plasma treatment does not adversely affect the structural properties of the FR on cotton textiles.

## 8.2 The Overview

In this thesis, we have reported for the first time the FR properties of 8 new compounds. We also attempted to establish a relationship between their structures to their FR efficiencies by the comparison and assessment of the FR efficiencies of different category of bonds. Namely, between phosphate silyl esters and phosphate esters, between hypophosphates and pyrophosphates, between pyrophosphates and imidodiphosphates and between phosphoramidates and phosphorohydrazidates.

The results of our investigations through LOI, TGA and PCFC measurements reveal that the FR can be most efficiently enhanced by having silyl ester side groups. This enhancement is much more pronounced than modifying the phosphorus centre of the FR compound with either a direct P-P bond (hypophosphate) or with a bridging oxygen (pyrophosphate). The relative better FR efficiency observed in imidodiphosphates (P-N-P) over pyrophosphates (P-O-P) exemplifies the phosphorus-nitrogen synergism in FR efficiency studies. As the best FR compound in this thesis, **PNP-OTMS** revealed the possibility of combining silyl ester side groups and phosphorus-nitrogen synergism to achieve additional enhancement of FR efficiency. In the cases of phosphoramidates, phosphorohydrazidates and N-silylated phosphoramidates, the modification of amide side groups brings about limited enhancement to the flame retardant properties of the compound.

The most important finding in this thesis lies in the reduced molecular size of phosphate silyl esters after desilylation: after losing TMS side groups, they become 'naked' phosphates, which can be packed more densely over the same surface area and have access to more primary OH sites on the cellulose chains. This facilitates and allows phosphorylation to take place at room temperature.

Assessing the role that silicon plays to the flame retardancy is a tricky task: the organosilicon compounds used in this thesis (APTMS, HDMSO) reveals that silicon possess very limited FR efficiency compared to phosphorus, and does not enhance the FR efficiency of phosphorus-based FRs when present as physical mixtures on the surface of cotton textiles. However, in phosphate silyl esters one could say that they play a role in enhancing the FR efficiency of the compound – by acting as a leaving group. Unlike in phosphorus-nitrogen synergism, where the nitrogen atom usually remains in the condensed phase, silicon in phosphate silyl esters achieve the same effect by leaving the condensed phase. In this aspect, naming this effect as

“synergism” or “cooperativity” would be ironic, as silicon does not directly participate in the condensed phase action to the thermal degradation of cellulose.

To avoid altering the physical properties of the cotton textiles, a condition of maximum 3% P content (or 20% of FR to the weight of textile, depending on the molecular weight of the FR) with LOI 26 is set for most industrial applications. A big advantage of using phosphate silyl esters as FRs here lies therein, that they already possess very high LOI values (>30) at low P contents (< 2%) on textiles. Essentially, these silyl ester flame retarded textiles are self-extinguishing at ambient conditions. Furthermore, through PIGP we protected the FR-treated textile by graft polymerization of a hydrophobic monomer on the surface of textile without affecting the FR efficiency of the compound on cotton fabric. Finally, the atmospheric plasma processing shows promising results in conferring water repellence to the FR-treated textiles. With our current attempt towards conferring washing durability onto these phosphate silyl ester treated textiles, the potential towards a large scale production and application of commercially viable self-extinguishing textiles will be well in sight.

### **8.3 Outlook**

Combining our findings in this thesis and in the works of previous students in the laboratory, we have identified the following key aspects of designing the ideal flame retardant molecule for cotton textiles:

1. A stable network of FR on the surface of textiles: A functional group that allows the graft polymerization of the flame retardant molecule onto the surface of cotton textiles.
2. Flame Retardancy: provided by the core of the molecule, consisting of phosphorus-nitrogen direct bond, utilizing the phosphorus-nitrogen cooperativity in flame retardancy.
3. Small molecules: With either “naked” reactive phosphoramidates/phosphates or suitable precursors, the use of phosphoric acid could be avoided. Too many carbon-containing FR side groups tend to contribute to the fuel during the burning.

It has already been shown in previous works about the efficiency of diethyl (2-acryloxyethyl) phosphoramidate, or DEAEPN, which demonstrates the possibility of combining the first and second criteria in the molecular design. In this thesis we have presented the possibility of

combining the second and third criteria of the ideal flame retardant.

### **DEAEPN: The Silyl Ester Derivative**

Therefore, it would be interesting to study next the possibility of combining all the above mentioned criteria for an excellent flame retardant that is also wash durable. This can be achieved by studying the silyl ester derivative of DEAEPN.

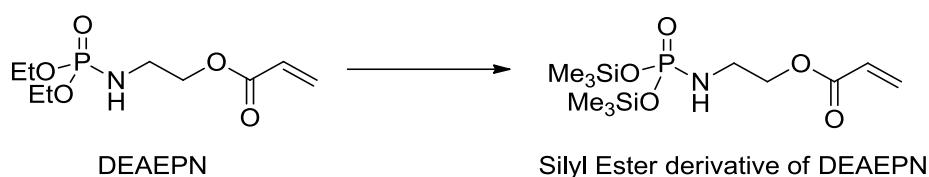


Figure 8.1: The chemical structure of a proposed silyl ester derivative of DEAEPN

### **Cyclic phosphate esters**



Figure 8.2: Cyclic phosphate esters with an oxygen (left) or a nitrogen (right) bridge.

In facilitating the phosphorylation reaction of the molecules to the cellulose chains, it would be worth while investigating on the feasibility of cyclic phosphate esters. These esters are expected to be more stable than the phosphate silyl esters, hence would be expected to exhibit considerably well flame retardant properties.

Last but not least, the development of atmospheric plasma processes in conferring desired additional properties onto cotton textiles will be crucial in determining the eventual viability of these FR-treated textiles towards large scale applications. Other than PeCVD processes, we could also attempt treatment on textiles already impregnated by FR compounds and the precursor of the compound that would eventually give the desired additional properties on the textile. For example, the treatment of textile impregnated with silyl ester derivative of DEAEPN and APTMS would potentially give the processed textile good FR efficiency that is durable to laundering processes.



# **Chapter 9**

## **Experimental, Miscellaneous and Appendices**

## 9.1 Chemicals and Materials

All experiments involving chemical synthesis were performed using Schlenk techniques under argon atmosphere. Solvents for synthesis such as dichloromethane, petroleum ether, formamide were used as purchased. Where necessary, solvents such as tetrahydrofuran or diethyl ether were dried and degassed prior to use. Solvents for impregnation of cotton textile samples were used as purchase without further purification. Diethyl phosphite (Sigma-Aldrich), diethyl chlorophosphate (Acros), triethyl phosphate (Sigma-Aldrich), N, N, N', N'-tetraethylethylenediamine (TEEDA) and tris(trimethylsilyl) phosphate (TCI-Deutschland) and used without further purification. Copper (I) chloride (CuCl) (Fluka) was purified as described in the literature<sup>83</sup> and kept under a dessicator before use. Bromotrimethylsilane (TMSBr) (ABCR) was kept in a refridgerator and allowed to warm to room temperature before use without further purification.

### NMR Spectra Measurements

Nuclear Magnetic Resonance (NMR) experiments were recorded on Bruker Avance 250, 300 or 500 MHz spectrometers. The spectral data were calibrated according to external standards (SiMe<sub>4</sub> for <sup>1</sup>H and <sup>13</sup>C, H<sub>3</sub>PO<sub>4</sub> for <sup>31</sup>P).

### Melting Points

Melting points were determined by using the Büchi apparatus. Samples were measured using open tube capillaries

### Boiling Points

Boiling points were determined during by distillation of the respective products to obtain pure samples.

## 9.2 Synthesis of Flame Retardant Compounds

### 9.2.1 Tetraethyl Hypophosphate (PP-OEt)

The synthesis of **PP-OEt** was carried out according to a procedure modified from the literature<sup>49</sup>. In a one-neck rbf, a solution of TEEDA (1.4 mL, 6 mmol, 0.3 equiv) in 2 mL acetone (absolute grade, used as purchase without further purification) was charged. CuCl (200 mg, 2 mmol, 0.1 equiv) was added into the mixture. The solution turned greenish yellow. To this solution, diethyl phosphite (2.56 mL, 20 mmol, 1.0 equiv) was then added. The mixture was



left to stir in air under a drying tube packed with anhydrous calcium chloride powder.

The colour of the solution changes gradually from yellowish green to green, turquoise then blue at the end of the reaction after 25.5 hours of stirring. The progress of the reaction was traced with  $^{31}\text{P}$  NMR spectroscopy. The reaction is deemed completed when a singlet peak at 6.5 ppm is observed in the proton-coupled  $^{31}\text{P}$  NMR spectrum.

To isolate the product, the solvent was first removed via rotavapor. Dichloromethane was then added to the mixture in a separation funnel. Here, 8 mL saturated ammonium chloride solution was added, thoroughly shaken, and the yellow organic phase was collected. This step was repeated twice. To the organic phase, the solvent was removed by rotavapor, followed by a distillation at 77°C under  $10^{-2}$  mbar. A colourless distillate is then obtained.

Yield: 70%

Boiling point: 77 - 79°C at  $10^{-2}$  mbar

NMR [ $\delta$ /ppm] ( $\text{CDCl}_3$ , RT)

$^{31}\text{P}$  (101.3 MHz) : 6.5 (s)  
 $^1\text{H}$  (250.13 MHz) : 1.37 (t,  $^2J_{\text{HH}} = 6.9$  Hz,  $\text{CH}_3$ , 3H); 4.27 (m,  $\text{OCH}_2$ , 2H)  
 $^{13}\text{C}$  (50.3 MHz) : 63.9 (dd,  $^2J_{\text{C-P}} = 3.1$  Hz,  $\text{CH}_2$ ), 16.4 (dd,  $^2J_{\text{C-P}} = 3.1$  Hz,  $\text{CH}_3$ ).

### 9.2.2 Tetraethyl Pyrophosphate (POP-OEt)

To a solution of water (0.71 mL, 0.039 mol, 1 equiv) in pyridine (6.4 mL) under a water bath, diethyl chlorophosphate (11.2 mL, 0.0775 mol, 2 equiv) was added. White precipitate appeared almost immediately after addition. The mixture was left to stir for another 10 minutes and then filtered. Pyridine was then removed via reduced pressure, giving a viscous colourless liquid.

Yield: 85%

Boiling point: 135 – 138°C,  $10^{-2}$  mbar

NMR [ $\delta$ /ppm] ( $\text{CDCl}_3$ , RT)

$^{31}\text{P}$  (101.3 MHz) : -13.1 (s)  
 $^1\text{H}$  (250.13 MHz) : 1.21 (b,  $\text{CH}_3$ , 3H) ; 4.09 (b,  $\text{OCH}_2$ , 2H)  
 $^{13}\text{C}$  (50.13 MHz) : 15 (t,  $^3J_{\text{CP}} = 3.7$  Hz,  $\text{CH}_3$ ) ; 64.2 (t,  $^2J_{\text{CP}} = 2.7$  Hz,  $\text{OCH}_2$ )

### 9.2.3 Tetrakis(trimethylsilyl) Pyrophosphate (POP-OTMS)

**POP-OTMS** was synthesized according to a modified procedure<sup>53</sup>. In a 250 mL rbf, dihydrogen disodium pyrophosphate (2.22g, 0.01 mol) and formamide (25 mL) were loaded. Under vigorous stirring, trimethylsilyl chloride (4.55 g, 0.044 mol) was added drop wise while the flask was placed under an ice bath. After 1 hour of stirring, petrol ether (100 mL) was added to the mixture. After 5 minutes of further stirring, the mixture was allowed to settle. The top colourless layer of liquid was transferred to a Schlenk tube, then the solvent and excess trimethylsilyl chloride were removed via reduced pressure to give a colourless liquid. This liquid can be stored at -30°C as a clear and colourless solid.

Yield: 82%

Melting point: 150°C (decomp.)

NMR [ $\delta$ /ppm], CDCl<sub>3</sub>

<sup>31</sup>P (101.3 MHz) : -30.8 (s)

<sup>1</sup>H (250.13 MHz) : 0.24 (s)

<sup>13</sup>C (50.13 MHz) : 0.6 (s)

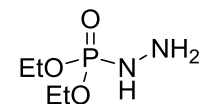
<sup>29</sup>Si (59.5 MHz) : 55.6 (s)

### 9.2.4 Diethyl Phosphorohydrazidate (PNN-OEt) and N, N'-Bis(diethyl)phosphoryl Hydrazidate (PNNP-OEt)<sup>54</sup>

To a mixture of tetrachloromethane (120 mL), dichloromethane (200 mL), anhydrous, finely powdered potassium carbonate (4.14 g, 0.03 mol) and triethylbenzylammonium chloride (40 mg, 1 mol%), 80% hydrazine hydrate (1.25 g, 0.02 mol) was added dropwise at 20°C. The stirring was continued for 15 min at room temperature. Then, a solution of diethyl phosphite (2.56 mL, 0.02 mol) in dichloromethane (30 mL) was added at 20°C under a water bath. After the addition has completed, the mixture was left to for another 4 hours at room temperature. The solid is then filtered off the mixture, and washed with dichloromethane. After evaporation of the solvent, the residue was placed under reduced pressure (10<sup>-3</sup> mbar) for at least 2 hours to remove traces of volatile impurities. The resulting product is a colourless liquid of **PNN-OEt**.

To synthesize **PNNP-OEt**, the same procedure is repeated until the filtration of potassium carbonate. After the filtration, anhydrous magnesium sulphate (4 g) and trimethylamine (2.75 mL, 0.02 mol) were added to the filtrate. A solution of diethyl phosphite (2.56 mL, 0.02 mol) was then added dropwise, with the mixture stirring at 20°C under a water bath. The stirring remained for 2 hours after addition at room temperature. The resulting mixture was then

filtered, evaporated, diluted with toluene, then filtered again to remove trimethylamine hydrochloride salt. The subsequent evaporation of solvent yields the colourless crystalline solid of **PNNP-OEt**, which can be purified by crystallization from toluene: hexane (1:1)



**PNN-OEt**

Yield: 91.2%

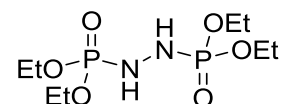
Boiling point: 160 – 162°C

NMR [ $\delta$ /ppm], CDCl<sub>3</sub>

<sup>31</sup>P (101.3 MHz) : +8.5 (s)

<sup>1</sup>H (250.13 MHz) : 4.74 (NH, d, 1H) <sup>2</sup>J<sub>H-P</sub> = 29.6 Hz; 4.05 (OCH<sub>2</sub>, p, 4H) <sup>3</sup>J<sub>H-P</sub> = 6 Hz; 3.31 (NH<sub>2</sub>, b, 2.3H); 1.28 (CH<sub>3</sub>, t, 3H)

<sup>13</sup>C (50.3 MHz) : 63.0 (OCH<sub>2</sub>, s); 16.4 (CH<sub>3</sub>, s)



**PNNP-OEt**

Yield: 80.4%

Melting point: 99 – 101°C

NMR [ $\delta$ /ppm], CDCl<sub>3</sub>

<sup>31</sup>P (101.3 MHz): +6.8 (s)

<sup>1</sup>H (250.13 MHz): 5.25 (NH, d, <sup>2</sup>J<sub>H-P</sub> = 25 Hz, 2H); 4.12 (OCH<sub>2</sub>, t, <sup>3</sup>J<sub>H-P</sub> = 7 Hz, 8H); 1.33 (CH<sub>3</sub>, t, <sup>3</sup>J<sub>H-P</sub> = 6 Hz, 12H)

<sup>13</sup>C (50.3 MHz): 63.2 (CH<sub>2</sub>, t, <sup>2</sup>J<sub>C-P</sub> = 2 Hz, 4C); 16.1 (CH<sub>3</sub>, t, <sup>2</sup>J<sub>C-P</sub> = 4Hz, 4C)

### 9.2.5 *N*-Trimethylsilyl Phosphoramidate (PN-TMS)

To a solution of diethyl phosphoramidate (3.06 g, 0.02 mol, 1 equiv) in dichloromethane in a 2-neck rbf, trimethylsilyl chloride (2.54 mL, 0.02 mol, 1 equiv) was added in the presence of trimethylamine (2.8 mL, 0.025 mol, 1.25 equiv). During the addition, a white precipitate quickly appeared while the solution remained colourless. The mixture was left on stirring for a further 2 hours after the addition, and then filtered. After removal of the solvent via reduced pressure, colourless crystals were obtained.

Yield: 91%

Melting point: 53 – 54.5°C

NMR [ $\delta$ /ppm], CDCl<sub>3</sub>

<sup>31</sup>P (101.3 MHz): 9.4 (s)

<sup>1</sup>H (250.13 MHz): 4.1 (CH<sub>2</sub>, q, <sup>3</sup>J<sub>HP</sub> = 6 Hz, 4H); 2.2 (Si(CH<sub>3</sub>)<sub>3</sub>, s, 12H), 1.43  
(CH<sub>3</sub>, q, <sup>2</sup>J<sub>HP</sub> = 6Hz, 6H)

<sup>13</sup>C(50.3 MHz): 30.9 (s), 16.2 (s); 0.63 (s)

## 9.2.6 Tetrakis(trimethylsilyl) Imidodiphosphate (PNP-OTMS)

### Intermediate **B1**: Diethyl Phosphoroazidate<sup>64</sup>

Sodium azide\* (17 g, 0.26 mol, 3 equiv) was first added into an oven-dried, argon-filled 500-mL three neck rbf. This solid is then suspended in 120 mL of freshly distilled acetone (from CaSO<sub>4</sub>). Diethyl phosphorochloridate (15 g, 0.086 mol, 1 equiv) was then added into the suspension. The resultant mixture was then brought to reflux at an oil bath temperature of 80 °C.

After 20 hours, monitoring by <sup>31</sup>P NMR of the solution indicated a complete reaction (change in chemical shift from 4.3 ppm to 0.1 ppm). The resulting white suspension was then filtered and acetone was removed from the filtrate via reduced pressure, yielding a colourless liquid of diethyl phosphoroazidate **1**.

\*(**CAUTION**: Danger of **EXPLOSION** when handling sodium azide with metallic equipments. Keep **AWAY** from sources of heat.)

Yield: 84 %

NMR [δ/ppm], neat

<sup>31</sup>P (101.3 MHz): 0.1 (s)

### Intermediate **B2**: Diethyl (triethoxy-λ<sup>5</sup>-phosphanylidene)phosphoramidate

The colourless liquid of **B1** was first dissolved in 120 mL of dry toluene. Under a water bath, triethyl phosphite (17.9 mL, 0.104 mol, 1.2 equiv) was slowly added to this solution. Effervescence was observed during the addition. When the addition was completed, the resulting mixture was heated to 60°C for the next 12 h. At the end of the reaction, toluene was removed via reduced pressure to yield a faint yellow liquid of diethyl (triethoxy-λ<sup>5</sup>-phosphanylidene)phosphoramidate **B2**. To remove the excess triethyl phosphite, the remaining liquid was placed for an additional three hours in an oil bath at 50°C under reduced pressure. In <sup>31</sup>P NMR, the isolation of pure **B2** is identified with a characteristic AB quartet centered at -2.3 ppm.

NMR [δ/ppm], neat

<sup>31</sup>P (101.3 MHz): -2.3 (ABq, 2P, Δδ<sub>PP</sub> = 0.575, <sup>2</sup>J<sub>PP</sub> = 69 Hz)

**Intermediate B3: Tetraethyl Imidodiphosphate (PNP-OEt)**

In an oven dried, argon-filled 500 mL three-neck rbf, 150 mL of 2.0 M HCl (0.104 mol, 2 equiv) in diethyl ether solution was charged. In the dropping funnel, 100 ml diethyl ether was first added, followed by **B2** (16 g, 0.050 mol, 1 equiv). The resulting solution was dropwise added into the HCl in diethyl ether solution. This mixture was brought to reflux in an oil bath at 50 °C for 24 h.

The reaction is complete when the characteristic quartet peak is no longer observed, giving a singlet peak at -2 ppm in its <sup>31</sup>P NMR spectrum. Diethyl ether was then removed by reduced pressure to afford an off pink viscous liquid of tetraethyl iminodiphosphate (**PNP-OEt**) **B3**.

To remove excess HCl, the resulting liquid was placed under reduced pressure, passing through KOH powder over a filter for 24 hours. The disappearance of a broad singlet at 8 ppm in the <sup>1</sup>H NMR spectrum signifies a complete removal of HCl from the mixture.

Yield: 76.2%

Boiling point: 145°C (decomp.)

NMR [δ/ppm], Et<sub>2</sub>O

<sup>31</sup>P (101.3 MHz): -2 (s)

**Final Product B4: Tetrakis(trimethylsilyl) Imidodiphosphate (PNP-OTMS)**

To a solution of **B3** (5 mL, 0.017 mol, 1 equiv) in dichloromethane under a water bath, trimethylsilyl bromide (14 mL, 0.104 mol, 6 equiv) was added slowly. The resulting mixture was kept under reflux for 60 hours. The reaction is considered complete when only a singlet at -17 ppm is observed in the <sup>31</sup>P NMR spectrum. The final product was isolated as a white viscous paste, which can be recrystallized in hexane giving slightly brown crystalline solid of tetrakis(trimethylsilyl) iminodiphosphate (**PNP-OTMS**). The solid can be stored in the glovebox under room temperature as it is sensitive towards hydrolysis. Yield: 70%

Melting point: 152 °C (decomp.)

NMR [δ/ppm], CDCl<sub>3</sub>

<sup>31</sup>P (101.3 MHz): -17 (b, s)

<sup>1</sup>H (250.13 MHz): 0.32 (b, s)

<sup>13</sup>C (50.3 MHz): 0.81 (b, s)

### **9.3 Preparation of Flame Retardant-Impregnated Cotton Textile Sample**

#### **Elemental Analysis (EA)**

EA were carried out by Micro-Laboratory (Institute of Organic Chemistry), ETH Zurich. Before carrying out the elemental analyses, all samples were dried. Bulk elemental analysis (C, H, N and O) of the samples was carried out on a LECO CHN-932 microanalyzer. All samples were analysed in triplicate and the values are reproducible within  $\pm 0.4\%$  (relative standard deviation).

#### **Sample Preparation**

Cotton textile samples are cut into dimensions of 10 cm x 5 cm, and placed in a standard climate of humidity ( $65 \pm 2$ ) % at ( $20 \pm 2$ ) °C for at least 24 hours (DIN EN 20 139). For this standard climate, a glass container containing a saturated aqueous solution of ammonium nitrate ( $\text{NH}_4\text{NO}_3$ ) was used.

#### **Impregnation of Flame Retardants on Cotton Textile**

For 1 g of textile sample, 1 mL of total liquor is used (*total* volume of flame retardant and, where necessary, photoinitiators and cross-linking agents). The amount of flame retardant for application was calculated based on the percentage to the weight of textile. The quantity of photoinitiator and cross-linking agent were calculated based on the percentage to the weight of the flame retardant.

The liquor was prepared by dissolving the relevant materials in THF (for the case of most phosphate esters and silyl esters only) or dichloromethane (for the case of AC8) to a total of 1 mL. The textile samples, pre-conditioned under the standard climate, were first weighed and then placed on a glass petri dish. Thereafter, the liquor was then collected with a syringe and transferred drop wise onto across the area of the textiles. The transfer was done carefully to ensure the entire area of the sample has been immersed with the same volume of liquor.

After complete evaporation of the solvent (constant weight of the textiles obtained), the increase in weight of the textile is recorded and is ready for the next course of action.

## **9.4 Plasma Treatment of the Textiles**

PIGP is performed in our laboratory with the microwave plasma generated by a *Europlasma DC300PC* system. This system is made up of three parts:

1. A microwave generator (2.46 GHz) with a tunable power ranging from 0 to 600 W which generates the glow discharge
2. A vacuum chamber (27 L, aluminum-based container)
3. A pumping system generating the vacuum (E2M28 PFPE, *Edwards*)

The gas flow is monitored by unit mass flow controllers.

In a typical experiment, a cotton textile sample is placed on a glass petri dish and inserted into the vacuum chamber. In general, the plasma treatment time is 20 mins for all monomers, except for AC8 which is 10 mins. The flow of argon is set at 130 sccm, power of the microwave generator at 100 W and the base pressure at 40 Pa). After the treatment, the textile samples are placed in the standard climate for at least 24 hours before proceeding with the next course of action.

## **9.5 Characterization of Flame Retardancy**

### ***Limiting Oxygen Index (LOI)***

LOI measurements were performed according to the standard ISO 4589-2 using an Oxygen Index Test Apparatus (Fire Instrumentation Research Equipment Ltd) with digital oxygen concentration readout to an uncertainty of 0.1 %. Textile samples of 10 cm x 5 cm dimension was fixed on a sample holder before being placed onto the LOI burning chamber. The air in the chamber was set to contain a mixture of nitrogen and technical grade oxygen, with a total air flow of 18.0 L min<sup>-1</sup>. Fire is then directed from the top and removed once ignition and sustained burning has taken place on the substrate. The LOI value is taken to be the lowest percentage of oxygen at which a self-sustained combustion could take place.

### **Pyrolysis Combustion Flow Calorimetry (PCFC)**

PCFC measurements were performed to measure the heat release rate (Fire Testing Technology). The heat release rate was calculated from the principle of oxygen consumption calorimetry<sup>15</sup>, where there is an average of 13.1 MJ released per kg of O<sub>2</sub> consumed during a combustion process. The maximum pyrolysis temperature was set at 750 °C and the combustor temperature at 900 °C. Before measurements, the PCFC instruments were calibrated to the purity of the oxygen source. The gas flow is set at 80% N<sub>2</sub> and 20% O<sub>2</sub> at a



total flow rate of  $100 \text{ cm}^3 \text{ min}^{-1}$ . PCFC measurements were typically performed on textile samples of weight  $(2.0 \pm 0.5) \text{ mg}$ . These samples were placed on a ceramic crucible before being loaded onto the sample holder.

### **Thermogravimetric Analysis – Infrared – Mass Spectrometry (TGA-FTIR-MS)**

TGA were performed on NETZSCH STA449F5 instrument connected to Mass Spectrometer AEOLUS III. Transmission Infra-Red (IR) experiments were recorded on Bruker TENSOR II spectrometer. About 2.5 mg of the samples was heated from  $40^\circ\text{C}$  to  $900^\circ\text{C}$  at a rate of  $10 \text{ K min}^{-1}$  under argon flow. The line that transfers evolved gases from TGA to IR was maintained at  $200^\circ\text{C}$ , while the line that transfers from TGA to MS was maintained at  $230^\circ\text{C}$ . The FTIR spectra were recorded from  $4000 \text{ cm}^{-1}$  to  $600 \text{ cm}^{-1}$  at a resolution of  $4 \text{ cm}^{-1}$  with 32 scans per sample. The TGA data obtained during the measurement was analyzed using Netzsch Proteus – Thermal Analysis Software. The IR spectra are analyzed using the OPUS software.

## **9.6 Characterization Methods for Compounds and Surface Modified Textiles**

### **Scanning Electron Microscopy (SEM)**

SEM was performed on a LEO1530 Gemini Microscope (Zeiss) with a field gun emission operated at a different voltages (from 1 to 3 kV). For the preparation, small samples were stuck on an aluminium holder with a gluey carbon film.

### **Energy-Dispersive X-Ray Spectroscopy (EDX)**

TEM was performed on a Tecnai F30 (FEI, USA; FEG (field emission gun), Super Twin lens, point resolution ca. 0.2 nm microscope operated at 300 kV. Local elemental analysis was done with an energy-dispersive X-ray spectrometer (EDAX, USA) which is attached to the microscope.

### **X-Ray Photoelectron Spectroscopy (XPS) Measurements**

XPS spectra presented in this thesis were acquired with a Sigma-II probe of Thermo Fischer Scientific. Analyses were carried out with a non-monochromatic Al K $\alpha$  (1486.6 eV) source. Full-width-at-half-maximum (fwhm) of Ag  $3d_{5/2}$  was 1.27 eV. Survey spectra were acquired with a pass energy of 50 eV and a step size of 1 eV. The pass energy and the step size for narrow scan were 25 and 0.1 eV, respectively. In both cases, the emission angle was 50°. The spectrometer was calibrated according to ISO 15472:2001 with an accuracy of  $\pm 0.2$  eV. The textile samples were placed under  $10^{-3}$  mbar for at least 20 days at room temperature to remove all moisture.

### **Measurement of Hydrostatic Permeability (Schmerber Pressure)**

The Schmerber Pressure was measured according to the Standard ASTM using the TexTest instrument FX 3000. For this measurement, a textile sample of dimension 10 cm x 10 cm was cut and placed under constant atmosphere for at least 24 hours. The sample was then placed under the instrument and the pressure gradient is set at 10 mbar per minute. The Schmerber Pressure of the textile sample was determined as the hydrostatic pressure at which three droplets of water are present on the upper surface of the textile sample.

## Appendix

### Solid state structure data via X-Ray determination

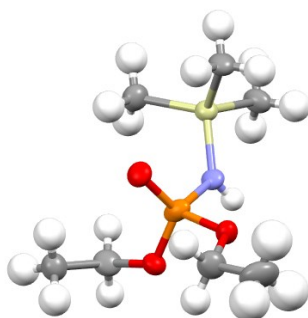


Table 1 Crystal data and structure refinement for ***P-NTMS***.

Identification code	sad
Empirical formula	$C_{14}H_{40}N_2O_6P_2Si_2$
Formula weight	450.60
Temperature/K	100.4
Crystal system	monoclinic
Space group	$P2_1/n$
$a/\text{\AA}$	11.1850(6)
$b/\text{\AA}$	18.4539(10)
$c/\text{\AA}$	12.7366(7)
$\alpha/^\circ$	90
$\beta/^\circ$	105.968(2)
$\gamma/^\circ$	90
Volume/ $\text{\AA}^3$	2527.5(2)
$Z$	4
$\rho_{\text{calc}}/\text{g/cm}^3$	1.184
$\mu/\text{mm}^{-1}$	0.294
$F(000)$	976.0
Crystal size/ $\text{mm}^3$	$0.69 \times 0.24 \times 0.2$
Radiation	MoK $\alpha$ ( $\lambda = 0.71073$ )
$2\theta$ range for data collection/ $^\circ$	4.832 to 58.33
Index ranges	$-12 \leq h \leq 15, -23 \leq k \leq 25, -17 \leq l \leq 13$
Reflections collected	17204
Independent reflections	6737 [ $R_{\text{int}} = 0.0271, R_{\text{sigma}} = 0.0352$ ]
Data/restraints/parameters	6737/0/297
Goodness-of-fit on $F^2$	1.023
Final $R$ indexes [ $I \geq 2\sigma(I)$ ]	$R_1 = 0.0455, wR_2 = 0.1012$
Final $R$ indexes [all data]	$R_1 = 0.0665, wR_2 = 0.1139$
Largest diff. peak/hole / $e \text{\AA}^{-3}$	0.61/-0.76

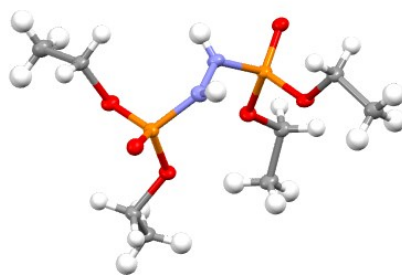


Table 2 Crystal data and structure refinement for **PNNP-OEt**.

Identification code	JE0143_C2c_publishable
Empirical formula	C <sub>8</sub> H <sub>22</sub> N <sub>2</sub> O <sub>6</sub> P <sub>2</sub>
Formula weight	304.22
Temperature/K	296.15
Crystal system	monoclinic
Space group	C2/c
a/Å	18.4984(12)
b/Å	8.0064(4)
c/Å	9.7274(7)
α/°	90.00
β/°	98.847(4)
γ/°	90.00
Volume/Å <sup>3</sup>	1423.54(16)
Z	4
ρ <sub>calc</sub> /cm <sup>3</sup>	1.419
μ/mm <sup>-1</sup>	0.326
F(000)	648.0
Crystal size/mm <sup>3</sup>	0.4 × 0.12 × 0.04
Radiation	MoKα (λ = 0.71073)
2θ range for data collection/°	4.46 to 52.04
Index ranges	-22 ≤ h ≤ 22, -9 ≤ k ≤ 9, -11 ≤ l ≤ 11
Reflections collected	5089
Independent reflections	1398 [R <sub>int</sub> = 0.0190, R <sub>sigma</sub> = 0.0194]
Data/restraints/parameters	1398/0/88
Goodness-of-fit on F <sup>2</sup>	1.082
Final R indexes [I ≥ 2σ (I)]	R <sub>1</sub> = 0.0361, wR <sub>2</sub> = 0.0926
Final R indexes [all data]	R <sub>1</sub> = 0.0435, wR <sub>2</sub> = 0.0975
Largest diff. peak/hole / e Å <sup>-3</sup>	0.88/-0.45

# **Chapter 10**

## **Bibliography**

- (1) N. N. Brushlinsky, M. Ahrens, S. V. Sokolov, P. W. *World Fire Statistics 2016*; 2016.
- (2) Charles Mock, Michael Peck, Catherine Juillard, David Meddings, Andrea Gielen, L. M. *Burn Prevention: Success Stories Lesson Learned*; 2011.
- (3) Association, T. G. **2014**, No. 29, 12.
- (4) Alongi, J.; Malucelli, G. *Rsc Adv.* **2015**, 5 (31), 24239.
- (5) Salimova, V. Structure-Property Relationship Studies on Various Phosphoramidates as Potential Flame Retardants for Cellulose, ETH Zürich, 2013.
- (6) Prinz, K. Flame retardant and dyeing treatment of cellulose fabrics using a combined ' grafting from ' and PIGP process, 2011.
- (7) Akita, K.; Kase, M. *J. Appl. Polym. Sci.* **1967**, 5 (4), 833.
- (8) Capart, R.; Khezami, L.; Burnham, A. K. *Thermochim. Acta* **2004**, 417 (1), 79.
- (9) Franklin, W. E. *J. Macromol. Sci. Part A -Chemistry J. MACROMOL. SCL-CHEM* **1983**, 194 (194), 619.
- (10) Horrocks, A. R. *Polym. Degrad. Stab.* **2011**, 96 (3), 377.
- (11) Kandola, B. K.; Horrocks, a. R.; Price, D.; Coleman, G. V. *Flame-Retardant Treatments of Cellulose and Their Influence on the Mechanism of Cellulose Pyrolysis*; 1996; Vol. 36.
- (12) Willard, J. J.; Wondra, R. E. *Text. Res. J.* **1970**, 40 (3), 203.
- (13) International, A. ASTM International 2010, pp 1–14.
- (14) Lyon, R. E.; Walters, R. N. *J. Anal. Appl. Pyrolysis* **2004**, 71 (1), 27.
- (15) Lyon, R. E.; Walters, R. N. *J. Anal. Appl. Pyrolysis* **2004**, 71 (1), 27.
- (16) Huggett, C. *Fire Mater.* **1980**, 4 (2), 61.
- (17) Schreder, E. D.; La Guardia, M. J. *Environ. Sci. Technol.* **2014**, 48 (19), 11575.
- (18) Klemm, D.; Heublein, B.; Fink, H.-P.; Bohn, A. *Angew. Chemie Int. Ed.* **2005**, 44 (22), 3358.
- (19) Roy, D.; Semsarilar, M.; Guthrie, J. T.; Perrier, S. *Chem. Soc. Rev.* **2009**, 38 (7), 2046.
- (20) Vail, S. L. In *Carbohydrate Research*; T. P. Nevell and S. H. Zeronian, Ed.; 1985; Vol. 142, pp 384–422.
- (21) M. P. Stevens. *Polymer Chemistry*; Oxford University Press, New York, 1999.
- (22) Tsafack, M. J.; Levalois-Grützmacher, J. *Surf. Coatings Technol.* **2007**, 201 (12), 5789.
- (23) Odian, G. *Principles of polymerization*; 2004; Vol. 58.
- (24) Pritchard, M.; Sarsby, R. W.; Anand, S. C. *Handbook of Technical Textiles*; 2000.
- (25) Muthu, S. S. *Handbook of Sustainable Apparel Production*; CRC Press, 2015.
- (26) Gaan, S.; Sun, G.; Hutches, K.; Engelhard, M. H. *Polym. Degrad. Stab.* **2008**, 93 (1), 99.
- (27) Tsafack, M. J.; Levalois-Grützmacher, J. *Surf. Coatings Technol.* **2006**, 200 (11), 3503.
- (28) Tesoro, G. C.; Sello, S. B.; Willard, J. J. *Text. Res. J.* **1969**, 39 (1937), 180.
- (29) Horrocks, A. R.; Kandola, B. K.; Davies, P. J.; Zhang, S.; Padbury, S. A. In *Polymer Degradation and Stability*; 2005; Vol. 88, pp 3–12.
- (30) Gaan, S.; Rupper, P.; Salimova, V.; Heuberger, M.; Rabe, S.; Vogel, F. *Polym. Degrad. Stab.* **2009**, 94 (7), 1125.
- (31) Tsafack, M. J.; Levalois-Grützmacher, J. *Surf. Coatings Technol.* **2006**, 201 (6), 2599.

- (32) Ruffin, C. New Phosphorus Containing Flame Retardants for Cotton Fabrics, ETH Zürich, 2006.
- (33) Tsafack, M. J. Polymerization of Organophosphorus Approach to Flame Retard Polyacrylonitrile and Cotton Textiles presented by, ETH Zurich, 2005.
- (34) Lecoeur, E.; Vroman, I.; Bourbigot, S.; Delobel, R. *Polym. Degrad. Stab.* **2006**, *91* (8), 1909.
- (35) Lecoeur, E.; Vroman, I.; Bourbigot, S.; Lam, T. M.; Delobel, R. *Polym. Degrad. Stab.* **2001**, *74* (3), 487.
- (36) Alongi, J.; Ciobanu, M.; Tata, J.; Carosio, F.; Malucelli, G. *J. Appl. Polym. Sci.* **2011**, *119* (4), 1961.
- (37) Ruffin, C.; Fischbach, U.; Grützmacher, H.; Levalois-Grützmacher, J. *Heteroat. Chem.* **2007**, *18* (7), 721.
- (38) Wang, S.; Sui, X.; Li, Y.; Li, J.; Xu, H.; Zhong, Y.; Zhang, L.; Mao, Z. *Polym. Degrad. Stab.* **2016**, *128*, 22.
- (39) Przybylak, M.; Maciejewski, H.; Dutkiewicz, A.; Wesolek, D.; Władyka-Przybylak, M. *Polym. Degrad. Stab.* **2016**, *128*, 55.
- (40) Tobita, H.; Hamielec, A. E. In *Ullmann's Encyclopedia of Industrial Chemistry*; Wiley-VCH Verlag GmbH & Co. KGaA: Weinheim, Germany, 2015; pp 1–50.
- (41) Mayer-Gall, T.; Knittel, D.; Gutmann, J. S.; Opwis, K. *ACS Appl. Mater. Interfaces* **2015**, *7* (18), 9349.
- (42) Tibbitt, J. M.; Jensen, R.; Bell, A. T.; Shen, M. *Macromolecules* **1977**, *10* (3), 647.
- (43) Johnson, D. R.; Osada, Y.; Bell, A. T.; Shen, M. *Macromolecules* **1981**, *14* (1), 118.
- (44) Horrocks, A. R.; Tune, M.; Cegielka, L. *Text. Prog.* **1988**, *18* (1–3), 1.
- (45) Baudler, M. *Zeitschrift für Anorg. und Allg. Chemie* **1956**, *288* (3–4), 171.
- (46) Leininger, E.; Chulski, T. *J. Am. Chem. Soc.* **1949**, *71* (7), 2385.
- (47) Stec, W.; Zwierzak, A. *Can. J. Chem.* **1967**, *45* (21), 2513.
- (48) Błaziak, D.; Guga, P.; Jagiełło, A.; Korczyński, D.; Maciaszek, A.; Nowicka, A.; Pietkiewicz, A.; Stec, W. *J. Org. Biomol. Chem.* **2010**, *8* (24), 5505.
- (49) Zhou, Y.; Yin, S.; Gao, Y.; Zhao, Y.; Goto, M.; Han, L.-B. *Angew. Chemie Int. Ed.* **2010**, *49* (38), 6852.
- (50) TOY, A. D. F. *J. Am. Chem. Soc.* **1948**, *70* (11), 3882.
- (51) McKenna, C. E.; Higa, M. T.; Cheung, N. H.; McKenna, M.-C. *Tetrahedron Lett.* **1977**, *18* (2), 155.
- (52) Kühnel, E.; Laffan, D. D. P.; Lloyd-Jones, G. C.; Martínez del Campo, T.; Shepperson, I. R.; Slaughter, J. L. *Angew. Chemie Int. Ed.* **2007**, *46* (37), 7075.
- (53) Wessjohann, L. A.; Dessoy, M. A. *Polyhedron* **2014**, *70*, 133.
- (54) ZWIERSZAK, A.; SULEWSKA, A. *Synthesis (Stuttg.)* **1976**, *1976* (12), 835.
- (55) Atherton, F. R.; Openshaw, H. T.; Todd, A. R. *J. Chem. Soc.* **1945**, 660.
- (56) Atherton, F. R.; Todd, A. R. *J. Chem. Soc.* **1947**, 674.
- (57) Georgiev, E.; Roundhill, D. M.; Troev, K. *Inorg. Chem.* **1992**, *31* (10), 1965.
- (58) Georgiev, E. M.; Kaneti, J.; Troev, K.; Roundhill, D. M. *J. Am. Chem. Soc.* **1993**, *115* (23), 10964.

- (59) Mitova, V.; Koseva, N.; Troev, K. *RSC Adv.* **2014**, 4 (110), 64733.
- (60) Le Corre, S. S.; Berchel, M.; Couthon-Gourvès, H.; Haelters, J.-P.; Jaffrès, P.-A. *Beilstein J. Org. Chem.* **2014**, 10, 1166.
- (61) Sabaté, C. M.; Delalu, H. *Eur. J. Inorg. Chem.* **2012**, 2012 (5), 866.
- (62) Groom, C. R.; Bruno, I. J.; Lightfoot, M. P.; Ward, S. C. *Acta Crystallogr. Sect. B Struct. Sci. Cryst. Eng. Mater.* **2016**, 72 (2), 171.
- (63) Reynolds, M. A.; Oppenheimer, N. J.; Kenyon, G. L. *J. Label. Compd. Radiopharm.* **1981**, 18 (9), 1357.
- (64) M. Timperley, C.; Cooper, N. In *Best Synthetic Methods*; Elsevier, 2015; pp 563–632.
- (65) Riesel, L.; Steinbach, J.; Herrmann, E. *Zeitschrift für Anorg. und Allg. Chemie* **1983**, 502 (7), 21.
- (66) Riesel, L.; Steinbach, J.; Thomas, B. *Zeitschrift für Anorg. und Allg. Chemie* **1979**, 451 (1), 5.
- (67) Halonen, H.; Larsson, P. T.; Iversen, T. *Cellulose* **2013**, 20 (1), 57.
- (68) Granja, P. L.; Pouysgu, L.; Ptraud, M.; De Jso, B.; Baquey, C.; Barbosa, M. A. *J. Appl. Polym. Sci.* **2001**, 82 (13), 3354.
- (69) Amaral, I. F.; Granja, P. L.; Barbosa, M. a. *J. Biomater. Sci. Polym. Ed.* **2005**, 16 (12), 1575.
- (70) Ghanadpour, M.; Carosio, F.; Larsson, P. T.; Wågberg, L. *Biomacromolecules* **2015**, 16 (10), 3399.
- (71) Shi, Y.; Belosinschi, D.; Brouillette, F.; Belfkira, A.; Chabot, B. *Carbohydr. Polym.* **2014**, 106 (1), 121.
- (72) Naumkin, A. V.; Kraut-Vass, A.; Gaarenstroom, S. W.; Powell, C. J. NIST X-ray Photoelectron Spectroscopy Database, Version 4.1 <http://srdata.nist.gov/xps/>.
- (73) Trevor, D. J.; Sakka, S. *H A N D B O O K of SOL GEL SCIENCE and TECHNOLOGY Processing , Characterization and Applications VOLUME III APPLICATIONS of SOL-GEL TECHNOLOGY*; Vol. 3.
- (74) Inagaki, N.; Toyoshima, T.; Katsuura, K. *J. fire Retard. Chem.* **1981**, 8 (1).
- (75) Gaan, S.; Sun, G. *J. Anal. Appl. Pyrolysis* **2007**, 78 (2), 371.
- (76) Gleria, M.; De Jaeger, R. *Topics in Current Chemistry*. 2005, pp 165–251.
- (77) Hippler, R. Wiley-VCH Verlag GmbH & Co. KGaA, 2008; p 891.
- (78) Harry, J. E. *Introduction to plasma technology*; Wiley-VCH Verlag GmbH & Co. KGaA, 2010.
- (79) Bour, J.; Bardon, J.; Aubriet, H.; Del Frari, D.; Verheyde, B.; Dams, R.; Vangeneugden, D.; Ruch, D. *Plasma Process. Polym.* **2008**, 5 (8), 788.
- (80) Mahltig, B.; Böttcher, H. *J. Sol-Gel Sci. Technol.* **2003**, 27 (1), 43.
- (81) Mahltig, B.; Haufe, H.; Böttcher, H. *J. Mater. Chem.* **2005**, 15 (41), 4385.
- (82) Hoefnagels, H. F.; Wu, D.; de With, G.; Ming, W. *Langmuir* **2007**, 23 (26), 13158.
- (83) Armarego, W. L. F.; Chai, C. In *Purification of Laboratory Chemicals*; Elsevier, 2013; pp 555–661.



## Curriculum Vitae: LOW JIA EN

### Personal Details

---

Last Name            Low  
First Name           Jia En  
Born                    15 October 1984, Malaysia  
Address                ETH Zurich / HCI H136  
                              Vladimir-Prelog-Weg 1  
                              CH-8093 Zurich, Switzerland  
Email                   lowj@inorg.chem.ethz.ch

### Education

---

11/2012 – 12/2016    **Doctorate in Chemistry**  
                              ETH Zurich  
  
09/2010 – 10/2012    **Master of Science in Chemistry**  
                              ETH Zurich  
  
08/2004 – 06/2008    **Bachelor of Science in Chemistry**  
                              National University of Singapore (NUS)

### Work Experience

---

11/2012 – 04/2017    **Research Assistant at ETH Zurich**  
  
08/2008 – 07/2010    **Research Officer at Institute of Materials Research and Engineering (IMRE), Singapore**

### Language Skills

---

<b>Chinese</b>	<b>Mandarin</b> Native	<b>Cantonese</b> Fluent	<b>Hokkien</b> Elementary
<b>German</b>	Professional (Goethe Zertifikat C1)		
<b>English</b>	Bilingual		
<b>Malay</b>	Professional		
<b>French</b>	Elementary		
<b>Spanish</b>	Elementary		

---

## Conferences and Workshops attended

---

03.2016	13 <sup>th</sup> European Workshop for Phosphorus Chemistry	Berlin, Germany
Poster	„Phosphate Silyl Esters: Synthesis and Application as Flame Retardants Applied onto Cotton Fabrics“	
02.2016	COST MP1105 Workshop on Flame Retardants	Turin, Italy
Poster	„Flame Retardant Behaviour of Water Resistant Cotton Fabrics Modified by Phosphate Silyl Ester“	
06.2015	Flame Retardancy and Protection of Materials	Berlin, Germany
Poster	„Towards Wash Durable Phosphoramidate Flame Retardants on Cellulose-based Cotton Textiles via Plasma-Induced Graft Polymerization (PIGP)“	
06.2015	Flame Retardancy and Protection of Materials	Berlin, Germany
Oral	„Flame Retardants Containing Phosphorus, Nitrogen and Silicon in Different Combinations for Cellulose-based Cotton Textiles“	
02.2015	COST MP1105 Workshop: Advances in Flame Retardancy of Materials	Madrid, Spain
Oral	„Phosphate-based Compounds Containing Additional Elements as Flame Retardants on Cellulose-based Cotton Fabrics“	
09.2014	Swiss Chemical Society Fall Meeting	Zurich, Switzerland
Poster	„The Effect of Additional Elements along with Phosphorus on the Flame Retardancy of Cellulose-based Cotton Textiles“	
05.2014	10 <sup>th</sup> Coating Science International	Noordwijk aan Zee, Netherlands
Oral	„Effects of Phosphorus-, Nitrogen- and Silicon-based Coatings Applied by Plasma-Induced Graft Polymerization Processes on the Flammability of Cellulose-based Cotton Textiles“	
09.2013	Swiss Chemical Society Fall Meeting	Lausanne, Switzerland
Poster	„Synergistic Effects of Phosphorus, Nitrogen and Silicon in the Flame Retardancy of Cotton Textiles Processed by Plasma-Induced Graft Polymerization“	
08.2013	International Science Plasma Conference	Cairns, Australia
Poster	„Synergistic Effects of Phosphorus, Nitrogen and Silicon in the Flame Retardancy of Cotton Textiles Processed by Plasma-Induced Graft Polymerization“	